THE ROLE OF HSP90 IN B CELL RECEPTOR SIGNALING AND NOVEL COMBINATORIAL THERAPIES FOR ABC DLBCL

A Dissertation
Presented to the Faculty of the Weill Cornell Graduate School
of Medical Sciences
in Partial Fulfillment of the Requirements for the Degree of
Doctor of Philosophy

by
Rebecca Lynn Goldstein
May 2015

© 2015 Rebecca Goldstein

“I am but one small instrument.”

- Jimmy Eat World, “Goodbye Sky Harbor”

THE ROLE OF HSP90 IN B CELL RECEPTOR SIGNALING AND NOVEL COMBINATORIAL THERAPIES FOR ABC DLBCL

Rebecca Goldstein, Ph. D.

Cornell University 2015

Rational combinatorial targeted therapies for cancer are likely required to achieve potent durable responses. We mapped the interactome of a tumor-enriched isoform of Hsp90 (teHsp90), using a pharmacoproteomics approach trapping teHsp90 with the small molecule PU-H71. This strategy yielded enrichment of the proximal B cell receptor (BCR) signalosome. In functional assays we identified a novel mechanism for teHsp90 in facilitating BCR signaling dynamics by enabling phosphorylation of key BCR signalosome components including SYK and BTK. Consequently, PU-H71 attenuated BCR signaling, calcium flux and NF-κB signaling, ultimately leading to growth arrest in BCR-dependent ABC DLBCL cells. Combined exposure to PU-H71 and BCR pathway inhibitors, most notably ibrutinib, resulted in more potent suppression of BCR signaling than either drug alone in ABC DLBCL cell lines. PU-H71 combined with ibrutinib correspondingly induced synergistic killing of ABC DLBCL cell lines, primary human specimens *ex vivo*, and lymphoma xenografts *in vivo*, without significant toxicity. Pharmacoproteome driven rational combination therapy thus provides the basis for more potent BCR-directed therapy for ABC-DBLCL patients.

teHsp90 inhibition induces broad attenuation of lateral pathways that contribute to the greater BCR signaling network and DLBCL survival such as PI3K/AKT and ERK signaling, likely contributing to the synergistic growth inhibition induced by the PU-H71-ibrutinib combination treatment. In viability assays of many different combinations of BCR pathway inhibitors in ABC DLBCL cell lines, we observed differential combination growth inhibition effects that suggest general principles required for rational combination treatment design. Namely, inhibition of lateral pathways within a signaling network induces maximal synergistic growth arrest.

BIOGRAPHICAL SKETCH

Rebecca Goldstein grew up in Atlanta, Georgia, where she graduated from Yeshiva Atlanta High School. After studying abroad in Jerusalem, Israel, for one year, she went on to obtain a Bachelors of Arts degree *cum laude* in Biochemistry from Barnard College of Columbia University in New York, NY in 2007. For the next two years, Rebecca worked as a laboratory technician in the laboratory of Dr. Carol Troy at the Columbia University Medical College studying Alzheimer's Disease. In August of 2009, Rebecca began her doctoral studies at the Weill Graduate School of Biomedical Sciences of Cornell University. She joined the lab of Dr. Ari Melnick the following fall. Her thesis work, presented herein, identifies a novel role of Hsp90 in regulating B cell receptor (BCR) signaling in diffuse large B cell lymphoma and preclinical validation of novel therapies for this disease combining inhibition of Hsp90 with inhibitors of the BCR pathway. This work has been submitted for publication and presented at international conferences.

ACKNOWLEDGEMENTS

First and foremost, I want to thank my advisor and mentor, Dr. Ari Melnick for his support and guidance throughout my thesis project. His encouragement and mentorship has truly allowed me to grow into an independent scientist in many realms including experimentation, critical thinking, scientific writing and presentation skills. His belief that nothing is impossible was challenging at times, but ultimately helped me achieve my goals. He ensures the availability of seemingly unlimited resources that allowed my scientific curiosity to expand.

Next, I want to thank Dr. Leandro Cerchietti who has been a second mentor throughout this process. When I rotated in the lab, Leandro was an instructor, sitting just a bench away, always available to discuss an experiment. He has since become an assistant professor with his own lab, but he has remained an invaluable source of guidance and knowledge throughout this project.

I would also like to thank my thesis committee, Dr. Ethel Cesarman, Dr. David Scheinberg and Dr. Gabriela Chiosis for generously giving of their time and expertise to advance my project over the past few years. In particular, I want to thank Dr. Chiosis, who has served as a third mentor on this project. Her expertise and suggestions – and drug – have been instrumental in developing this work. I am very grateful to Dr. Katherine Borden for traveling to New York to serve as an external examiner for my defense.

Thanks to my collaborators who helped with this project. Tony Taldone who provided PU-H71 and PU-H71-beads. The proteomics mass spectrometry was performed in the laboratory of Dr. Kojo Elenitoba-Johnson at the University of

Michigan. TIRF microscropy was heavily assisted by Dr. Kaye Thomas at the Rockefeller University Bio-Imaging Resourse Center. Patient samples were generously provided by Dr. Wayne Tam and Dr. Giorgio Inghirami of the Weill Cornell Medical College.

There are many past and present members of the Melnick lab to whom I am tremendously indebted. Shao Ning Yang taught me almost everything I know from the very early days of my rotation culturing cells clear through animal experiments and everything in between. Thank you to post-docs Dr. Yanwen Jiang, Dr. Karen Bunting, Dr. Lorena Fontan-Gabas and Dr. Wendy Beguelin were always available to discuss results and next steps and to Dr. Katerina Hatzi and Dr. Mariano Cardenas for their friendship and coffee-based support. Perhaps most importantly, I want to thank (almost-)Dr. Tharu Fernando who has been with me from the very first day we started as graduate students in the pharmacology department. From those early days studying signaling transduction and chemical biology and our joint rotation in Ari's lab through our defenses a mere 6 days apart, she has provided tremendous amounts of support and friendship through qualifying exams, committee meetings, lab meetings, and everything in between. Thanks to everyone else in the lab for their help and teamwork.

Finally, I want to thank my friends and family for their continual love and support. Special thanks to my mom for giving me a boost when I needed it and my fiancée, Ariela, for all of her love and support throughout the second half of my PhD.

Funding for this work was provided in part by NIH grants F31 CA174239-02 and R01 CA155226.

TABLE OF CONTENTS

LIST OF FIGURES

CHAPTER FOUR

CHAPTER FIVE

LIST OF TABLES

CHAPTER ONE

INTRODUCTION

Cancer is not a single disease; rather, it is a collection of molecularly distinct illnesses united by shared traits. Most subtypes arise from numerous molecular lesions linked to either somatic mutations or the hijacking of normal proteins by tumors resulting in non-oncogene addiction. Targeted therapies against these proteins and pathways administered as single agents are unlikely to be curative due to the genetic complexity, clonal heterogeneity and development of resistance of most tumors. The signaling pathways that direct the abnormal cellular growth of cancer contain functional redundancy, further complicating efforts to therapeutically target these malignancies. In order to improve treatment for cancer patients, a better understanding of the complex signaling pathways governing tumor growth is required. Greater suppression of these pathways may be achieved through the design of rational combinations of targeted agents that affect parallel or complementary pathways, leading to tumor eradication.

1. Heat shock protein 90 (Hsp90)

Structure and Function

Heat shock protein 90 (Hsp90) is a ubiquitously expressed molecular chaperone that assists the proper folding, assembly and transportation of hundreds of cellular proteins – collectively known as “clients” – involved in numerous processes including cell growth, proliferation and survival (1). Hsp90 is a conformationally flexible protein dimer; each monomer contains a

C-terminal protein-binding region and an amino-terminal ATP-binding pocket linked by a middle domain. With the assistance of certain co-chaperones, Hsp90 hydrolyzes ATP to propel the Hsp90-chaperone cycle in which client proteins are bound in an inactive state, chaperoned for proper folding, and ultimately released (2) (Figure 1.1).

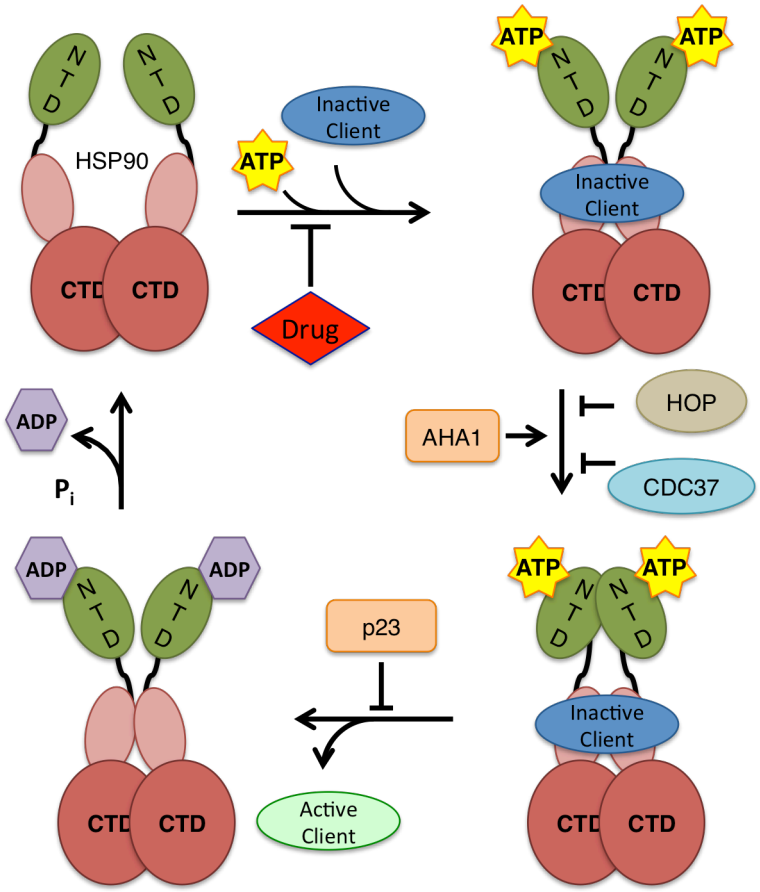

Figure 1.1 The Hsp90 chaperone cycle. Clockwise from top left, ATP binding to the N-termial ATPase domain (NTD) of Hsp90 induces a conformational change and NTD dimerization, forming the closed Hsp90 dimer necessary for ATP hydrolysis. Inactive client proteins bind mostly to the middle domain of Hsp90 and are conformationally activated as Hsp90 advances through the ATPase cycle that is facilitated or inhibited by certain cofactors including AHA1, HOP, CDC37 and p23. CTD, C-terminal domain. Adapted from (2).

Hsp90 is expressed constitutively, but can also be induced upon cellular stress, such as heat shock, in order to maintain the function of damaged

proteins. This function may have played a role in the evolutionary process, allowing cells to tolerate an accumulation of inherent genetic mutations (3, 4). Similarly, because it sustains the viability of cells under transforming pressure, Hsp90 plays an important role in maintaining the cancer phenotype.

The role of Hsp90 in cancer

Six hallmark characteristics are shared by most if not all cancers: (i) self-sufficiency in growth signaling, (ii) insensitivity to anti-growth signaling, (iii) ability to evade apoptosis, (iv) limitless replicative potential, (v) sustained angiogenesis, and (vi) tissue invasion and metastasis (5). Hsp90 regulates proteins and pathways involved in each of these capabilities (Figure 1.2) Hsp90 also maintains the functional stability of damaged proteins, especially in cells under transformative pressure. It is therefore not surprising that cancer cells often hijack this mechanism to promote their malignant phenotype. Indeed, Hsp90 is highly expressed in most tumor cells. Moreover, Hsp90 has been shown to regulate nearly every protein that is involved in cell-specific oncogenic processes (6).

Hsp90 inhibition

Because Hsp90 maintains the stability and activity of many oncogenic client proteins that cause and maintain malignant phenotypes, it is an attractive therapeutic target. Several inhibitors of the N-terminal ATPase pocket of Hsp90 have been discovered and developed. These compounds block ATP from binding Hsp90, locking the chaperone and preventing the conformational changes necessary for the Hsp90 chaperone cycle to proceed. Interruption of chaperone cycling induces targeting of client proteins to the proteasome

where they are degraded (6-8). In a cancer cell, degradation of the oncogenic proteins chaperoned by Hsp90 can result in decreased proliferation or cell death.

The first Hsp90 inhibitors discovered were N-terminal ATP pocket binders, including natural products, such as ansamycins (geldanamycin (GM), 17-allylamino-17-demethoxygeldanamycin (17-AAG), and 17-dimethylaminoethyl-amino-17-demethoxy-geldanamycin (17DMAG) (9-11) and radicicols (RDs) (RD (12), cycloproparadicicol (13), and pochonin D (14)). Two of these early Hsp90 inhibitors, 17AAG and 17DMAG, were the first to enter the clinic. Rational design or high-throughput screening was used to discover later

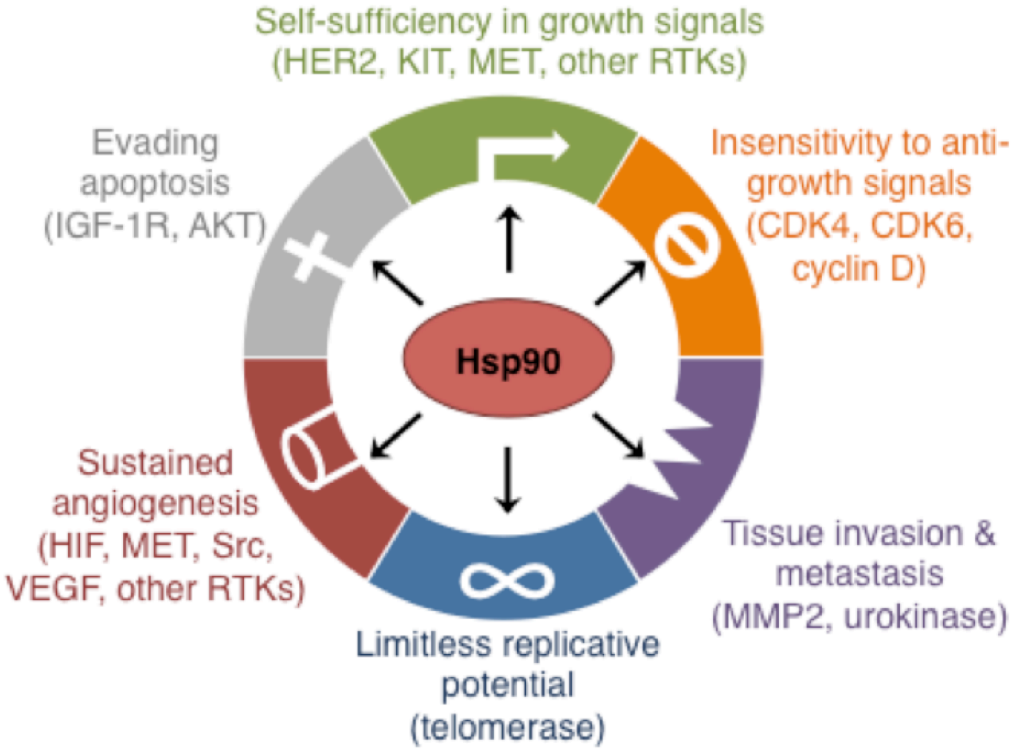

Figure 1.2 Hsp90 chaperones proteins that establish each of the six hallmarks of cancer (Adapted from 1, 5).

Hsp90 N-terminal inhibitors. These include purine-scaffold derivatives (PU-class) (15) and other scaffolds types (16).

Compounds that bind to the C-terminal and middle domains of Hsp90 and disrupt its chaperone function have also been described. Novobiocin, a coumarin-containing DNA gyrase inhibitor, weakly binds the C-terminal domain of Hsp90 (17) that binds a second ATP molecule after the N-terminal pocket has bound either ATP or an inhibitor. The C-terminal ATP binding site may regulate the N-terminal ATPase activity, thereby affecting the Hsp90 chaperone cycle (17, 18).

Agents that interfere with the binding of Hsp90 and its co-chaperones or client proteins have also been described. Shepherdin, a peptidomimetic of minimal span that retains Hsp90 inhibitory activity of the anti-apoptotic and mitotic regulator survivin, binds the ATP pocket of Hsp90, causing destabilization of client proteins (19).

Inhibition of histone deacetylases (HDACs) can induce Hsp90 acetylation, which prevents its ability to bind ATP, which blocks chaperone function and induces degradation of client proteins. This effect has been shown using different HDAC inhibitors including the depsipeptide FR-901228 (20), LAQ824 (Nimmanapalli cancer research 2003), LBH589 (21), suberoilanilide hydroxamic acid (22) and by inhibition of HDAC6 by specific short-interfering RNA (siRNA) (22, 23). Hsp90 chaperone function is also dependent on several post-translational modifications including phosphorylation (24, 25), acetylation (23), ubiquitylation (26) and S-nitrosylation (27). Indirect inhibition

of Hsp90 via modulation of its post-translational modifications may be another route to therapeutically target Hsp90.

Hsp90 is expressed in normal cells, comprising 1-2% of total cellular protein, where it assists the folding of hundreds of proteins including kinases, transcription factors and receptors. Constitutive Hsp90 genetic knockout in eukaryotes is lethal (28), calling into question the therapeutic window required for Hsp90 to be viable drug target. However, it was the discovery and investigation of Hsp90-selective compounds that revealed principles that validated Hsp90 as a *bona fide* target in cancer. Several classes of these inhibitors bind selectively to Hsp90 in tumor cells (19, 29-32). Importantly, cancer cells are significantly more sensitive to Hsp90 inhibition than their normal counterparts (12, 19, 29-34). Further, Hsp90 inhibitors have anticancer effects in animal models at nontoxic doses (19, 32, 33, 35, 36). Some of these inhibitors accumulate in animal model tumors while exhibiting rapid clearance from the blood and normal tissues (11, 29, 32, 37-39).

Tumor selectivity of Hsp90 inhibitors

The astonishing tumor selectivity of Hsp90 inhibitors remains to be fully explained, but data in the field has led to several hypotheses. One idea is that Hsp90 exists in a higher affinity state in cancer cells (30). This notion was first supported by experiments showing that 17AAG exhibits a 100-fold difference in affinity between Hsp90 in transformed cells and that of normal cells (30). Reports with other Hsp90 inhibitors of the PU-class (31, 32) as well as shepherdin (19) confirm this finding. *In vivo* studies demonstrating extensive retention of Hsp90 inhibitors in tumors while being rapidly cleared from blood

also support this hypothesis. The PU-class Hsp90 inhibitor PU24Cl (32) was the first agent to demonstrate this behavior, accumulating at pharmacologically relevant doses in MCF7 xenograft tumors. Studies showing similar results were reported with 17DMAG in MDA-MB-231 xenograft tumors (39), 17AAG in human ovarian xenograft tumors (37), and IPI-504, the reduced form of 17AAG in a multiple myeloma xenograft model (40). Hsp90 inhibitors of several classes exhibit the phenomenon of tumor accumulation, which may be due to the higher affinity state of tumor Hsp90.

A second hypothesis to explain the tumor selectivity of Hsp90 inhibitors is the post-translational modification status of Hsp90 (41). Hsp90 is modified by serine-, threonine- and tyrosine-phosphorylation (42-45). Phosphorylation of Hsp90 results in loss of binding to client proteins (24, 46). As discussed above, acetylation of Hsp90 may be required for chaperone cycle function. Studies in HDAC6-deficient cells show that the glucocorticoid receptor (GR), a client of Hsp90, has diminished ligand binding, nuclear translocation and gene activation (47). More, cytosolic Hsp90 from HDAC-knockdown cells has less ATP-binding affinity and cannot assemble into a complex with GR (23). Acetylated Hsp90 shows decreased association with other clients including HER2, mutant p53, Raf-1 and androgen receptor (48, 49). S-nitrosylation of Hsp90 has also been shown to inhibit its chaperone activity (27). Hsp90 is ubiquitinated at several residues by the ubiquitin ligase C-terminus of Hsc70 interacting protein (CHIP) (50), targeting it to the proteasome (51). Protein methyltransferases have been identified as Hsp90 interacting proteins (52) and Hsp90 lysine methylation by SMYD2 has been described (53, 54). These post-translational modifications may play a role in Hsp90 activity and affinity

for inhibitors. Similar to post-translational modification, the interaction of Hsp90 with certain sets of co-chaperones (30, 55-59) and the post-translational modifications of these co-chaperones (57, 60-64) may play a role in the enhanced affinity of tumor Hsp90 for inhibitors.

Finally, the intrinsic nature and function of Hsp90 may provide the solution. Hsp90 and its co-chaperones can be genetically deregulated in cancer cells (65-68). However, protein expression is unlikely to account for the ability of Hsp90 and its co-chaperones to regulate such an astonishingly diverse repertoire of stressed proteomes (67, 69-71). In normal cells, Hsp90 comprises 1-2% of cellular protein, and in tumor cells, this amount increases to 4-6%. In the *in vivo* Hsp90 inhibitor experiments described above, inhibitors are administered in great excess (50 – 200 mg/kg) of the amount of Hsp90 protein (~500 μM) found in the tumors. At these concentrations, the drugs inhibit tumor growth, but only 0.5-50% of drug is retained in the tumors, suggesting that only a small fraction of total Hsp90 binding sites are bound by inhibitor (72). These calculations suggest that there exists a pool of Hsp90 in a high-affinity conformation that specifically chaperones the small fraction of cellular proteins that drive the malignant phenotype.

Taken together, these complementary hypotheses illustrate a scenario with two states of Hsp90. “Latent state” Hsp90, found in normal cells, (and to a lesser extent in stressed or cancer cells,) chaperones normal proteins and exhibits low-affinity for ATP as well as Hsp90 inhibitors. Cancer cells or other chronically stressed cells, preferentially contain “activated state” Hsp90, which is found in megacomplexes with co-chaperones and has a high affinity for

client proteins, which are often involved in driving and regulating the malignant phenotype (Figure 1.3). Under transforming pressure, such as mutation, activation or other stress, Hsp90 client proteins in cancer cells develop an increased requirement for chaperoning. This tumor-enriched Hsp90 (teHsp90) has a higher affinity for inhibitors, which may explain the therapeutic window of this class of drugs (72).

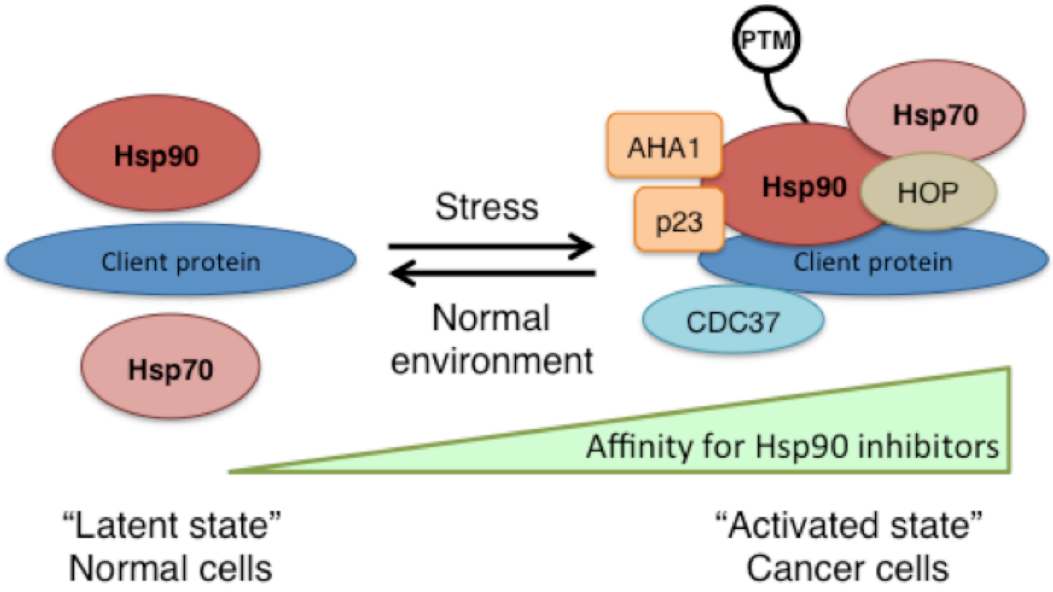

Figure 1.3 The two states of Hsp90. Tumor cells preferentially contain Hsp90 in higher-order multi-chaperone complexes. This tumor-enriched Hsp90 (teHsp90) has a higher affinity for Hsp90 inhibitors than normal tissues, which contain latent, uncomplexed Hsp90. Modified from (72).

Hsp90 complexes in cancer cells are not comprised of only activated state Hsp90. Rather, cancer cells contain both a pool of latent state or "housekeeping Hsp90" with low affinity for Hsp90 inhibitors in addition to the activated or "oncogenic Hsp90" pool which chaperones the proteome required for the malignant phenotype (58). Exactly how these two fractions differ remains to be resolved, but may be explained by one or more of the above

hypotheses. This difference, however, provides the rationale for targeting Hsp90 in cancer cells.

Hsp90 inhibitors as chemical tools

While the definitive source of the tumor selectivity of Hsp90 inhibitors has yet to be elucidated, this principle can be exploited to identify tumor specific teHsp90 client proteomes. By immobilizing Hsp90 inhibitors on solid supports, these compounds can be used as chemical tools to affinity purify cell-specific teHsp90 megacomplexes. This method allows not only for the identification of the cell-specific teHsp90 proteome, but also the investigation of the molecular mechanisms by which teHsp90 regulates specific subtypes of cancer.

This approach goes back to the first Hsp90 inhibitor, geldanamycin. Originally identified in a screen of compounds that could revert the phenotype of cells transformed with the v-src oncogene, it was eventually shown that the tumoricidal activity of GM was not related to src-inhibition (34). Rather, using solid phase immobilized GM affinity precipitation, Hsp90 was identified as the molecular target of GM, highlighting the role of Hsp90 in oncogenic processes (73).

In fact, this method (Figure 1.4) was used to describe the oncogenic pool of teHsp90-chaperoned complexes in cancer cells. Moulick et al (58) used PU-H71, a purine-scaffold small molecule inhibitor of Hsp90, conjugated to agarose beads to chemically precipitate teHsp90 in the breast cancer cell line MDA-MB-468. After seven sequential chemical precipitations, the fraction of Hsp90 bound to PU-H71 was drastically reduced as shown by immunoblot for

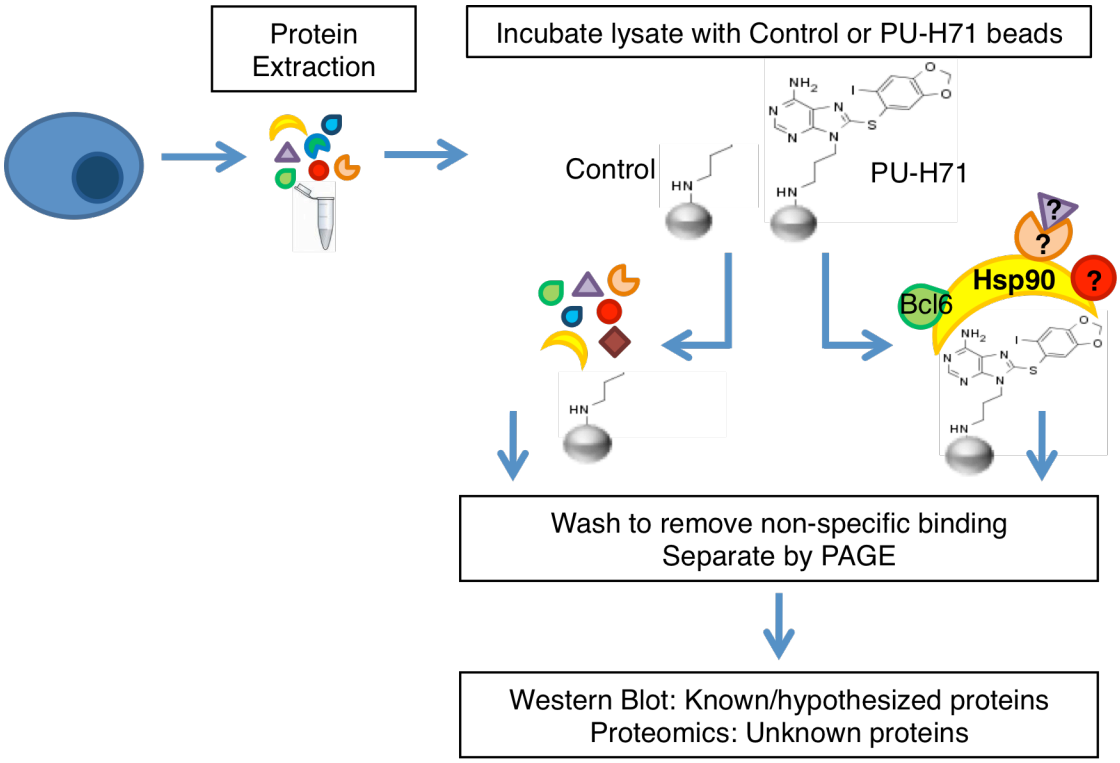

Figure 1.4 PU-H71 chemical precipitation. Following cell lysis, protein extracts are precleared, then incubated with agarose beads conjugated to an Hsp90 inert chemical (control) or PU-H71 beads to precipitate teHsp90 complexes. Beads are washed, complexes are eluted by boiling in SDS loading buffer and resolved by SDS PAGE followed by mass spectrometry (unknown clients) or immunoblotting (known/hypothesized clients).

Hsp90 (58). Although the pool of Hsp90 bound by these compounds was nearly depleted, immunoprecipitation of the remaining supernatant with an antibody to Hsp90 effectively isolated substantial amounts of Hsp90, which showed no depletion after three sequential immunoprecipitations (58). This finding demonstrates that PU-H71 interacts with a specific fraction of Hsp90 in cancer cells. Along these lines, the authors went on to show that some Hsp90 inhibitors can deplete cancer cells of Hsp90-chaperoned oncoproteins. Using extracts from the BCR-ABL+ CML cell line K562, the authors first demonstrated that an antibody to Hsp90 co-immunoprecipitates both BCR-ABL and its normal counterpart c-Abl, and that both of these proteins are

present in the remaining supernatant. By contrast, chemical precipitation of teHsp90 complexes with PU-H71 beads preferentially sequestered BCR-ABL, while the remaining supernatant contained only Abl, furthering the notion that the pool of PU-H71-bound teHsp90 can be depleted (58). To further demonstrate this, the authors performed sequential chemical precipitations using PU-H71 beads followed by immunoprecipitation with an antibody to Hsp90 of the remaining supernatant. Sequential PU-H71 chemical precipitations depleted cell extracts of BCR-ABL to the extent that the final immunoprecipitation isolated only Abl and not BCR-ABL, though this antibody was previously shown to co-immunoprecipitate equal amount of both proteins (58). The authors observed similar results for the synthetic Hsp90 inhibitor SNX-2112, while NVP-AUY922 behaved like the Hsp90 antibody. GM beads were less efficient at co-precipitating BCR-ABL. The authors also showed that the PU-H71-bound fraction of teHsp90 in K562 cells co-precipitates with the chaperones Hsp70, Hsp40 and HOP (58). This data clearly shows that teHsp90 inhibitors interact with a restricted fraction of Hsp90 that preferentially chaperones oncoproteins. Finally, the authors used PU-H71 chemical precipitation combined with mass spectrometry to identify the aberrant signalosome of CML cells (58). From these experiments, the authors identified the STAT pathway as clients of Hsp90 and described a novel role of teHsp90 in regulating STAT activation in CML.

In a collaboration project, work from our laboratory demonstrates that teHsp90 chaperones viral proteins that drive Kaposi's sarcoma-associated herpesvirus (KSHV) positive primary effusion lymphomas (PELs). Using PU-H71 chemical precipitation, both vFLIP, the viral homolog of cellular FLIP (cFLIP), and its

downstream target IKKγ were identified as clients of teHSP90 in four KSHV$^+$ PEL cell lines (Figure 1.5) (74). Together, vFLIP and and IKKγ form the vFLIP signalosome which induces NF-κB activity, leading to anti-apoptotic and pro-proliferative signaling in PEL cells (75). Importantly, PU-H71-bound teHsp90 associates only with cFLIP$_L$ (long isoform) and not cFLIP$_S$ (short isoform) (74). Though vFLIP is more closely structurally related to cFLIP$_S$, it is the long isoform of cFLIP that induces NF-κB activity (75). This finding confirms that PU-H71 selectively precipitates oncocomplexes. Taken together, these studies clearly demonstrate the usefulness of Hsp90 inhibitors, specifically the purine scaffold inhibitor PU-H71, as chemical tools to probe known and unknown client oncoproteins of Hsp90 to reveal underlying mechanisms of teHsp90 regulation of cancer.

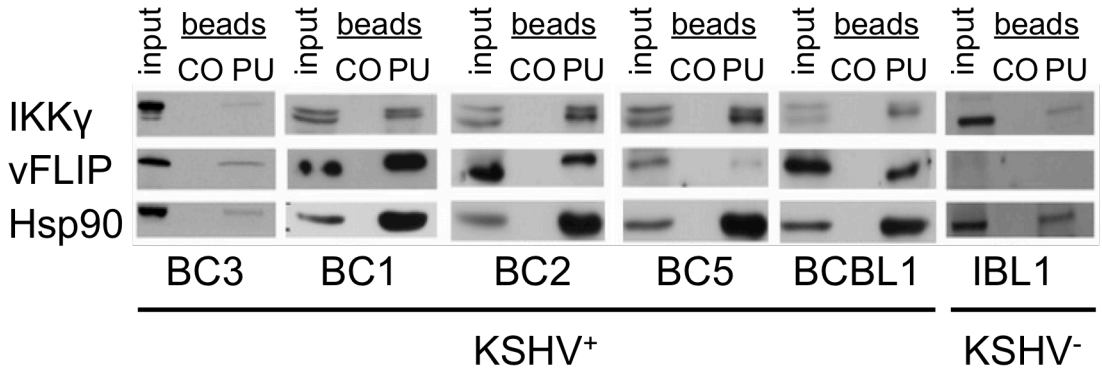

Figure 1.5 teHsp90 chaperones the vFLIP signalosome in KSHV$^+$ PELs. Immunoblots of PU-H71-bead (PU), but not control-bead (CO) pulldowns in KSHV$^+$ PEL cell lines recognized vFLIP and IKKγ. IBL1, a KSHV$^-$ cell line, was included as a negative control for vFLIP (74).

Hsp90 inhibitors target oncoproteins

While the exact mechanism of the tumor selectivity of Hsp90 inhibitors remains to be elucidated, teHsp90 selectively chaperones those proteins required for cancer cell survival, many of which are mutated or chimeric. As a

result, these oncoproteins are degraded upon teHsp90 inhibition. For example, anaplastic large cell lymphoma is characterized by the expression of the constitutively active chimeric protein NPM-ALK, a fusion of the nucleophosmin (NPM) and the membrane receptor anaplastic lymphoma kinase (ALK). NPM-ALK is a client of Hsp90 and is destabilized and degraded in cells exposed to Hsp90 inhibitors (76). Exposure to Hsp90 inhibitors causes selective apoptosis in acute myeloid leukemia (AML) cells harboring mutant FLT3 receptor tyrosine kinase (77) through rapid loss of FLT3 activity as well as several of its downstream targets. The BCR-ABL fusion protein results from a chromosomal abnormality associated with chronic myelogenous leukemia (CML) and is a client of Hsp90 (58, 78). Mutations in the c-*kit* proto-oncogene cause constitutive activity of the KIT protein associated with gastrointestinal stromal tumors (GIST). This activity as well as activity of downstream effector molecules is abrogated upon exposure to Hsp90 inhibition (79). Mutant B-Raf often associated with melanomas is highly dependent on Hsp90 and accordingly sensitive to Hsp90 inhibition (80, 81). Prostate cancer is often driven by overexpression, mutation or post-translational modification of the androgen receptor (AR), even in the presence of anti-androgens. AR is an Hsp90 client whose expression is decreased with Hsp90 inhibition in a prostate cancer cell line (82). Moreover, Hsp90 inhibition prevents nuclear translocation of ligand-bound AR and diminishes transcriptional activity of nuclear AR (36). The BCL6 transcription factor gene is often translocated and hypermutated in diffuse large B cell lymphoma (DLBCL). BCL6 is chaperoned by Hsp90 and degraded upon Hsp90 inhibition (38). Just as teHsp90 selectively chaperones oncogenic proteins, teHsp90 inhibition disrupts the function and stability of these client onocoproteins in a variety of tumor types.

Hsp90 inhibition overcomes resistance to targeted therapies of Hsp90 client proteins

Many targeted therapies for cancer are aimed at proteins that drive the malignant phenotype either through mutation or non-oncogene addiction. One of the major deficits of single agent targeted therapy is the acquisition of resistance either through mutation of the drug binding site or upregulation of a compensatory molecule or pathway. Many of these targeted oncoproteins are clients of Hsp90, and cells that have become resistant to first line therapeutics targeted to these molecules are sensitive to Hsp90 inhibitors. For example, imatinib is a small molecule inhibitor of the BCR-ABL fusion protein that drives Philadelphia chromosome-positive leukemia (83). These cells can acquire imatinib resistance through mutations in the BCR-ABL kinase domain or gene amplification (84), but have been shown to increase or maintain their dependence on Hsp90 and sensitivity to Hsp90 inhibition (85). In tumors with MET gene amplifications, c-Met inhibition only causes a modest decrease in downstream signaling, but 17AAG destabilizes c-Met protein and also causes significant disruption of downstream signaling (86). Tumor xenografts harboring MET-amplifications that are both sensitive and resistant to c-Met inhibitors are sensitive to Hsp90 inhibtion (87). Non-small cell lung cancer (NSCLC) cells acquire resistance to the tyrosine kinase inhibitors gefinitib and erlotinib through a T790M mutation in EGFR. Hsp90 inhibition in these cells reduces EGFR expression levels as well as downstream and compensatory signaling (88). Some EGFR mutations are intrinsically resistant to gefitinib and erlotinib, but Hsp90 inhibitors destabilize these mutants as well as downstream signaling, resulting in decreased tumor cell viability (89). Other

NSCLC tumors express the EML4-ALK fusion oncogene and initially respond to the tyrosine kinase inhibitor crizotinib, which targets ALK. These tumors gain resistance through gene amplifications and a kinase domain mutation, but resistant cells are highly sensitive to 17AAG (90). Breast cancer patients with amplification of the HER2 oncogene are effectively treated with trastuzumab, a fully humanized monoclonal antibody to HER2, until resistance emerges through truncation of HER2, dimerization with other receptor tyrosine kinases, activation of downstream kinases or deletion of downstream tumor suppressors. HER2-positive cell lines with intrinsic or acquired resistance to trastuzumab are sensitive to Hsp90 inhibition, and show degradation of HER2 as well as inhibition of downstream signaling (91). Triple negative breast cancers, which do not express HER2, estrogen receptors or progesterone receptors, are insensitive to most targeted therapies. They are, however, sensitive to Hsp90 inhibition because of loss of multiple signaling pathways, causing decreased proliferation and induction of apoptosis in cellular and animal models (92).

Hsp90 inhibitors can overcome resistance to other non-targeted therapies as well. For example, mantle cell lymphoma is effectively treated with the proteasome inhibitor bortezomib. Resistance emerges quickly through upregulation of the co-chaperone Grp78, which depends on Hsp90 chaperoning activity. Resistant cells treated with bortezomib combined with Hsp90 inhibitors disrupt the Grp78/Hsp90 complex and cause apoptosis *in vitro* and *in vivo* (93).

Hsp90 inhibitors in the clinic

As discussed, teHsp90 is a promising therapeutic target for cancer. As such, many inhibitors have been tested in the clinic. Geldanamycin, an ansamycin and the first Hsp90 inhibitor, displayed poor solubility in addition to significant hepatotoxicity in animals, preventing its clinical evaluation (94). 17AAG, a derivative of GM with similar biological activity but an improved toxicity profile (10) was the first to enter the clinic. In a phase II clinical trial of women with trastuzumab-resistant HER2+ breast cancer, the addition of 17AAG caused significant response (8). Other trials of 17AAG plus bortezomib in relapsed/refractory multiple myeloma also demonstrated promising results (11). A more water soluble derivative of 17AAG, 17-desmethoxy-17-N,N-dimethylaminoethylaminogeldanamycin (17DMAG), was synthesized by the NCI. This compound was explored in various trials of prostate cancer, melanoma, breast cancer, and AML (92, 93). Though 17DMAG was well-tolerated and showed some clinical activity, this research program was terminated possibly due to competition from upcoming second generation inhibitors as well as the difficult synthesis of 17AAG (95). Infinity pharmaceuticals developed a water-soluble salt of 17AAG called IPI-504, the reduced hydroquinone of 17AAG. *In vivo*, these compounds exist in a redox equilibrium. The quinone of 17AAG may have been the source of the compound's hepatotoxicity; reduction to a hydroquinone resulted in the less toxic, more potent IPI-504. Hsp90 inhibitors from the purine class have also entered the clinic, including BIIB021, the second purine scaffold-based Hsp90 inhibitor developed by Biogen Idec, CUDC-305 developed by Curis, and PU-H71 developed at Memorial Sloan Kettering (96). Several Hsp90 inhibitors from the resorcinol family have also been evaluated clinically. STA-9090

(ganetespib) developed by Synta Pharmaceuticals showed activity in clinical trials of advanced solid tumors as well as NSCLC patients. AUY922 developed by Novartis has shown clinical activity in breast cancer and GIST and is currently being evaluated in DLBCL patients (96).

Hsp90 inhibition as a platform for combination therapies

The tumor selectivity of Hsp90 inhibitors created the basis for therapeutically targeting teHsp90 in cancer. Another attractive feature of Hsp90 as a therapeutic target is its broad relevance to different types of cancer regardless of genetic background. Because teHsp90 chaperones a plethora of different oncoproteins in multiple signaling pathways, it stands to reason that Hsp90 inhibition constitutes a simultaneous attack on multiple nodes of a cancer cell's signaling network. Hsp90 inhibition can break or at least weaken concurrently multiple oncogenic signaling pathways. This feature is highly attractive because single agent therapy is unlikely to be curative in cancer due to acquisition of resistance, tumor heterogeneity and redundant signaling pathways. All of these issues can be addressed, at least partially, by Hsp90 inhibition, because Hsp90 inhibitors target multiple proteins and pathways at the same time. As discussed, Hsp90 inhibition can overcome de novo and acquired resistance to targeted therapies in several types of cancer. In this regard, Hsp90 inhibition serves as an optimal platform for combination with targeted therapies against Hsp90 client proteins. This approach could show increased anti-tumor effect through maximal suppression of critical signaling nodes by inhibiting directly with targeted inhibitors in addition to Hsp90 inhibition. Furthermore, as the client protein is destabilized and degraded in the presence of Hsp90 inhibition, synergistic antitumor effects may be

observed, as less of the targeted agent is required to hit its target. The identification of druggable teHsp90 client proteins and pathways specifically required for cancer cell survival may highlight rational targets for combinatorial therapies for cancer. These combination treatments may evade the emergence of resistance due to the broad dampening of cellular signaling that results from Hsp90 inhibition.

Diffuse large B cell lymphoma (DLBCL)

B cell development

Many of the key processes required for normal B-cell differentiation and survival also contribute to the transformed phenotype of B-cell lymphomas. B cell receptor (BCR) expression on the cell surface is the hallmark of B cells. This receptor comprises two heavy-chain and two light-chain immunoglobulin (Ig) polypeptides covalently linked by disulfide bridges. The Igα/Igß (CD79A/CD79B) heterodimer, the signaling moiety of the BCR, contains cytoplasmic immunoreceptor tyrosine activation motifs (ITAMs) that transmit signals to downstream signaling effectors of the BCR pathway upon BCR crosslinking.

Early B-cell development, which occurs in the bone marrow, is the process by which B cell precursors rearrange the Ig heavy- and light-chain gene loci to produce a functional surface BCR (97). Accordingly, each step of this progression is characterized by the specific structure of the BCR. The Ig molecules contain variable and constant regions, which bind to antigen and mediate downstream signaling, respectively. Pre-B cells rearrange the genetic

loci that encode the heavy- and light-chain regions of the variable regions through V(D)J recombination. In this process the 50 V_H, 27 D_H, and 6 J_H gene segments are joined to produce the heavy-chain variable region. The variety of gene segments available for rearrangement ensures the generation of a diverse repertoire of V_H gene rearrangements. D_H-J_H rearrangements occur first, followed by V_H-D_HJ_H rearrangements. If productive, this process culminates in expression of a pre-B-cell receptor. Pre-B cells then carry out rearrangements of the light-chain from V_L and J_L gene segments. Ultimately the rearranged VDJ is joined to an Ig constant region (98). Following this process, pre-B cells that express a functional BCR differentiate into mature B cells and leave the bone marrow; those that do not undergo apoptosis (98).

Following VDJ recombination, mature B cells are activated by antigen binding of the BCR during immune response. In T-cell-dependent immune responses, mature B cells enter transient structures called germinal centers that are found in secondary lymphoid organs such as the lymph nodes. The histological appearance of these structures divides the germinal center into two distinct sections: the dark zone, which contains large proliferating B cells (centroblasts), and the light zone, which contains smaller, non-dividing B cells (centrocytes). Germinal center formation begins when a naïve mature B cell in the B cell follicle encounters antigen. Once in the germinal center, B cells enter the dark zone where they undergo massive clonal expansion (99). These rapidly proliferating cells undergo somatic hypermutation of the genes of the Ig variable region in an attempt to further increase the affinity of the BCR for antigen (100). Disadvantageous mutations that lead to reduced affinity of the BCR for antigen causes cells to undergo apoptosis. The few germinal center B

cells with increased affinity for antigen are positively selected for survival by $CD4^+$ T cells and follicular dendritic cells in the light zone (101).

After somatic hypermutation, cells undergo a process of class switching where the constant region of the heavy chain is replaced with that of another Ig gene, such as IgM being replaced by IgG. Finally, these germinal center B cells differentiate into memory B cells or plasma cells and leave the germinal center microenvironment (97). This process is illustrated in Figure 1.6.

The considerable genotoxic stress associated with the processes of B cell development is tightly regulated. The BCL6 (B cell lymphoma 6) transcription factor is a critical transcriptional regulator of germinal center formation and antibody affinity maturation. BCL6 knockout mice fail to develop germinal centers and lack antibody affinity maturation, suggesting its essential role for these processes (102, 103). In fact, BCL6 is upregulated by both B and T cells in the B cell follicle following antigenic stimulation of naïve B cells (104, 105). The transcriptional program of BCL6 in the germinal center enables GC B cells to tolerate this level of damage. By repressing expression of genes involved in cell cycle arrest, apoptosis and DNA damage response such as *TP53*, *CDKN1A*, *ATR, CHK1* and *ATM* (106-110). BCL6 allows GC B cells to undergo rapid proliferation despite an excess of DNA damage including double-stranded breaks that normally causes apoptosis. In order to prevent premature activation of GC B cells by T cells, BCL6 also represses genes involved in B cell activation such as *CD69*, *CD44*, *CD23b* and *NF-κB1* (111-113). BCL6 also maintains the germinal center phenotype by blocking terminal differentiation of GC B cells to plasma cells by repressing *PRDM1* (113). BCL6

downregulation is required for centroblasts to differentiate into centrocytes and ultimately plasma cells. Following antigen engagement of the BCR, mitogen-activated protein kinases (MAPKs) phosphorylate BCL6, leading to its ubiquitin-mediated proteasomal degradation (114). Follicular helper T cells expressing CD40 ligand interact with GC B cells, inducing CD40 signaling, leading to NF-κB-mediated activation of IRF4. Binding of the BCL6 promoter by IRF4 results in downregulation of BCL6 (115). Overall, BCL6 is a master transcriptional regulator of the germinal center program.

Non-Hodgkin's lymphoma (NHL) is the seventh most common type of cancer. This group of about 15 different malignancies can be formed from either B-cells or T-cells, the most common of which is diffuse large B cell lymphoma (DLBCL). In 2014, the NIH estimates over 70,000 new cases of DLBCL resulting in almost 19,000 deaths (www.cancer.gov). Historically, DLBCL patients exhibited clinical heterogeneity, with only about 40% of patients responding to therapy (116).

Because stages of B cell development are characterized by specific structures of the BCR and expression of differentiation markers, examination of these features can be used to distinguish the cells of origin of different subtypes of B cell lymphomas (117, 118). In order to improve diagnosis and treatment of DLBCL, many studies have attempted to classify this molecularly heterogeneous disease. One gene expression profiling study divided DLBCL into two major subtypes (119). Germinal center B cell like (GCB) DLBCL can be characterized by the expression of genes important for germinal center differentiation including BCL6 and CD10, whereas activated B cell like (ABC)

DLBCL is distinguished by a gene expression profile resembling that of activated peripheral blood B cells. The NF-κB pathway is more active and often mutated in ABC DLBCL (119). Each of these subtypes differs not only in gene expression and apparent cell of origin, but also in the process of malignant transformation, clinical presentation, chemotherapy cure rates and response to targeted therapies, making each a distinct cancer.

These prospective classifications were made using patient samples and while they have advanced the understanding of the molecular mechanisms underlying DLBLCL to a degree, they have not been the final answer for diagnosis or treatment of patients. Until these details are better understood, treatments cannot be individually tailored. Because patient samples are comprised of heterogeneous populations of cells and tumor microenvironment plays a role in the disease (120), DLBCL cell lines do not classify as well as patient samples. However, well-characterized cell lines can be used as models of the different subtypes of DLBCL in which to investigate the molecular mechanisms behind the disease.

DLBCL pathogenesis

An accumulation of genotoxic stress accompanies B cell development, including double stranded DNA breaks. The double-stranded DNA breaks that occur during VDJ recombination can result in recombinations that drive lymphomas (121, 122). During the GC reaction, B cells undergo additional double stranded DNA breaks during class switch recombination (123) and somatic hypermutation (124) that mainly affect the Ig locus. In DLBCLs trapped in the GC stage of differentiation, somatic hypermutation is an ongoing

process. These mutations can affect genes that are not usually targets of this process, which may introduce additional mutations to promote tumor survival (125, 126). For example, translocation of BCL6 occurs in about 25% of DLBCLs (127). Most of these translocations occur in the region that contains the first exon and the 5' region of the first intron (128). BCL6 regulates an important group of oncogenes in normal B cells including *BCL2*, *MYC*, *CCND1* and *BMI1* (129). Downregulation of BCL6 is required for exit from the GC and differentiation. In the presence of activating BCL6 translocations, GC B cells repression of these genes is disrupted (129), enabling tumor proliferation and survival. Accordingly, mice with constitutive expression of BCL6 in germinal center B-cells develop tumors that resemble human DLBCL (130, 131). Further, BCL6 is a therapeutic target in DLBCL (132). GCB DLBCLs may also exhibit BCL2 translocations (133), deletion of the tumor suppressor *PTEN* (134) or p53 mutations (135).

ABC DLBCL exhibits genetic abnormalities unique to its subtype. Blimp-1, encoded by *PRDM1*, which represses BCL6, is frequently deleted in ABC DLBCL, blocking full differentiation into plasma cells (115, 128, 133, 136, 137). Other genetic aberrations include overexpression of BCL2 and amplification of the *BCL2* locus (133). These lymphomas also exhibit deletions of the *INK4A-ARF* locus, which encodes p16, an inhibitor of senescence, and $p14^{ARF}$, an inhibitor of p53 activation (133, 138). The actions of chemotherapy are prevented in the absence of these tumor suppressors, which may explain why ABC DLBCLs have a poorer prognosis with conventional chemotherapy (133).

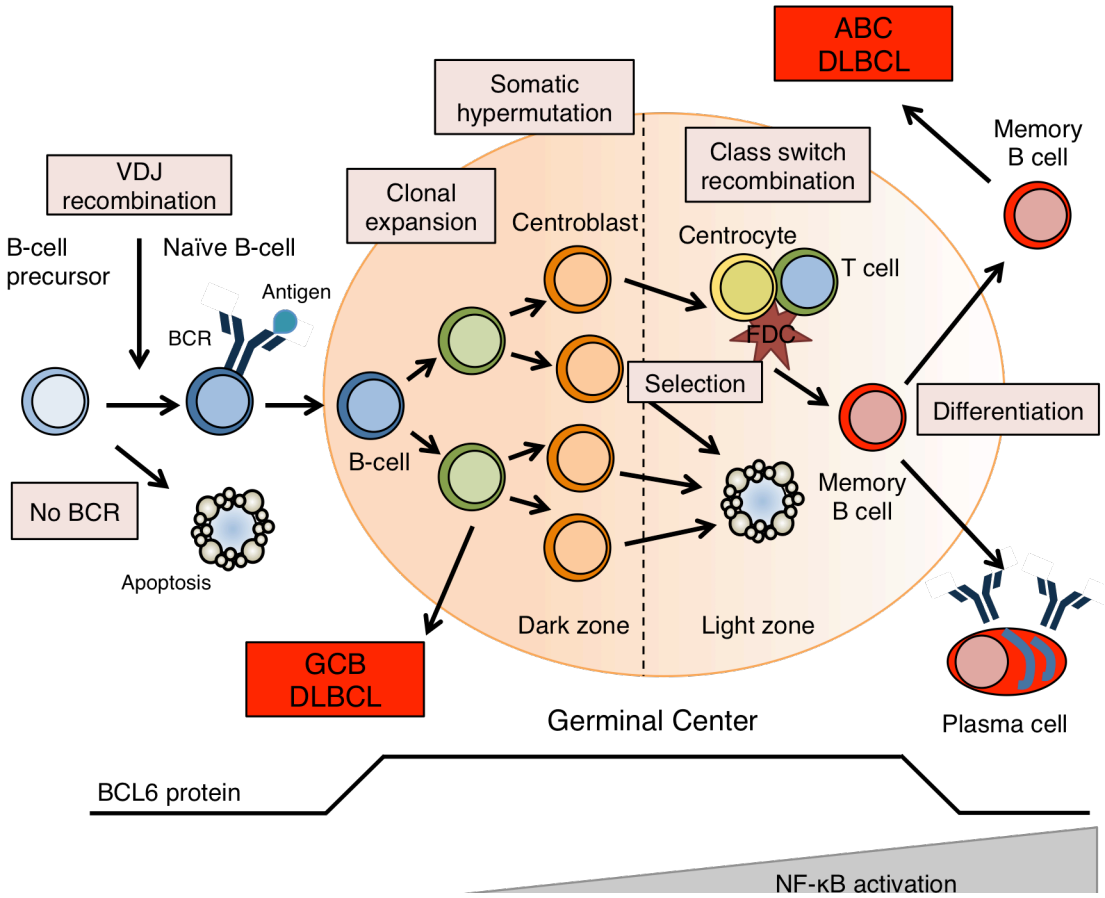

Figure 1.6 B-cell differentiation and germinal center reaction. B cell precursors undergo V(D)J recombination to rearrange Ig heavy- and light-chain genes until equipped with functional surface B cell receptor (BCR). Naïve B cells are activated when antigen binds BCR, then enter germinal centers (GCs) to proliferate into memory B cells. There, naïve B cells are replaced by proliferating B cells in the dark zone and undergo somatic hypermutation of the V_H region to increase antibody affinity for antigen. Cells with mutations that increase the affinity of the receptor for antigen survive. Next cells undergo a process of class switching where the constant region of the heavy chain is replaced with that of another Ig gene. Interactions with T cells in the light zone can induce NF-κB activation. Finally, these cells differentiate into memory B cells or plasma cells and leave the GC. Modified from (97).

ABC DLBCL was initially identified and defined by a gene expression signature characteristic of normal B cells activated *in vitro* (119). Later studies showed that ABC DLBCL exhibits constitutive NF-κB activity that is required for lymphoma survival (139). In normal B cells, crosslinking of the BCR leads

to phosphorylation of IκBα, leading to its ubiquitylation and degradation. This protein functions to sequester NF-κB subunits in the cytosol. When IκBα is degraded, NF-κB subunits translocate to the nucleus and activate an anti-apoptotic transcriptional program. In ABC, but not GCB, DLBCL, interference with NF-κB signaling through retroviral transduction of a super-repressor form of IκBα or dominant negative forms of IκB kinase (IKK), the kinase that phosphorylates IκBα, killed lymphoma cells (139). Moreover, a target of NF-κB is the transcription factor IRF4 (140) that drives terminal B cell differentiation by transactivating Blimp-1 (141, 142). Together, IRF4 and Blimp-1 promote expression of XBP-1, a transcription factor that promotes the secretory phenotype (143-145). ABC DLBCLs express both IRF4 and XBP-1, but genetic inactivation of Blimp-1 blocks full plasmacytic differentiation of these cells (113, 128, 136, 137).

BCR signaling

Signaling through the BCR is required for B cell proliferation and survival. The BCR is a large transmembrane immunoglobulin receptor, most often IgM or IgD. The Igα/Igβ (CD79A/CD79B) heterodimer is associated with the BCR and acts as its signal transduction moiety. Ligand binding of the BCR causes aggregation of receptors, inducing phosphorylation of immunoreceptor tyrosine-based activation motifs (ITAMs) found on the cytoplasmic tails of CD79A/CD79B by src family kinases such as LYN, BLK and FYN. Spleen tyrosine kinase (SYK), a cytoplasmic tyrosine kinase is recruited to doubly phosphorylated ITAMs on CD79A/CD79B through its SH2 domain. Once docked, SYK is activated, and phosphorylates many downstream targets including the adaptor molecule BLNK. Concurrently, PI3-K is activated by

recruitment to the BCR coreceptor CD19, generating phosphatidylinositol 3,4,5-triphosphate (PIP_3), which activates the AKT/mTOR pathway. PIP_3 binds to Bruton's tyrosine kinase (BTK), recruiting it to the membrane, where it forms a complex with BLNK and phospholipase Cγ (PLCγ). Activation of these kinases by BCR aggregation results in the formation of the BCR signalosome at the cell membrane, comprised of the BCR, CD79A/CD79B heterodimer, src family kinases, SYK, BTK, BLNK and its associated signaling enzymes. The BCR signalosome mediates signal transduction from the receptor at the membrane to downstream signaling effectors.

PLCγ cleaves phosphatidylinositol 4,5-bisphosphose (PIP2) into diacylglyercol (DAG) and the second messenger inositol trisphosphate (IP3), which activates both calcium release through the calcium-release-activated calcium (CRAC) channel and NFAT. DAG activates protein kinase Cβ (PKC-β) which phosphorylates latent CARD-11 causing its translocation to the cell membrane where it forms a multiprotein complex with MALT1, BCL10 and TRAF6. The ubiquitin ligase TRAF6 becomes autoubiquitinated and forms a complex with TAB2 and TAK1, the latter of which phosphorylates IKKβ, activating IKK to phosphorylate IκBα, leading to its degradation and activation of NF-κB signaling. The deubiquitinase A20 is a target gene of NF-κB that inhibits NF-κB signaling by deubiquitinating IKK and TRAF6.

Signals from the BCR signalosome are also transduced to extracellular signal-related kinase (ERK) family proteins through Ras and to the MAPK family through Rac/cdc43. Activation of PLCγ causes increases in cellular calcium, resulting in activation of calcium-calmodulin kinase (CaMK) and NFAT. Many

other downstream effectors in this complex pathway (p38 MAPK, ERK1/2, CaMK) translocate to the nucleus to affect change in transcription of genes involved in cell survival, proliferation, growth and differentiation (Reviewed in 146, 147).

Chronic active BCR signaling in ABC DLBCL

In an attempt to identify new therapeutic targets for ABC DLBCL, an “Achilles heel” RNA interference screen was used to identify genes necessary for tumor survival (148). Using this method, CARD11, BCL10 and MALT1, the three proteins of the CBM complex, were identified as necessary for ABC but not GCB DLBCL survival (148). As discussed, the transient activation of this complex leads to activation of NF-κB signaling in normal lymphocytes. The discovery of somatic mutations in CARD11 in ABC DLBCL explains the continuous requirement for this complex (149). Mutations in CARD11 are present in about 10% of ABC DLBCLs and can constitutively activate NF-κB when introduced to heterologous cells. Further, following BCR stimulation, these mutants can potentiate NF-κB signaling (149).

In most ABC DLBCLs, CARD11 is not mutated, but these tumors still express high levels of NF-κB genes and wild-type CARD11 is required for ABC DLBCL cells. In these tumors, signaling molecules upstream of the CBM may activate CARD11 and NF-κB. An RNA interference screen identified that NF-κB signaling in ABC DLBCLs requires BTK, a tyrosine kinase required to connect BCR signaling to NF-κB signaling (150). The BCR itself activates BTK in these lymphomas, as knockdown of the BCR (immunoglobulin heavy or light chains), CD79A and CD79B is lethal to ABC DLBCLs with wildtype CARD 11 (150).

Total internal reflection fluorescent (TIRF) microscopy experiments demonstrated that the BCR of ABC DLBCLs exhibits prominent clustering with low diffusion in the cell membrane, as opposed to GCB DLBCLs that showed diffuse distribution of the BCR in the cell membrane (150). These clusters colocalized with phosphotyrosine suggesting that they represent active signaling (150). These clusters may form due to the presence of a yet unknown antigen or a defect in BCR membrane assembly. Genes in the BCR pathway were resequenced in order to provide genetic evidence of the role of BCR signaling in the pathogenesis of ABC DLBCL. These efforts revealed somatic mutations in CD79B in over one fifth of the ABC DLBCL patients examined as well as less frequent mutations in CD79A (150). These mutations occur in the ITAM motifs of CD79A and CD79B. As discussed, these motifs are the site of docking and activation for SYK as well as other kinases, and therefore critical for BCR signaling. Many of these mutations affect the first tyrosine of the CD79B ITAM motif. Other mutations affect other conserved ITAM residues or cause deletions in all or part of the ITAM motifs of CD79A and CD79B (150).

The mutations in the CD79 subunits are not loss of function because they sustained survival in ABC DLBCL cells with knockdown of endogenous CD79 isoforms. However, unlike CARD11 mutants, they do not spontaneously activate NF-κB when introduced into GCB DLBCL cells (150). Knock-in mice with loss or mutation of CD79A or CD79B ITAMs develop normal mature B cells that are, in fact, hyperresponsive to antigenic stimulation. B cells from these mice also exhibit higher levels of surface BCR expression because of

decreased receptor internalization (151-153). This phenomenon was also observed in ABC DLBCLs exhibiting or reconstituted with CD79 mutants of the first tyrosine residue of the ITAM. Mutations affecting the second tyrosine did not elevate surface BCR expression, nor have they been observed in patients, highlighting their functional nature. These mutations may have arisen in ABC DLBCLs to prevent signaling-induced receptor-internalization (150).

The CD79 mutations also function to block negative regulation by the src family kinase LYN. Following BCR stimulation, LYN phosphorylates CD79 ITAM residues as an early step in BCR signaling. However, LYN also negatively regulates this pathway (154, 155). LYN phosphorylates immunoreceptor tyrosine-based inhibitory motifs (ITIMs) on CD22 and the Fc γ-receptor, to which the phosphatase SHP1 is promoted, leading to ITAM dephosphorylation. LYN also phosphorylates SYK at a negative regulatory site, decreasing its activity. Lyn-deficient mice exhibit hyperactive BCR signaling that causes a severe autoimmune disease (156). ABC DLBCL cells reconstituted with mutant CD79B show less LYN kinase activity than with wildtype CD79B (150).

This constitutive BCR activity in ABC DLBCLs was coined “chronic active BCR signaling” to distinguish it from the “tonic” BCR signaling that is a basal, ongoing requirement for mature B cell survival. Chronic active BCR signaling requires CARD11 and the CBM complex, whereas tonic BCR signaling does not (157). Also, chronic active BCR signaling is characterized by BCR clustering, which has not been observed in resting mature mouse B cells which require tonic BCR signaling for survival (158). Taken together, a model

of ABC DLBCL pathogenesis emerges in which CD79 mutations arise, allowing cells to avoid negative regulation of BCR signaling, activate NF-κB and escape cell death (Figure 1.6).

Therapeutic targeting of BCR signaling in DLBCL

Because it promotes cell growth, proliferation and survival, BCR signaling is a rational therapeutic target in DLBCL. As described, mutations in this pathway lead to its chronic activation, highlighting the therapeutic relevance of BCR signaling in ABC DLBCL. In fact, many components of the BCR pathway have been targeted in DLBCL, some of which have already been translated to patients (Figure 1.6). Overexpression of protein tyrosine phosphatase receptor-type truncated (PTPROt), a negative regulator of SYK, inhibits proliferation and induces apoptosis in DBLCL, identifying SYK as a target in DLBCL (159). Inhibition of SYK by the small molecular fostamatinib disodium (R406) blocks proliferation and induces apoptosis in DBLCL cell lines (160). This orally available compound has also shown significant clinical activity with good tolerance in DLBCL patients (161). Cerdulatinib (PRT2070), developed by Portola, is a dual SYK-JAK inhibitor that shows antitumor effect in a subset of DLBCL cell lines and is currently under clinical evaluation (162). PRT2607, a SYK-specific inhibitor, is also being developed in their pipeline.

The constitutive activation of NF-κB in ABC DLBCL is an extremely attractive therapeutic target. NF-κB can be targeted through different approaches. IKK inhibition blocks phosphorylation of IκB, preventing release and nuclear translocation of NF-κB subunits. MLX105, a selective IKK inhibitor, potently kills ABC DLBCL cell lines (140). NEDD8-activating enzyme (NAE) regulates

the ubiquitination of phosphorylated IκB, resulting in its degradation and the release of NF-κB subunits to the nucleus. Inhibition of NAE by small molecules such as MLN4924 induces apoptosis in ABC DLBCL and shows strong tumor burden regression in DLBCL patient and xenograft models. Expectedly, the effects of MLN4924 are more potent in ABC DLBCL (163). Inhibition of PKCβ, the upstream activator of IKK, with sotrastaurin (STN) selectively inhibits the growth of CD79-mutant ABC DLBCL cell lines and xenograft models (164). MALT1 inhibitors comprise the newest class of compounds that target the constitutive NF-κB activity of ABC DLBCL. In 2012, two groups simultaneously reported selective inhibitors of MALT1 that induce cytotoxicity in ABC DLBCL cells, xenografts and patient models (165, 166).

The PI3K/AKT/mTOR pathway is deregulated in many cancers including DLBCL (167). Small molecule inhibitors of this pathway have been heavily researched. Rapamycin (sirolimus), a macrolide antibiotic that targets mTOR, is an FDA approved oral immunosuppressant (168). Everolimus, an orally available rapamycin analog, has also been approved as a transplant immunosuppressant (169). These compounds have antitumor activity in DLBCL cell lines and patient samples, but their effect is mostly antiproliferative and only narrowly cytotoxic (167). Phase II clinical studies of everolimus in DLBCL have been moderately successful with an ORR of 35% (170). Inhibition of AKT is also a promising cancer therapy and can be targeted through several approaches. Perifosine, a lipid-based inhibitor that blocks the PIP_3-binding pleckstrin homology (PH) domain of AKT, preventing its translocation to the membrane, has shown antitumor activity both *in vitro* and *in vivo*. Small

molecule inhibitors of AKT, such as GSK690693, cause growth inhibition and apoptosis in lymphomas and leukemias (171).

Many PI3K inhibitors have also been investigated in DLBCL. Pan-PI3K inhibitors, which block activity of all PI3K isoforms, such as buparlisib (NVP-BKM120) have shown efficacy in both *in vitro* and *in vivo* models and is currently under clinical investigation in a phase II study of relapsed NHL including DLBCL (172). Inhibitors of specific isoforms of PI3K are also being investigated for DLBCL. For example, idelalisib (formerly CAL-101 or GS-1101) is an oral, selective inhibitor of the p110δ isoform of PI3K that induces apoptosis in DLBCL cell lines and patient samples (173). A phase I clinical study of idelalisib showed efficacy in relapsed indolent lymphoma, but in another study of relapsed and refractory NHL patients, no response was observed in the DLBCL group (174).

The MAPK pathway is another interesting therapeutic target in DLBCL. The oncogene MCT-1 is highly expressed in DLBCL patient specimens and regulated by ERK. Inhibition of ERK causes apoptosis in DLBCL xenograft models (175). Small molecule inhibitors or ERK and MEK have been developed and demonstrate excellent safety profiles and tumor suppressive activity in the clinic. Initial responses to these drugs, however, were not robust, with four partial patient responses observed and stable disease reported in 22% of patient (176). Inhibition of MEK may be insufficient to cause cytotoxicity because of mutations in RAS and RAF, the upstream regulators of the MAPK pathway, may activate other kinases that maintain cell survival despite MEK inhibition. Despite these limitations, a small molecule inhibitor of

MEK, selumetinib (AZD6244), causes apoptosis in DLBCL cell lines, xenografts and patient samples and has entered the clinic (177).

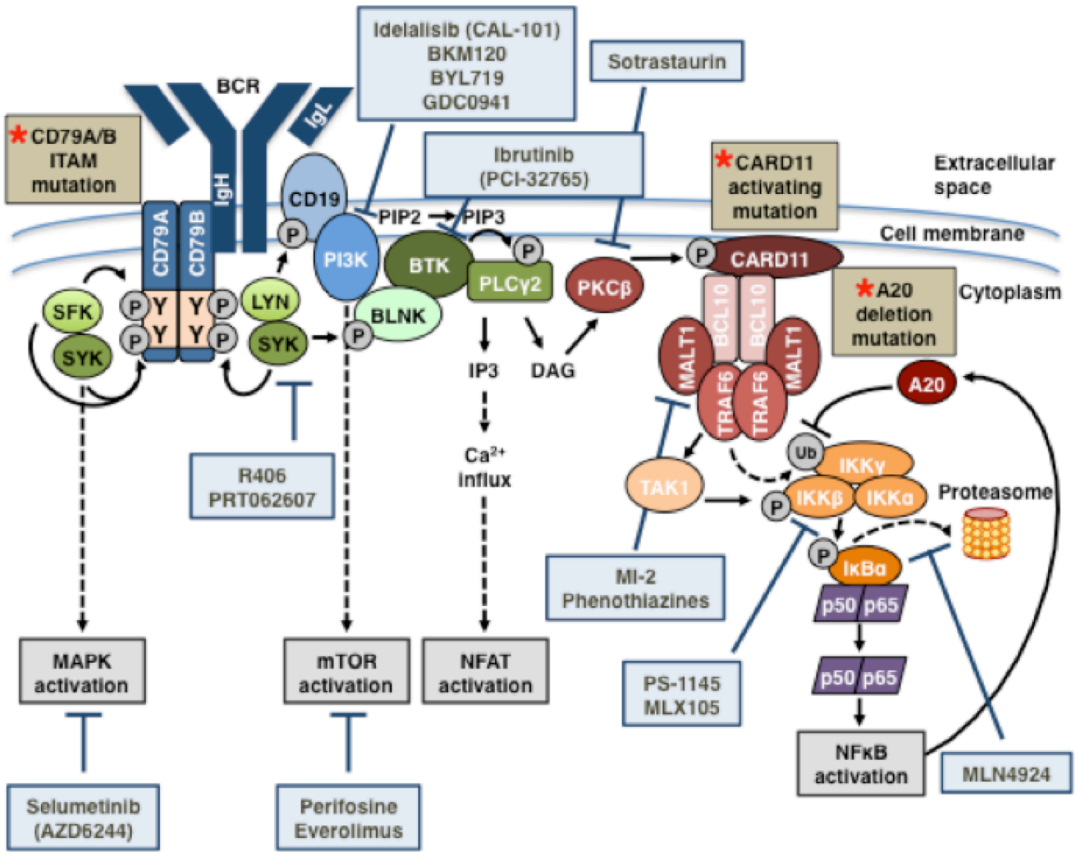

Figure 1.7 B cell receptor signaling in ABC-DLBCL. Schematic of B cell receptor signaling in ABC DLBCLs. Frequent mutations activate this pathway, elevating NF-κB signaling as well as other proliferation and survival pathways. As a result, inhibitors targeting many of these signaling molecules are in development. Adapted from (147).

Perhaps the most advanced targeted therapy for DLBCL is BTK inhibition. An RNA interference screen showed that BTK knockdown was highly toxic for DLBCL cell lines, specifically ABC DLBCL, initially identifying BTK as a potential target (148). Ibrutinib (PCI-32765) is a potent, selective, irreversible, orally available small molecule inhibitor of BTK developed by Pharmacyclics, Inc. and Janssen Pharmaceuticals (178). Ibrutinib lacked significant activity

against a panel of 19 BTK-related kinases and maintains over 1000-fold selectivity for B cells over T cells demonstrating its selectivity. Full BTK occupancy is achieved at 10 nM, and binding is irreversible as ibrutinib covalently binds to Cys481 of BTK. *In vivo* activity was shown in canine models of lymphomas (178). Ibrutinib also potently and selectively kills ABC DLBCL cell lines (150). Phase I clinical trials demonstrated that ibrutinib was well tolerated and had significant, durable activity in relapsed refractory B cell NHL and CLL, warranting further investigation in phase II trials of specific B cell malignancies (179, 180). In Phase II clinical trials, ibrutinib demonstrated a 5.3% overall response rate (ORR) in GCB DLBCL and a 40% ORR in ABC DLBCL, with 8 out of 40 patients achieving complete response (CR) (181). Phase III studies evaluating ibrutinib as a frontline therapy for non-GCB DLBCL patients are ongoing (ClinicalTrials.gov identifier NCT01855750).

Remarkably, ibrutinib achieved a 93% ORR in phase II studies of patients with relapsed refractory chronic lymphocytic leukemia (CLL) (182), and, in combination with rituximab, a monoclonal antibody against CD20, ibrutinib achieved a 95% ORR in high risk CLL patients (183). These promising studies led to FDA approval for CLL patients who have received at least one prior therapy and inspired numerous combination trials for other patients with B cell malignancies. A phase II clinical trial of ibrutinib in 111 patients with mantle cell lymphoma showed an ORR of 68% (21% CR) (184). These results led to FDA approval of ibrutinib for mantle cell lymphoma patients who have received at least one prior therapy. Other small molecule inhibitors of BTK are in various stages of development and have shown activity in laboratory and clinical settings (184-186).

Need for novel therapies

Standard chemotherapy regimens for DLBCL such as the combination of cyclophosphamide, doxorubicin and vincristine, three chemotherapeutics, and prednisone, a steroid, (CHOP) cure about 40% of DLBCL patients, with 5-year overall survival rates for GCB and ABC patients of 60% and 30%, respectively (187). The addition of rituximab, a monoclonal antibody against CD20, to this treatment schedule (R-CHOP) increases survival of DLBCL patients by 10 to 15% (188). However, 40% of DLBCL patients do not respond to R-CHOP. In the more aggressive ABC DLBCL subtype, the three year progression-free survival rate after R-CHOP is only 40% (147). Moreover, the side effects of this combination immunochemotherapy are not well tolerated, emphasizing the need for identifying novel targets and treatment regimens for this disease.

Enormous advances have been made in targeted therapy for DLBCL, but as discussed, many of these agents do not achieve complete, durable responses. Single agent therapy is unlikely to be curative in DLBCL because of tumor cell heterogeneity, complex signaling pathways and feedback mechanisms and the emergence of resistance. Accordingly, many of the compounds for targeted therapy discussed above show increased efficacy when used in combination with chemotherapeutics or other targeted agents. The benefits of combination therapy include increasing therapeutic efficacy, minimizing the development of drug resistance, and decreasing toxicity.

Consider ibrutinib, an FDA approved drug that has shown activity in ABC DLBCL. In Phase II clinical trials, as a single agent, ibrutinib exhibited moderate clinical activity, achieving 40% ORR in ABC DLBCL, with 8 out of 40

patients achieving complete response (181). When evaluated in combination with R-CHOP in a phase II study of DLBCL patients, the combination of ibrutinib and R-CHOP achieved 100% ORR with 60% CR (189). Moreover, mutations that confer resistance to ibrutinib have been reported (190, 191). The BTK^{C481S} mutation observed in ibrutinib-treated CLL patients removed the cysteine required for ibrutinib action. Gain-of-function mutations in PLCγ2, a direct downstream target of BTK, have also been detected in CLL patients treated with ibrutinib. A large high-throughput combinatorial screen identified numerous drugs that synergize with ibrutinib to kill ABC DLBCL cells (192). Taken together, these studies demonstrate that even the most promising targeted therapies are unlikely to be curative as single agents and may be most effective when used in therapeutic combinations. However, the design of rational therapeutic combinations can be challenging given the massive numbers of drugs and the difficulty of defining the proteome that drives tumor cell survival independent of whether they are affected by somatic mutations.

The role of Hsp90 in DLBCL

The emerging role of Hsp90 inhibition in cancer therapy prompted our laboratory to investigate the role of PU-H71, a purine-scaffold Hsp90 inhibitor, in DLBCL (38). Cell viability assays showed that PU-H71 inhibits growth and induces apoptosis in a panel of DLBCL cell lines. This effect was more prominent in BCL6-dependent DLBCL cell lines with average GI_{50} 1.39 μM (±1.00 μM) as compared to 71 μM (±41 μM) in BCL6 independent DLBCL cell lines, suggesting that PU-H71-induced apoptosis may occur through BCL6. Using PU-H71 chemical precipitation BCL6 was shown to interact physically with Hsp90 in DLBCL cells. More, exposure to PU-H71 resulted in time- and

dose-dependent degradation of BCL6 protein and mRNA, showing that it is a bona fide client of Hsp90. Immunohistochemical studies showed high expression of Hsp90 in 60 out of 70 DLBCL patient samples (85.7%). Of these samples, 87% were positive for BCL6, and 81% were positive for both Hsp90 and BCL6, with a strong correlation of BCL6 and Hsp90 ($r = 0.996$, $p < 0.00001$). Moreover, among 21 patient samples treated with PU-H71 (2.5 μM), 19 cases showed greater than 25% loss of viability compared to vehicle treated controls. *In vivo* studies of PU-H71 showed potent suppression of tumor growth in three DLBCL xenograft models. Like other Hsp90 inhibitors, PU-H71 showed preferential uptake and retention in xenograft tumor tissue compared to normal tissues (38). Taken together, these studies demonstrate the effectiveness of targeting Hsp90 with PU-H71 in DLBCL. PU-H71 recently entered the clinical arena where it is well tolerated and accumulates in tumors at micromolar concentrations (193).

In a later study from our laboratory (194), the gene signature induced by RI-BPI, a peptidomimetic inhibitor of BCL6, was used to identify BCL6 targets and potential classes of drugs for therapeutic synergy in killing DLBCLs. The RI-BPI-induced gene signature included genes associated with the actions of HDAC and Hsp90 inhibitors. Cerchietti et al (194) hypothesized that drugs with overlapping gene signatures with RI-BPI might enhance BCL6 inhibition thereby increasing downstream antilymphoma effects. Specifically, the lysine acetyltransferase p300 is directly repressed by BCL6, and exposure to RI-BPI induced expression of p300 and acetylation of its targets including Hsp90. Furthermore, combined inhibition of BCL6 with RI-BPI and Hsp90 with PU-H71 synergized to kill a panel of DLBCL cell lines and also more potently inhibited

the growth of DLBCL xenograft models *in vivo* and human DLBCL patient samples *ex vivo* greater than either drug alone (194). These findings act as proof of principle that combined inhibition of Hsp90 and its client protein(s), in this case, BCL6, can achieve therapeutic synergy in DLBCL.

Hypothesis

Inhibition of teHsp90 with PU-H71 causes potent antilymphoma effects in DLBCL. The mechanism of this action occurs through inhibition of BCL6, one of the major oncogenes in DLBCL and a verified Hsp90 client. Given the complex signaling pathways involved in lymphomagenesis and DLBCL survival, and the ability of teHsp90 to chaperone multiple pathways that contribute to the malignant phenotype of other cancers, teHsp90 likely chaperones many other proteins and pathways in DLBCL. We therefore hypothesized that identification of the teHsp90 oncoproteome will reveal additional mechanisms of DLBCL survival. Because combined inhibition of teHsp90 and its client protein(s) can produce therapeutic synergy, we further predict that identifying oncogenic clients of teHsp90 in DLBCL will lead to rational combinatorial therapies anchored by PU-H71, geared toward more thorough suppression of key oncogenic pathways.

CHAPTER TWO

teHsp90 pharmacoproteomics reveals multiple interactions with BCR pathway proteins in DLBCL

1. Introduction

Hsp90 is a ubiquitously expressed molecular chaperone that maintains the conformational stability and function of numerous cellular proteins (1). These "client" proteins regulate many cellular processes including proliferation, growth and survival (1). Perhaps unsurprisingly, in order to maintain their malignant phenotype, tumor cells have hijacked this survival mechanism. In fact, tumor cells are enriched for a pool of Hsp90 (teHsp90) that preferentially binds oncoproteins required for tumor survival including chimeric fusion proteins, mutated molecules and effectors relied on by tumors through non-oncogene addiction (1). teHsp90 exhibits a higher affinity for Hsp90 inhibitors than latent, housekeeping Hsp90, and can be depleted using Hsp90 inhibitors (30, 58). Upon Hsp90 inhibition, client proteins lose stability and are targeted for degradation by the proteasome, making teHsp90 inhibition an attractive therapeutic target in cancer (41).

Work from our laboratory confirms that teHsp90 inhibition with the purine-scaffold inhibitor PU-H71 is a viable therapeutic route in DLBCL. Experiments in DLBCL cells, xenografts and patient samples show that teHsp90 and BCL6 form a complex whose activity is disrupted upon teHsp90 inhibition with PU-H71, resulting in a potent antitumor effect (38). Further, we have shown that combined inhibition of teHsp90 and its client protein, BCL6, can synergistically kill DLBCL cells, xenografts and patient samples (194). The high affinity of PU-

H71 to teHsp90 stress complexes has been harnessed as a proteomics capture approach to identify the cellular component of oncoproteins specifically contributing to the growth and survival of tumors (58, 74). For example, PU-H71 pulldowns performed in BCR-ABL driven leukemia cells capture BCR-ABL, but not the normal counterpart ABL protein. Both BCR-ABL and ABL are Hsp90 clients as shown by immunoprecipitation with an antibody to Hsp90, but only BCR-ABL is bound and stabilized by teHsp90 (150).

Given the large number of proteins and pathways chaperoned by teHsp90 in other tumor types (1), we set out to identify the full teHsp90 oncoproteome in DLBCL. We hypothesized that identifying other teHsp90-chaperoned proteins and pathways critical to lymphomagenesis and DLBCL survival will further elucidate molecular mechanisms of DLBCL tumor biology. We further predicted that by focusing our analysis on druggable pathways, we could reveal translatable therapeutic combination treatments for DLBCL. Herein, we show that PU-H71 proteomics in DLBCL is a robust assay to identify signaling pathways critical to the tumor phenotype. We identified many BCR pathway proteins as components of teHsp90 complexes in DLBCL and show that several key kinases of this pathway are degraded with teHsp90 inhibition.

2. Results

2.1 Proteomic analysis of PU-H71 chemical precipitations in DLBCL cell lines

Our lab has previously shown that PU-H71 can be used as a tool to chemically precipitate the teHsp90-proteome of cancer cells (58, 74). We predicted that using this method in DLBCL cells would identify client proteins necessary for

DLBCL survival and lead to rational combinatorial therapies anchored by PU-H71. To identify the teHsp90 client proteins in DLBCL cell lines, we used agarose beads covalently attached to either an inert chemical or to PU-H71 to chemically precipitate teHsp90-client complexes in two GCB DLBCL cell lines, OCI-Ly1 and OCI-Ly7.

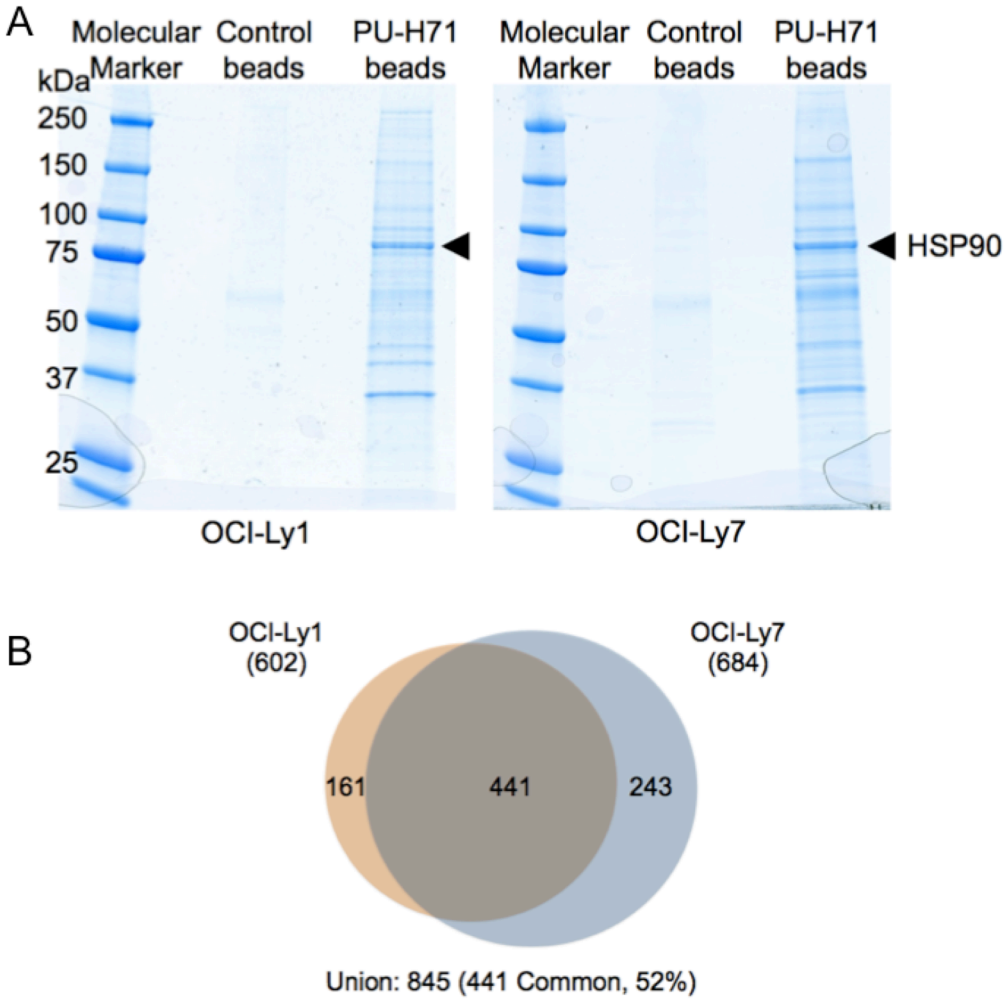

Figure 2.1 teHsp90 pharmacoproteomics in DLBCL cell lines (A) Lysates from OCI-Ly1 and OCI-Ly7 cells were subjected to chemical precipitation with PU-H71 or a control chemical followed by SDS PAGE and colloidal blue staining. The extracted proteins were examined by LC-MS/MS as shown in (B): Venn diagram is used to illustrate the numbers of overlapping and unique proteins identified by LC-MS/MS in each cell line.

These complexes were resolved by polyacrylamide gel electrophoresis followed by Coomassie blue staining of the gel in order to visualize the proteins. We observed that lysates incubated with control beads showed almost no detectable protein in the gel, especially when compared with the lanes of lysate incubated with PU-H71 beads, which showed a variety of proteins at all sizes (Figure 2.1 A). Bands were cut from the gel under sterile conditions and analyzed by liquid chromatography followed by tandem mass spectrometry (LC-MS/MS). After subtracting common contaminants and the agarose proteome (195), we identified 602 and 684 teHsp90 client proteins in OCI-Ly1 and OCI-Ly7, respectively (Figure 2.1 B, Table 2.1). Of the identified proteins, 52% were common to both cell lines, demonstrating the consistency of this assay across cell lines.

2.2 Visualization of teHsp90 client pathways

To identify the signaling networks most highly represented among the teHsp90 complexes in DLBCL, we analyzed the union of OCI-Ly1 and OCI-Ly7 client proteins using the Search Tool for the Retrieval of Interaction Genes/Proteins (STRING) with a confidence of 0.99 (196). Among the expected clusters of proteins chaperoned by teHsp90 stress complexes we identified components of the proteasome and ribosomal proteins. However, the teHsp90 complexes in our proteomics dataset were also highly enriched for proteins that form part of the B cell receptor (BCR) signaling pathway (Figure 2.2A). An orthogonal pathway analysis approach using Ingenuity Pathway Analysis (IPA) also identified the BCR pathway as highly represented in the teHsp90 DLBCL interactome (p=0.01) (Table 2.1).

Table 2.1 PU-H71 proteomics reveals teHsp90-chaperoned pathways. The union of proteins identified in OCI-Ly1 and OCI-Ly7 PU-H71 proteomics assays were subjected to Ingenuity Pathway Analysis. Significantly represented pathways are listed here. BCR pathway is highlighted in orange.

Ingenuity Canonical Pathways	-log(p-value)	Ingenuity Canonical Pathways	-log(p-value)
EIF2 Signaling	28.70	Ephrin B Signaling	4.80
Protein Ubiquitination Pathway	25.80	Huntington's Disease Signaling	4.79
Regulation of eIF4 and p70S6K Signaling	17.20	B Cell Development	4.67
tRNA Charging	13.20	Integrin Signaling	4.66
mTOR Signaling	11.80	CD28 Signaling in T Helper Cells	4.65
p70S6K Signaling	11.20	B Cell Receptor Signaling	4.49
Actin Cytoskeleton Signaling	10.30	DNA Double-Strand Break Repair by NHEJ	4.44
Purine Nucleotides De Novo Biosynthesis II	7.35	RhoA Signaling	4.35
PI3K/AKT Signaling	7.27	Methionine Degradation I (to Homocysteine)	4.24
Systemic Lupus Erythematosus Signaling	6.58	CTLA4 Signaling in Cytotoxic T Lymphocytes	4.23
RAN Signaling	6.15	PKCθ Signaling in T Lymphocytes	4.10
14-3-3-mediated Signaling	6.01	Protein Kinase A Signaling	4.06
Cell Cycle: G2/M DNA Damage Checkpoint Regulation	6.00	FAK Signaling	3.98
Breast Cancer Regulation by Stathmin1	5.84	fMLP Signaling in Neutrophils	3.95
VEGF Signaling	5.82	PRPP Biosynthesis I	3.88
Role of NFAT in Regulation of the Immune Response	5.77	5-aminoimidazole Ribonucleotide Biosynthesis I	3.88
Signaling by Rho Family GTPases	5.71	G Beta Gamma Signaling	3.87
ILK Signaling	5.60	Virus Entry via Endocytic Pathways	3.81
Fcγ Receptor-mediated Phagocytosis in Macrophages and Monocytes	5.40	RhoGDI Signaling	3.74
Glycolysis I	5.20	ERK/MAPK Signaling	3.69
Clathrin-mediated Endocytosis Signaling	5.10	PI3K Signaling in B Lymphocytes	3.57
Tight Junction Signaling	5.00	Calcium Signaling	3.54
Germ Cell-Sertoli Cell Junction Signaling	4.90	Cell Cycle Control of Chromosomal Replication	3.50
Gap Junction Signaling	4.90	Phospholipase C Signaling	3.50

Among the components of the BCR pathway present within teHsp90 stress complexes were the B-cell receptor itself (Igμ), as well as many canonical components including CD79A, CD79B, SYK, BTK, SHP1, PLCγ2, CD45, LYN, VAV, RAC, PI3K, mTOR, CSK, MEKK, JNK1/2 and several NF-κB components (Figure 2.2B).

2.3 teHsp90 complexes maintain protein expression of core components of the BCR pathway in GCB and ABC DLBCL cells

In order to validate the teHsp90 pharmacoproteomics assays, we next performed PU-H71 chemical precipitations in OCI-Ly1 and OCI-Ly7 cells followed by immunoblot for many of the BCR pathway proteins identified by LC-MS/MS. All of these protein interactions were confirmed by chemical precipitation/immunoblot, demonstrating the robustness and accuracy of the pharmacoproteomics assay. Additionally, B-cell linker protein (BLNK), a scaffolding protein in the BCR pathway, which was not present in the LC-MS/MS assays failed to be captured as a component of teHsp90 complexes in these validation studies, further confirming the accuracy of the proteomic analysis (Figure 2.3A).

Classical Hsp90-regulated client proteins depend on Hsp90 function for their stability. To determine if the stability of the BCR proteins identified by LC-MS/MS was dependent on teHsp90 complexes, we exposed OCI-Ly1 and OCI-Ly7 cells to increasing doses of PU-H71 for 24 hours and analyzed the abundance of the proximal enzymes of the BCR pathway by immunoblot. The proteins LYN, SYK, BTK and PLCγ2 were depleted in a dose-dependent

manner upon exposure to PU-H71, showng their dependency on teHsp90 complexes to maintain their expression (Figure 2.3B).

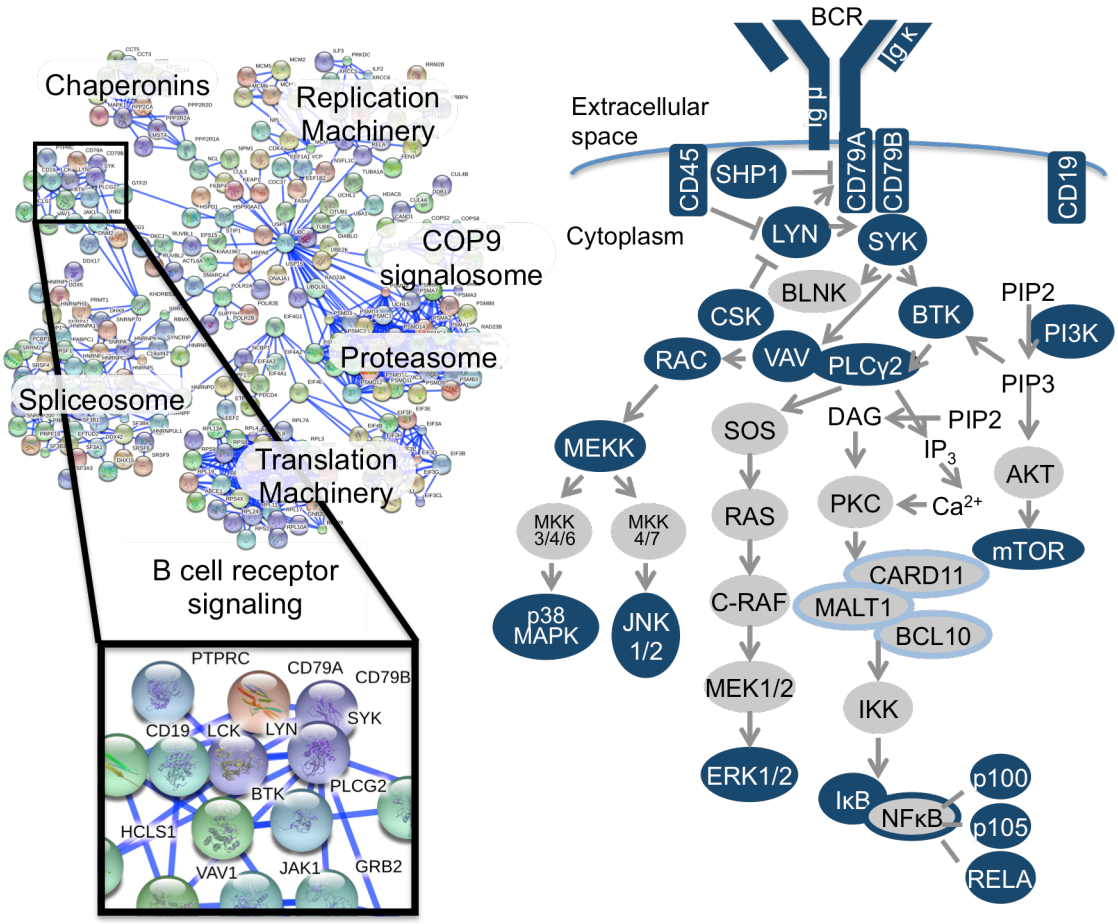

Figure 2.2 Pathways identified by PU-H71 proteomics in DLBCL (A) STRING representation of the union of proteins identified in OCI-Ly1 and OCI-Ly7 PU-H71 chemical precipitations at 0.99 confidence. (B) A representation of the BCR pathway is shown. Proteins with blue color were identified as components of the teHsp90 interactome by LC-MS/MS.

The more aggressive, therapy-resistant activated B cell like (ABC) subtype of DLBCL features chronic activation of BCR signaling, often due to the presence of somatic mutations of proteins in this pathway (150). As such, ABC DLBCLs are sensitive to targeted therapies that disrupt BCR signaling. We wondered whether the BCR proteins identified by proteomics were also associated with

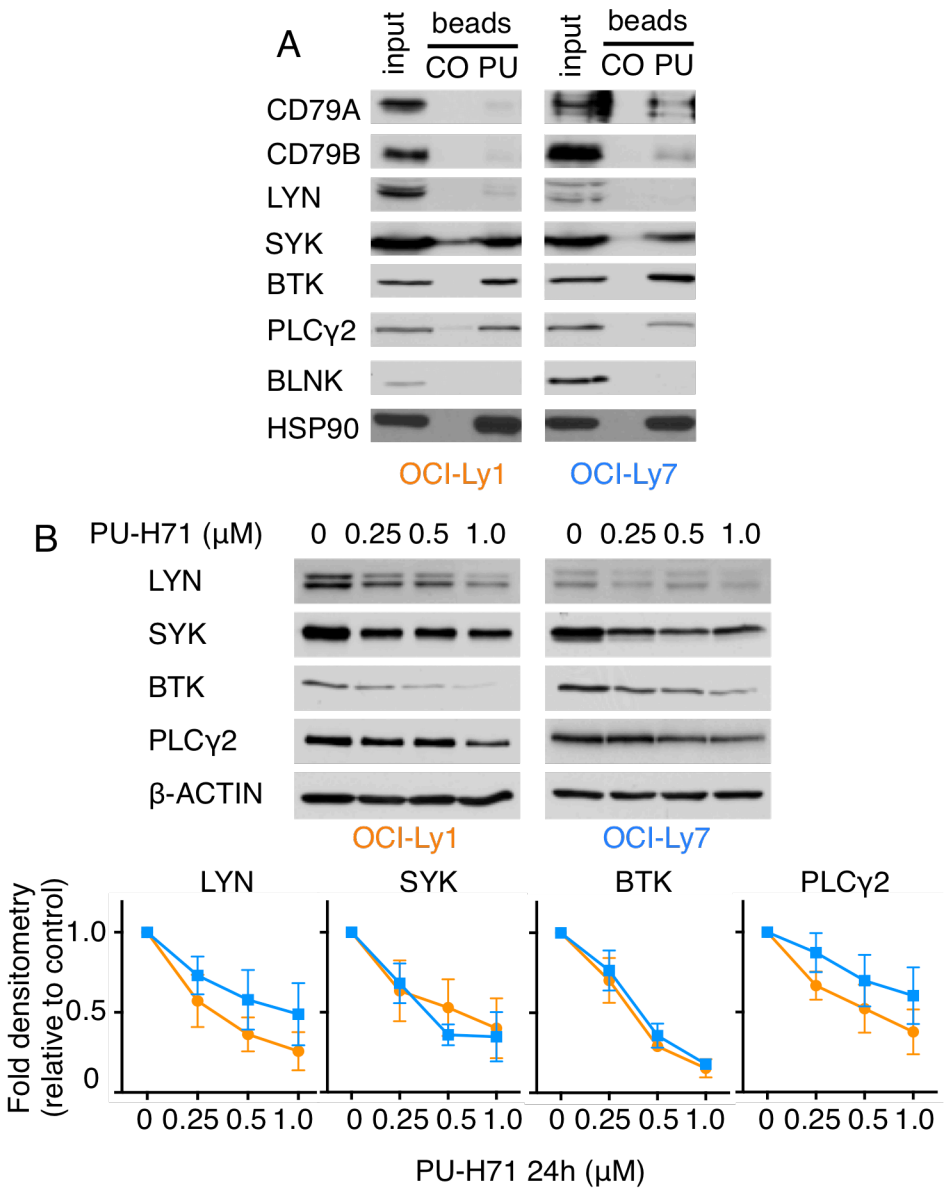

Figure 2.3 BCR pathway proteins interact with and require teHsp90 to maintain their expression. (A) Lysates from OCI-Ly1 and OCI-Ly7 were subjected to chemical precipitation with PU-H71 (PU) or control chemical (CO) beads followed by immunoblotting for the indicated BCR pathway proteins. Hsp90 is used as a positive control. (B) OCI-Ly1 and OCI-Ly7 cells were exposed to vehicle or increasing doses of PU-H71 for 24 hours as indicated. Lysates were subjected to immunoblotting with the indicated antibodies. β-actin was used as a loading control. The relative abundance of each protein relative to β-actin was quantified by densitometry for each timepoint represented in the line graph below as average ± SEM (n=3).

teHsp90 complexes in ABC DLBCL cell lines. If so, PU-H71 might serve as a candidate therapeutic agent for ABC DLBCLs. To test this, we performed PU-H71 chemical precipitations followed by immunoblot for BCR pathway proteins in two ABC DLBCL cell lines, HBL-1 and TMD8. We observed that the BCR proteins identified by LC-MS/MS in GCB DLBCL cell lines were also bound to teHsp90 complexes in these ABC DLBCL cells (Figure 2.4A). Moreover, the proteins SYK, BTK and PLCγ2 demonstrated dose-dependent expression reduction upon exposure to PU-H71 (Figure 2.4B). LYN showed the same trend, despite showing robust interactions with teHsp90-PU-H71 complexes in only one cell line tested. In HBL-1 and TMD8, CD79B was more abundant in teHsp90 complexes than in the GCB DLBCL cell lines tested, which may be because it is mutated and constitutively active in these cell lines (150).

3. Discussion

In this work, we identify the PU-H71 teHsp90 oncoproteome of DLBCL. The highly stable binding of PU-H71 to teHsp90 enables the enrichment of the teHsp90 proteome from cells using PU-H71 pulldowns (58, 74). This method can be used to specifically capture a unique functional class of Hsp90 complexes that exhibits greater association with biochemical effects specifically required by tumor cells to maintain their growth and survival (58, 74).

Some of the pathways enriched in teHsp90 complexes identified in our approach are well-characterized clients of Hsp90, including the proteasome, chaperonins, replication machinery and translation machinery. For example, Hsp90 client proteins identified by a yeast two-hybrid screen sorted

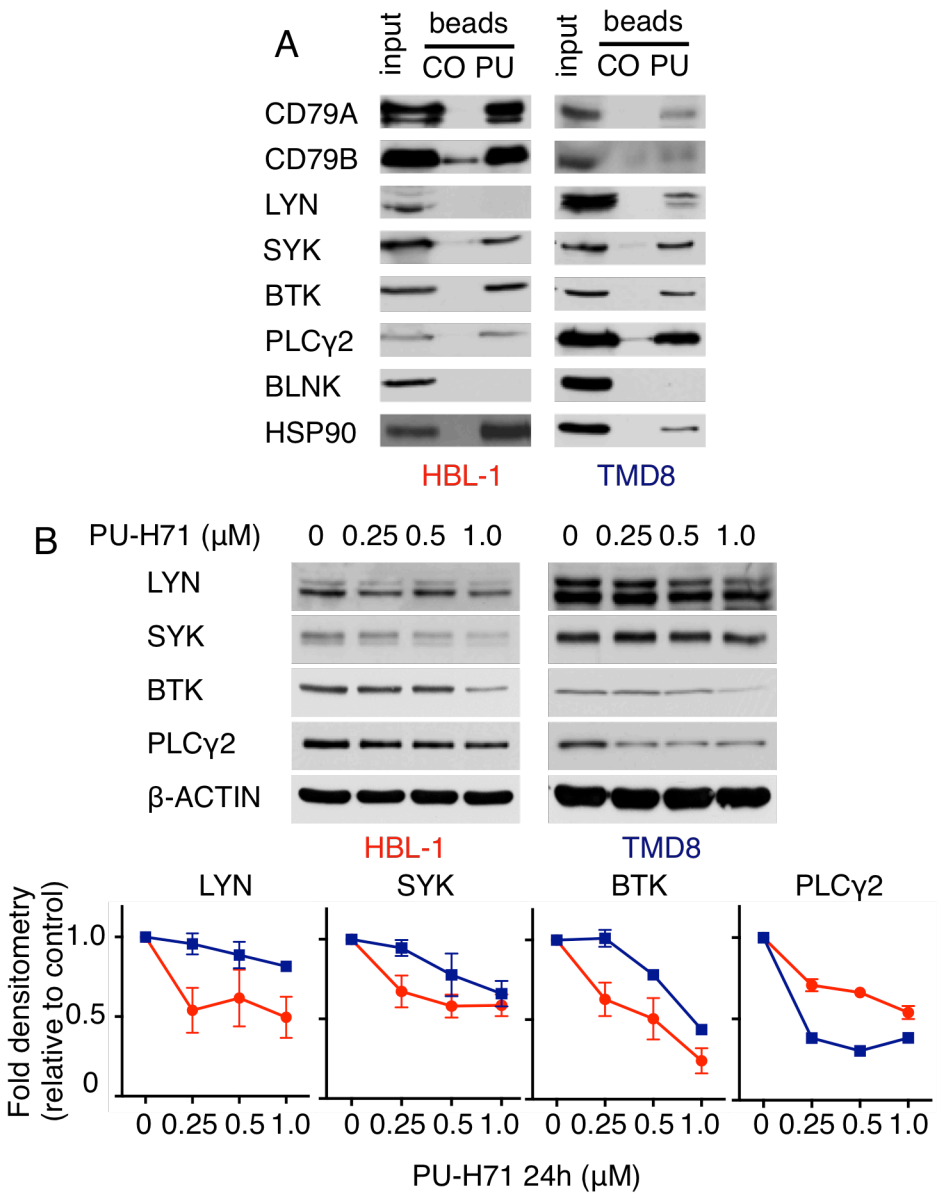

Figure 2.4 BCR pathway proteins interact with and require teHsp90 to maintain their expression in ABC DLBCLs. (A) Lysates from HBL-1 or TMD8 cells were subjected to chemical precipitation with PU-H71 (PU) or inert chemical (CO) beads followed by immunoblotting for the indicated BCR pathway proteins. Hsp90 is used as a positive control. (B) HBL-1 and TMD8 cells were exposed to vehicle or increasing doses of PU-H71 for 24 hours as indicated. Lysates were subjected to immunoblotting with the indicated antibodies. β-actin was used as a loading control. The relative abundance of each protein relative to β-actin was quantified by densitometry for each timepoint and is shown in the line graph below as average ± SEM (n=3).

into functional categories showed many interacting proteins to be involved in cell cycle and DNA processing, protein fate, and transcription (197). These experiments were performed in yeast, suggesting that the role of Hsp90 in regulating these processes required for cell survival is evolutionarily conserved.

In another study using HEK293T cells, proteins involved in transcription, ubiquitination, protein folding and the unfolded protein response were identified as Hsp90 clients, and that most ATP-dependent Hsp90 interactions were disrupted with GM treatment (198). Other approaches using immobilized Hsp90 as bait also revealed transcription and translation proteins as Hsp90 clients (199). In other efforts to map the global principles of Hsp90 interactions, using many different approaches, some complexes and pathways identified with our approach have been shown to be clients of Hsp90, placing our approach firmly within the field of Hsp90 affinity capture and confirming the accuracy of our technique.

The signaling pathways identified in our PU-H71 proteomics assays are more intriguing from a functional and therapeutic standpoint. Other proteomic methods have been utilized to explain the basis of Hsp90-kinase recognition (200) and to show that Hsp90 inhibition preferentially targets kinases and the DNA damage response (201), another pathway identified in our proteomics assay. In fact, the highest scoring signaling networks enriched by PU-H71 pulldown proteomics in BCR-ABL positive CML were those known to be used by BCR-ABL to propagate aberrant signaling in CML. These pathways include the PI3K-AKT-mTOR, NF-κB, Raf-MAPK, STAT, and focal adhesion. These

findings led to the discovery of a new STAT activation mechanism critical to CML survival (58). We used PU-H71 proteomics in a collaboration project to investigate KSHV$^+$ PELs. In these cells, the PU-H71 pulldowns enriched for proteins of the following pathways: NF-κB activation by viruses, apoptosis, autophagy, PI3K/AKT-mTOR, interleukin 6, angiogenesis, and vascular endothelial growth factor signaling (74). Representative proteins of these pathways were validated using PU-H71 pulldown followed by immunoblot in four KSHV+ PEL cell lines (74). Our proteomics assays in DLBCL revealed some of the same pathways that are well known to be important effectors of tumor cell signaling, including PI3K/AKT/mTOR signaling and ERK/MAPK signaling.

However, each of these studies also identified pathways uniquely required for survival by the specific type of cancer investigated. Similarly, our PU-H71 proteomics identified a signaling pathway known to be critical to DLBCL survival – the BCR pathway. Although expected, this result further demonstrates that PU-H71 affinity capture selects for the pool of teHsp90 that chaperones those proteins and pathways required for maintaining a specific tumor phenotype.

It is important to note that the initial proteomic assays were performed in GCB DLBCL cell lines as a hypothesis-generating experiment. The BCR pathway is known to be chronically active and therapeutically targetable in the ABC DLBCL subtype (150). However, GCB DLBCLs exhibit tonic BCR activity and are sensitive to inhibition of certain kinases in the pathway (160). Though teHsp90 preferentially chaperones oncogenic, often mutated client proteins,

the BCR pathway does not harbor mutations in the GCB DLBCL subtype, but is still chaperoned by teHsp90. Hence it is possible that Hsp90 is required for chaperoning of this pathway in both subtypes, albeit for different functions. Notably, CD79B, which is mutated in the HBL-1 and TMD8 ABC DLBCL cell lines (150), appears to be more abundantly present in teHsp90 complexes identified by PU-H71 chemical precipitation than in the GCB DLBCL cells.

4. Materials and methods

Cell lines and reagents The DLBCL cell lines OCI-Ly1 and OCI-Ly7 were grown in Iscove's Modified Dulbecco's Medium (IMDM) containing 10% FBS and supplemented with penicillin and streptomycin. The DLBCL cell lines HBL-1 and TMD8 were grown in medium containing 90% RPMI and 10% FBS, supplemented with L-glutamine, HEPES and penicillin and streptomycin. PU-H71 was synthesized as previously described (58). The following antibodies were used: CD79A clone HM47, Santa Cruz Biotechnology; CD79B clone SN8 and FL-229, Santa Cruz Biotechnology; LYN clone 44, Santa Cruz Biotechnology; SYK clone 4D10, Santa Cruz Biotechnology; BTK clone D3H5, Cell Signaling Technology; PLCγ2 clone Q-20, Santa Cruz Biotechnology; BLNK clone 2B11, Santa Cruz Biotechnology; Hsp90 catalog number ab13495, Abcam; β-actin clone AC-15, Sigma Aldrich.

Cell treatments Unless otherwise noted, cells were counted and assayed for viability using Trypan blue dye exclusion. Cells were centrifuged at 1500 rpm for 5 minutes at room temperature and resuspended in fresh media at a concentration of 2×10^6 cells/mL.

PU-H71 chemical precipitation PU-H71 and control (Hsp90 inactive chemical (2-methoxyethylamine)) beads were synthesized as previously reported (58). Before use, PU-H71 and control beads were washed three times in Felts buffers (20 mM HEPES, 50 mM KCl, 5 mM $MgCL_2$, 0.01% (w/v) NP-40, freshly prepared 20 mM Na_2MoO_4 and protease inhibitors (Roche, Indianapolis, IN)). For cell lysis, 40 million (immunoblot) or 100 million (proteomics) cells were spun down at 1500 rpm for 5 minutes, washed in 1X phosphate buffered saline (PBS), resuspended in 1 mL of Felts buffer and incubated on ice for 30 minutes. Pellets were vortexed for 15 seconds on high and centrifuged at 14,000 rpm for 15 minutes at 4°C. Supernatants were collected and precleared by incubating with 100 µL of washed control beads. For immunoblot, lysates were precleared for one hour rocking at 4°C. For proteomics, lysates were precleared for 8 hours rocking at 4°C, and then again with fresh beads overnight rocking at 4°C. Following preclearing, lysates were split, saving 10% of each pulldown to be used as input, and half of the remaining sample was incubated with 100 µL of either control of PU-H71 beads at 4°C overnight. Samples with PU-H71 beads were incubated in amber tubes to prevent PU-H71 light-sensitive degradation. Following incubation, beads conjugates were washed 3 times with Felts buffer by adding 1 mL fresh, cold Felts buffer, vortexing for 10 seconds, and spinning at 10,000 rpm for 1 minute. Precipitates were resolved by sodium dodecyl sulfate polyacrylamide gel electrophoresis (SDS-PAGE) following standard immunoblotting procedure. For proteomics, gels were stained with colloidal blue, cut into bands under sterile conditions, frozen on dry ice and sent for mass spectrometry analysis.

Mass spectrometry

In-gel trypsin-mediated digestion was carried out using standard procedures. Tryptic peptides were resolved on a nano-capillary reverse phase column and directly infused into a linear ion-trap mass spectrometer (LTQ Orbitrap XL, Thermo Fisher Scientific). The mass spectrometer was set to collect on survey scan (MS1), followed by MS/MS spectra on the 9 most intense ions observed in MS1 scan. Proteins were identified by searching the tandem mass spectra against human protein database using X!Tandem/TransProteomic Pipeline software suite. All proteins identified with a probability of >0.9 were retained for further analysis. Common contaminants and the agarose protome (195) were subtracted before further analysis.

Cell lysis for immunoblot

Cells were harvested, spun down at 1500 rpm for 5 minutes at room temperature. Pellets were washed in PBS, and then centrifuged again. After PBS aspiration, pellets were resuspended in lysis buffer (10 mM HEPES-KOH pH 7.9, 1.5 mM $MgCl_2$, 10 mM KCl, freshly prepared $NaMoO_4$, 1% Triton-X, 0.5 mM phenylmethylsulfonyl fluoride (PMSF), and protease and phosphatase inhibitors) by flicking the tube. Cells were incubated in lysis buffer on ice for 15 minutes, vortexed on high for 5 seconds, centrifuged at 14,000 rpm for 10 minutes at 4°C and prepared for downstream assays.

Statistical analysis

Two-tailed unpaired t test was used unless otherwise stated. All statistical analyses were carried out using Prism software (GraphPad).

CHAPTER THREE

Inhibition of teHsp90 induces broad attenutation of BCR signaling at multiple nodes

1. Introduction

Clients of teHsp90 depend on its chaperoning activity to maintain not only their stability, but also their function. As such, teHsp90 has been shown to mediate novel functions in protein physiology, independent of its effects on protein folding and stability (3,5). For example, in B-CLL, teHsp90 maintains LYN in an active conformation (10). In CML cells, teHsp90 regulates the conformation of STAT5 in order to sustain elevated levels of active pSTAT5 species in the cell (5). Further, in DLBCL, teHsp90 was shown to maintain the BCL6 transcriptional repressor in a DNA-bound active conformation (3). We therefore hypothesized that teHsp90 is required for the activity of the proximal enzymes of the BCR pathway independent of its function in maintaining the expression of these proteins. We further predict that due to the extensive interactions between teHsp90 and the BCR pathway identified by mass spectrometry, teHsp90 plays a broad role in regulating BCR pathway activity.

2. Results

2.1 teHsp90 is required for activation of BCR signaling proteins

Because teHsp90 is known to chaperone not only the stability but also the function of its client proteins, we wondered if teHsp90 function was required for the activity of the proximal enzymes of the BCR pathway, independent of its function in maintaining expression of these proteins. To test this, we treated three ABC DLBCL cell lines with PU-H71 at time points up to four hours, which

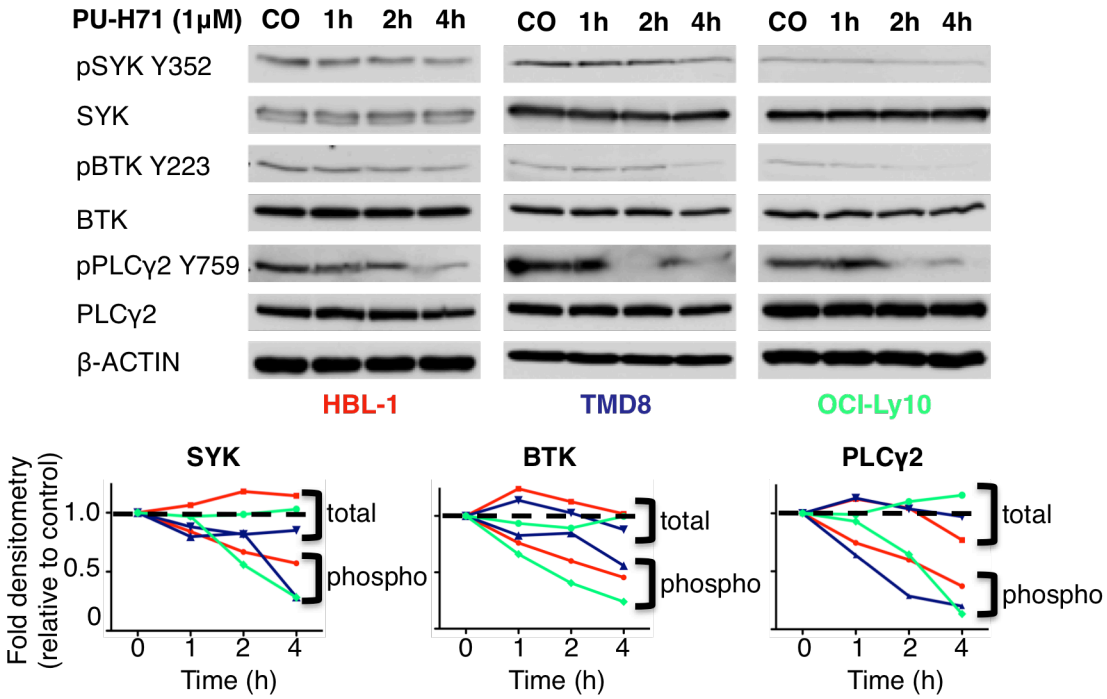

Figure 3.1 teHsp90 is required for basal BCR signaling in ABC DLBCL. HBL-1, TMD8 and OCI-Ly10 cells were exposed to vehicle or PU-H71 for increasing times as indicated. Lysates were subjected to imunoblotting with the indicated antibodies. β-actin was used as a loading control. The relative abundance of each phosphorylated protein relative to each total protein was and each total protein relative to β-actin was quantified by densitometry for each timepoint and is shown in the line graph (total).

is before reduction of protein abundance is observed. Immunoblots of these lysates were performed for total and activating phosphorylated forms of SYK, BTK and PLCγ2. In three ABC DLBCL cell lines, HBL-1, TMD8 and OCI-Ly10, phospho-SYK Y352, phospho-BTK Y223, and phospho-PLCγ2 Y759 decreased in a time-dependent manner upon exposure to PU-H71, independent of total protein levels (Figure 3.1).

2.2 teHsp90 is required for BCR signalosome complex function

2.2.1 Membrane localization of Hsp90 in DLBCL cells

teHsp90 regulates the activity and dynamics of signaling complexes required for cancer cell survival (58, 74). PU-H71 disrupts the dynamics of stress

complexes by maintaining teHsp90 in the ATP-bound configuration attached to its partner proteins (58). Given the interaction of teHSp90 with CD79A and CD79B, the BCR-associated transmembrane protein heterodimer that serves as the its signal transduction moiety, and the BCR itself, we wondered if teHsp90 chaperones the BCR at the cell membrane. To address this question, we first wanted to determine if Hsp90 is localized at the cell membrane in DLBCL cells. To test this, we used a cell fractionation method to purify membrane and cytosolic fractions of OCI-Ly7 and HBL-1 cells. Although not abundant, we detected expression of Hsp90 in the membrane fraction of both of these cell lines (Figure 3.2A) CD79A, which is predominantly localized in the membrane, was used as a control and showed the opposite localization pattern in these cells.

As an orthogonal assay to demonstrate membrane localization of Hsp90, we used total internal fluorescence microscopy (TIRFM), which is used for imaging of membrane biology. In these assays, HBL-1 or TMD8 cells were adhered to coverslips, fixed, and then stained with antibodies to Hsp90 or SYK followed by secondary antibodies conjugated to fluorophores and a fluorophore-conjugated antibody to IgM. TIRFM, which only penetrates 200 nm into sample allowing for imaging of membrane biology, was used to image these cells and revealed clear localization of Hsp90 at the membrane in both HBL-1 and TMD8 cells (Figure 3.2B). Moreover, these images depicted clustering of the B cell receptor (IgM) in TMD8 cells, as has been described (150). Our images also show considerable co-localization of Hsp90 with SYK at the membrane (Figure 3.2B). Taken together, this data suggests that Hsp90

is localized to the cell membrane in DLBCL cell lines, suggesting that its chaperone function may also take place in the membrane.

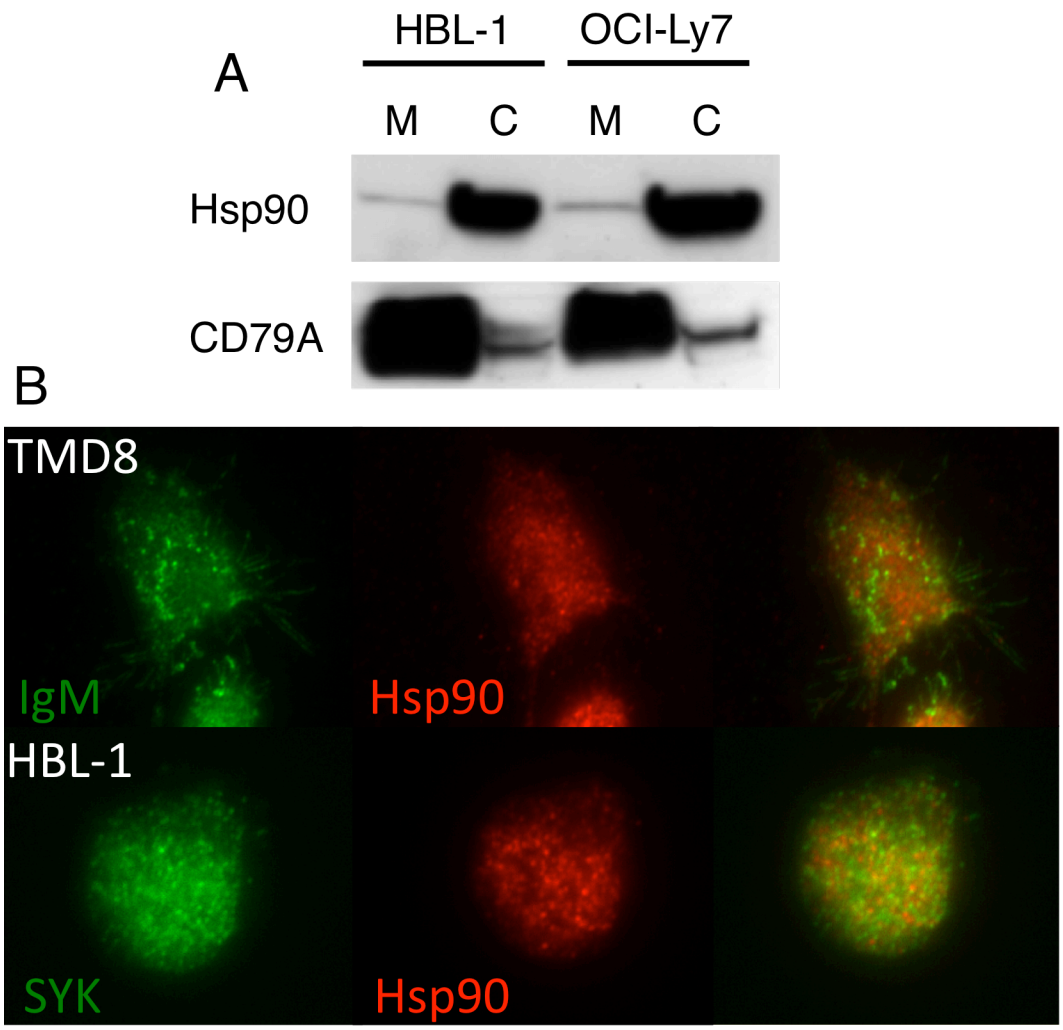

Figure 3.2 Membrane localization of Hsp90. (A) HBL-1 and OCI-Ly7 cells were subjected to cellular fractionation. Membrane (M) and cytoplasmic (C) fractions were immunoblotted with the indicated antibodies. (B) TMD8 cells were stained for IgM and Hsp90 with fluorescent conjugated antibodies and imaged using TIRFM (upper row). HBL-1 cells were stained for SYK and Hsp90 with fluorescent conjugated antibodies and imaged using TIRFM (lower row).

2.2.2 PU-H71 disrupts BCR-lipid raft association

Following ligation and aggregation of the BCR, the clustering and proximity of BCRs in lipid rafts causes amplification of BCR signaling (202). Because components of the BCR were identified in teHsp90 proteomics assays and exposure to PU-H71 diminished BCR signaling activity, we wondered if the PU-H71-induced loss of proximal BCR enzyme activity was due to decreased BCR-lipid raft association. To test this, we measured colocalization of the BCR with lipid rafts in DLBCL cells exposed to PU-H71 for 4 hours (the time when maximal decrease of SYK, BTK, and PLCγ2 activity independent of total protein degradation was observed). To visualize the BCR, we used an antibody to IgM conjugated to a fluorophore. To visualize lipid rafts, we stained cells with filipin, a small molecule that forms a fluorescent complex with cholesterol (203-205). Using confocal microscopy and the Costes' automatic thesholding method (206), we measured BCR-lipid raft colocalization in two ABC DLBCL cell lines in the presence of PU-H71 or vehicle. We observed a significant decrease in BCR-lipid raft colocalization in the presence of PU-H71 (Figure 3.3).

2.2.3 teHsp90 is required for dynamic assembly of the BCR signalosome complex

Given the observed attenuation of SYK, BTK and PLCγ2 phosphorylation upon PU-H71 exposure, we wondered whether teHsp90 was required for dynamic assembly of the BCR signalosome complex and if PU-H71 would disrupt this effect. To address this question, we interrogated the BCR signalosome using TIRFM in cells exposed to PU-H71 for four hours, the timepoint at which maximal suppression BCR signaling by PU-H71 independent of total protein

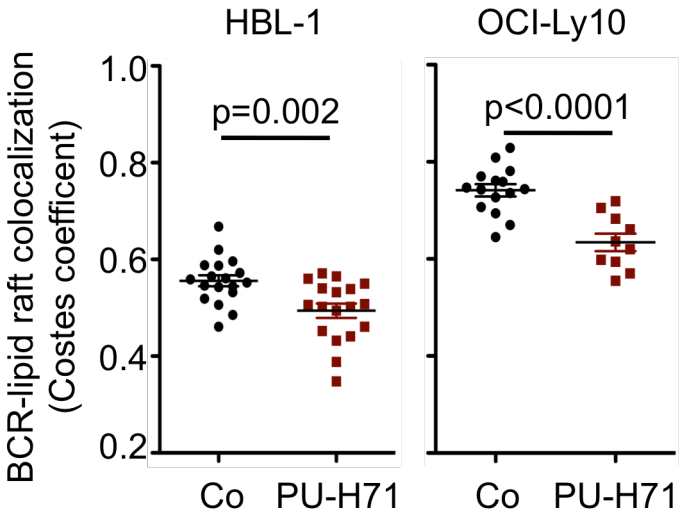

Figure 3.3 PU-H71 disrupts BCR-lipid raft association. IgM and lipid rafts of HBL-1 and OCI-Ly10 cells exposed to vehicle or PU-H71 (1 μM, 4h) were visualized by confocal microscopy (60X). Colocalization was quantified with the Costes method for at least 10 high power fields in at least two independent experiments. Unpaired t-test.

degradation was observed. For these assays, we used TIRFM to visualize IgM-SYK association in vehicle or PU-H71 treated cells. To visualize the BCR we used an antibody to IgM conjugated to a fluorophore. To visualize SYK we used a primary antibody against human SYK and then a secondary antibody conjugated to a different fluorophore. We imaged control and treated cells using TIRFM and quantified IgM:SYK colocalization by counting IgM clusters that were also SYK positive. We initially expected to see high basal IgM:SYK association that would be disrupted in the presence of PU-H71, but instead observed 36% of IgM clusters colocalized with SYK in vehicle treated cells compared to 53% of IgM clusters colocalized with SYK in PU-H71 treated cells ($p=0.03$) (Figure 3.4).

As an orthogonal method to test this hypothesis, we used a biochemical approach: endogenous co-immnoprecipitation assays in cells treated with

vehicle or PU-H71 at the short time points where loss of kinase phosphorylation was observed independent of effects on total protein abundance. Due to the chronic activation of the BCR pathway in these cell lines (150), we expected to observe high basal levels of CD79A interaction with SYK and BTK that would be disrupted upon exposure to PU-H71.

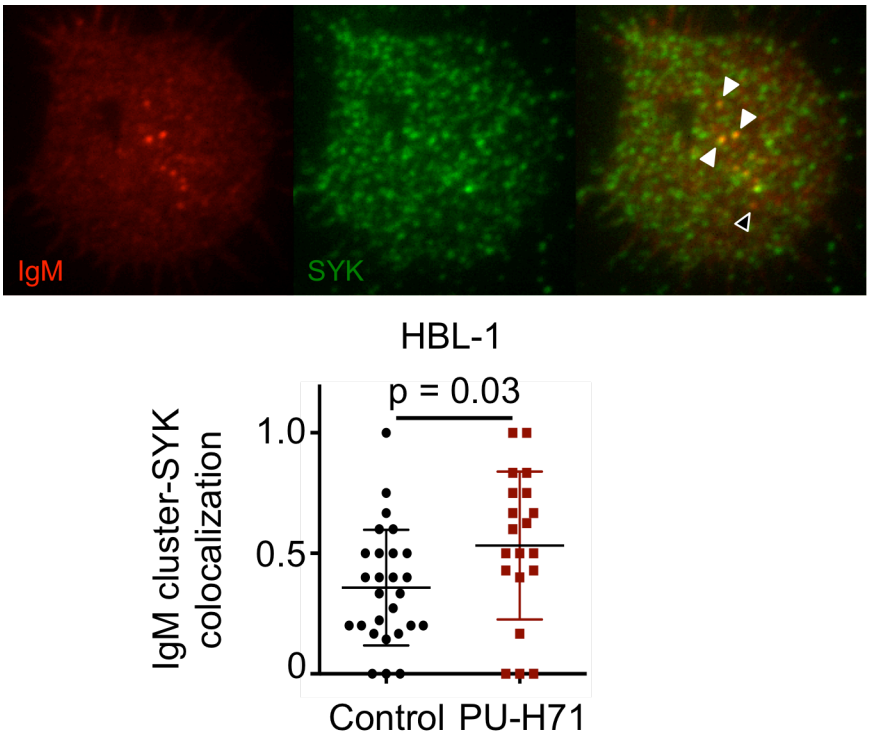

Figure 3.4 PU-H71 induces IgM cluster association with SYK. HBL-1 cells exposed to vehicle or PU-H71 (1 μM, 4h) were stained with fluorescent antibodies to IgM and SYK and visualized by TIRFM. Colocalization was quantified by counting IgM clusters that were SYK positive (white arrows, SYK-negative clusters represented with black arrow). Unpaired t-test.

However, we observed very low basal interaction of CD79A with SYK and no interaction of CD79A with BTK at basal levels (Figure 3.5) Further, we observed a time-dependent increase in the amount of SYK and BTK co-

immunoprecipitated with CD79A in cells exposed to PU-H71 (Figure 3.5). The presence of Hsp90 within the BCR signalosome complex was verified by probing the immunoblots of these assays with an antibody to Hsp90 (Figure 3.5). These immunoblots were also probed with an antibody to CD79A as a control for immunopreceipitation efficiency and observed no change.

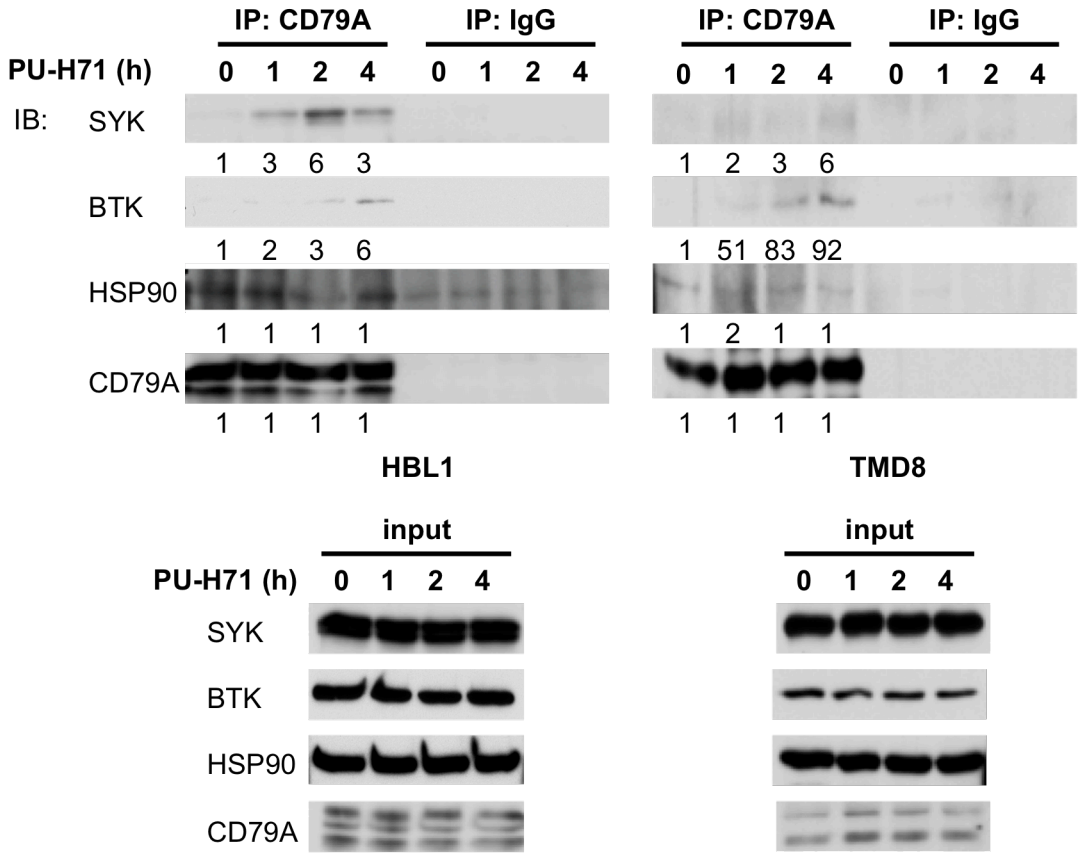

Figure 3.5 PU-H71 induces freezing of the BCR signalosome complex. Lysates of HBL-1 or TMD8 cells exposed to vehicle or PU-H71 (1μM) for the times indicated were immunoprecipitated with antibodies to CD79A or IgG and immunoblotted with the indicated antibodies. Input is 2% of each IP. Densitometry quantified using ImageJ relative to 0h is noted.

This PU-H71-induced accumulation of SYK and BTK on CD79A occurs at times of PU-H71 exposure when SYK and BTK exhibit reduced activity and decreased association of the BCR with lipid rafts is observed, suggesting that

this buildup of kinases on the BCR represents a loss of dynamic BCR complex function, likely due to inhibition of the Hsp90 chaperone cycle. Collectively these data suggest that teHsp90 contributes to BCR functionality by enabling lipid raft localization and dynamic interactions with its downstream mediators.

During signaling, BCR signalosome components must dynamically recycle configurations in order to provide ongoing BCR signaling required for cell survival. BCR surface expression is elevated in ABC-DLBCLs, which result from the CD79 mutations present in these cells to maintain chronic active signaling (150). We wondered if PU-H71-induced freezing of the BCR signalosome was associated with increased internalization of the receptor. To test this hypothesis, we performed a flow cytometry based BCR internalization assay in cells treated with vehicle or PU-H71. We observed mild, but significant increases in BCR internalization in cells treated with PU-H71 (Figure 3.6).

2.3 Signaling induced by BCR stimulation requires teHsp90 function

2.3.1 Antigen-induced BCR signalosome activation

To further demonstrate that accumulation of SYK and BTK with the BCR is associated with a loss of BCR signalosome complex function, we pretreated cells with 1 μM PU-H71 for 1 hour before stimulating the BCR with IgM + IgG (10 μg/mL), and then measured the activity of SYK and BTK by phospho-immunoblot in HBL-1 and TMD8 ABC DLBCL cells. We observed that PU-H71 inhibited BCR-stimulated activation of SYK by 33% in TMD8 cells, although there was only a minimal reduction in HBL-1 (Figure 3.7A). PU-H71 more powerfully inhibited BCR-stimulated activation of BTK by 50% and 62% in

HBL-1 and TMD8 cells, respectively (Figure 3.7A). We used intracellular phosphoflow cytometry as an orthogonal assay to further examine the BCR signaling pathway. In HBL-1 cells we observed a 20-30% decrease in SYK, BTK and PLCγ2 activation following BCR stimulation in cells pretreated with PU-H71 ($p \leq 0.0001$, Figure 3.7B). In OCI-Ly10 cells, we observed a 15-25% reduction in antigen-induced kinase activation in cell pretreated with PU-H71 ($p \leq 0.01$, Figure 3.7B). We also observed this effect in GCB DLBCL cells. In OCI-Ly1 cells pretreated with PU-H71, we observed a 15-25% decrease in BCR-stimulated kinase activation (Figure 3.7B).

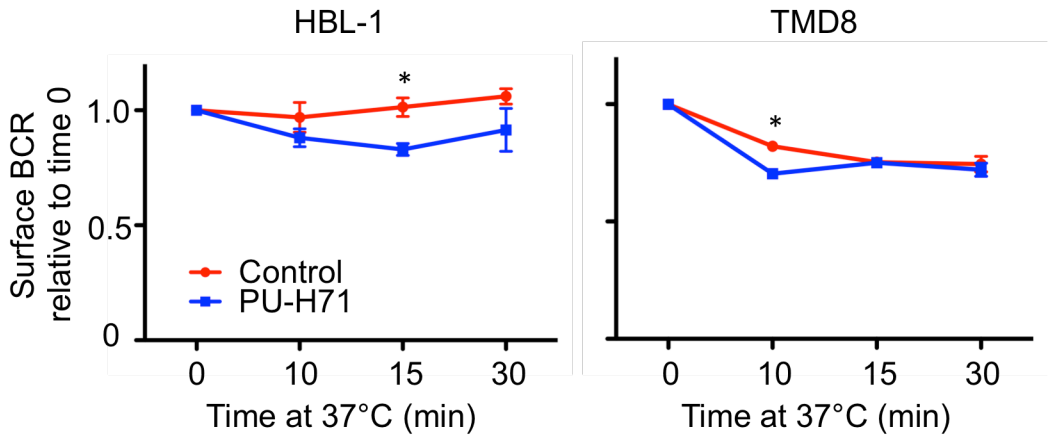

Figure 3.6 PU-H71 induces BCR internalization. HBL-1 and TMD8 cells treated with vehicle or PU-H71 (1 μM, 2h) were incubated with IgM (10 μg/mL) on ice before incubation at 37°C for the times indicated, then fixed and stained with a fluorescent-conjugated secondary antibody. BCR surface expression was quantified using flow cytometry (*$p<0.05$, $n=3$).

2.3.2 Calcium mobilization

Inhibition of teHsp90 with PU-H71 disrupts dynamic recycling of the BCR signalosome and prevents BCR-stimulated activation of SYK, BTK and PLCγ2, the proximal enzymes of the BCR pathway contained in the signalosome. We wondered if BCR signaling downstream of the membrane is teHsp90-dependent. To test this, we used a fluorescent calcium indicator (Fluo-4

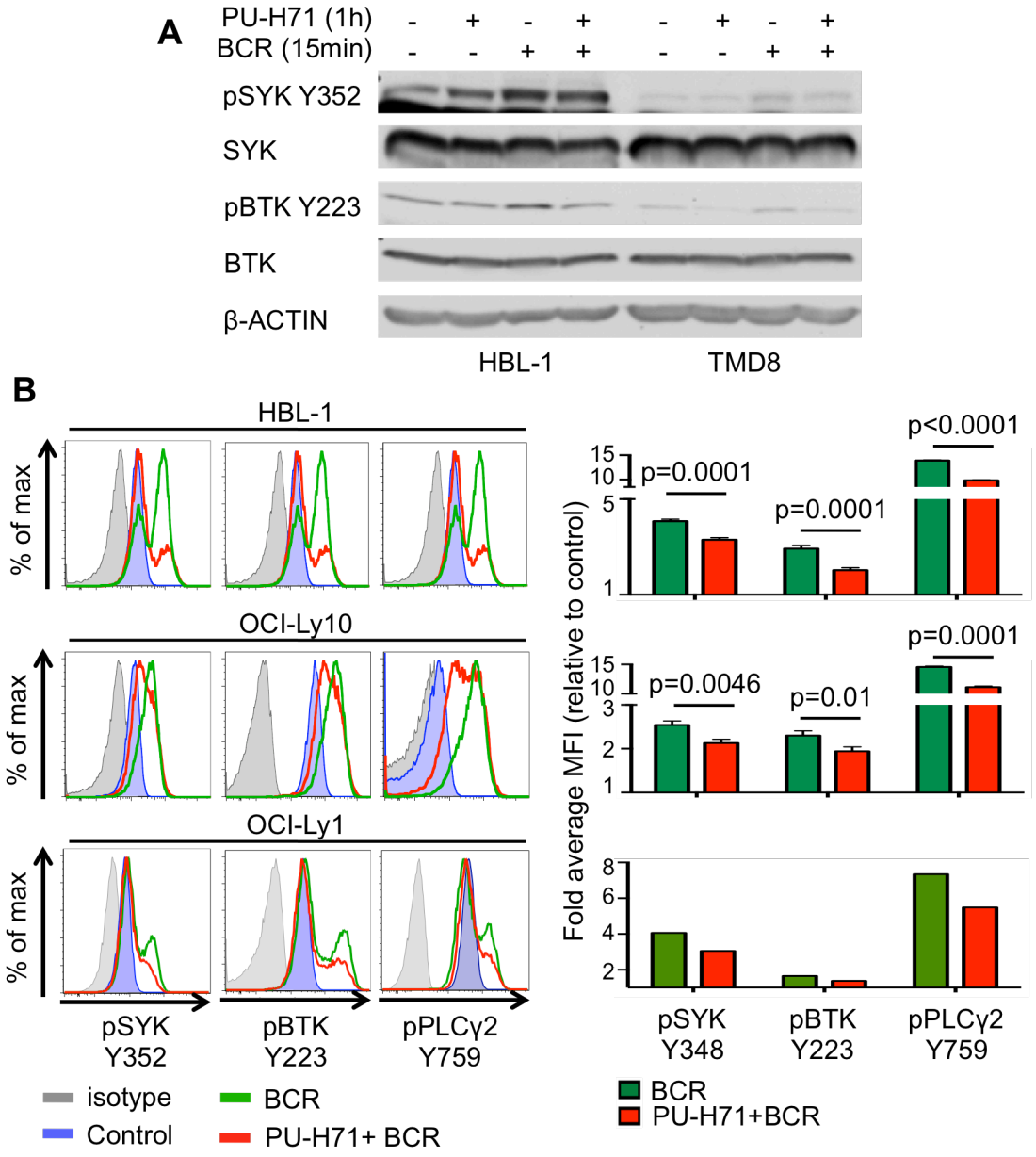

Figure 3.7 BCR-stimulated activation of proximal BCR signaling requires teHsp90 function. (A) Lysates of HBL-1 and TMD8 cells exposed to vehicle or PU-H71 (1 μM) before BCR stimulation (IgM+IgG 10 μg/mL) were subjected to immunoblotting. (B) HBL-1, OCI-Ly10 and OCI-Ly1 cells treated with vehicle or PU-H71 (1 μM, 1h) before BCR stimulation (IgM+IgG 10 μg/mL, 15min) were fixed, permeabilized and stained with phospho-antibodies or isotype controls. Phospho-proteins were quantified using flow cytometry. (n=3, unpaired t test).

AM) to measure calcium mobilization, a direct output of proximal BCR signaling, in DLBCL cells treated with vehicle or PU-H71. These experiments revealed profound suppression of BCR-induced calcium flux in both GCB and ABC DLBCL cells pretreated with PU-H71.

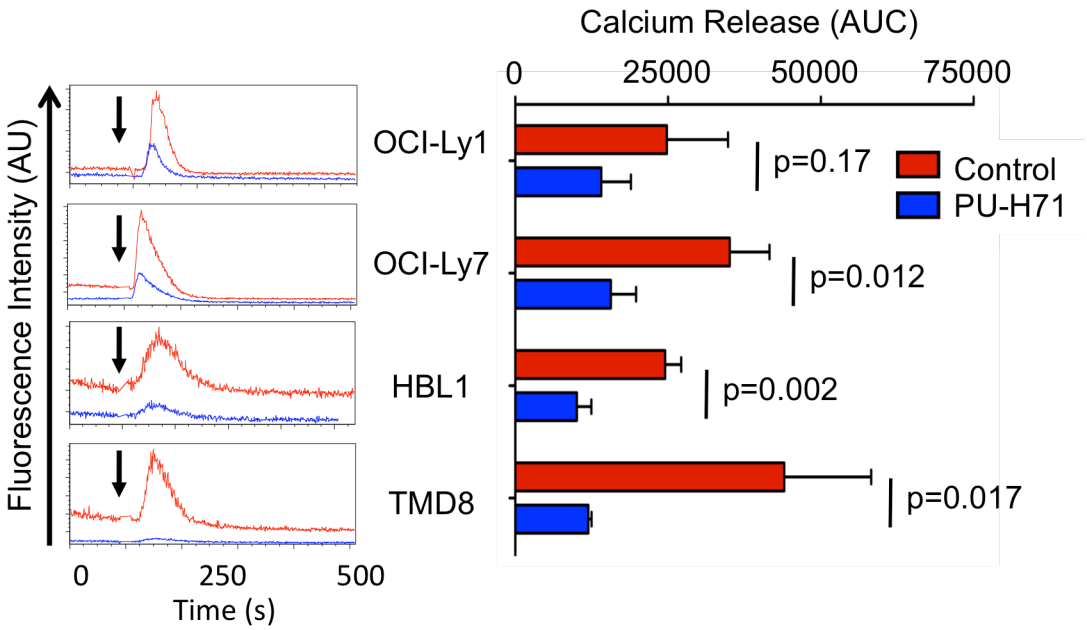

Figure 3.8 Calcium mobilization in DLBCL cells requires teHsp90 function. OCI-Ly1, OCI-Ly7, HBL-1 and TMD8 cells were treated with vehicle or PU-H71 (1 μM, 2h), then incubated with a fluorescent calcium indicator (Fluo-4 AM, 2 μM, 30min) then washed and resuspended in calcium free PBS. Calcium release was measured over time by flow cytometry before and after BCR stimulation (IgM+IgG 10 μg/mL at 120sec). n=3, unpaired t test.

2.3.3 Basal and BCR-induced NF-κB activity

After determining that teHsp90 function is required for proximal BCR signaling through calcium signaling, we sought to determine if impairment in BCR signaling was associated with downstream effects on NF-κB activity. To test this, we used the Ramos-blue cell line – a B cell lymphoma cell line engineered to express an NF-κB responsive reporter encoding alkaline phosphatase – to measure basal and BCR-induced NF-κB activity. In cells

treated with PU-H71 we observed a significant decrease in NF-κB reporter activity (p=0.02) and even more profound suppression of NF-κB activity after BCR stimulation of these cells (p=0.01 Figure 3.9A).

Next we wanted to determine if NF-κB activity in DLBCLs was teHsp90 dependent. To test this, we transfected OCI-Ly1 and HBL-1 cells with the NF-κB reporter vector $(NF\text{-}\kappa B)_5$-luc2CP-pGL4 which contains five copies of the NF-κB consensus-response element and a destabilized firefly luciferase. Exposure to PU-H71 diminished basal NF-κB reporter activity in transfected HBL-1 and OCI-Ly1 cells 50% and 90%, respectively (p=0.0001, Figure 3.9B). BCR stimulation with IgM+IgG induced a 1.5- and 3-fold increase in NF-κB reporter activity in HBL-1 and OCI-Ly1 cells, respectively (p=0.01, p<0.0001, Figure 3.9B). Further, treatment with PU-H71 decreased BCR-induced NF-κB reporter activity to 80% of control levels (p=0.02) in HBL-1 cells and just 5% of control reporter activity in OCI-Ly1 cells (p<0.0001, Figure 3.9B).

2.3.4 PU-H71 atteanuates signaling of lateral pathways within the BCR signaling network

Our proteomics assays identified teHsp90 client proteins within the BCR signaling network that are lateral to the canonical BCR signaling pathway such as PI3K, mTOR, MAPK, JNK1/2 and ERK1/2. Because teHsp90 is required not only for the stability was also the activity of its client proteins, we wondered teHsp90 function was required for activity of these signaling effectors. To test this, we treated ABC DLBCL cells with PU-H71 at short timepoints before total client protein degradation is observed and assayed for client activity by phospho-immunoblot. We observed a time-dependent decrease in ERK

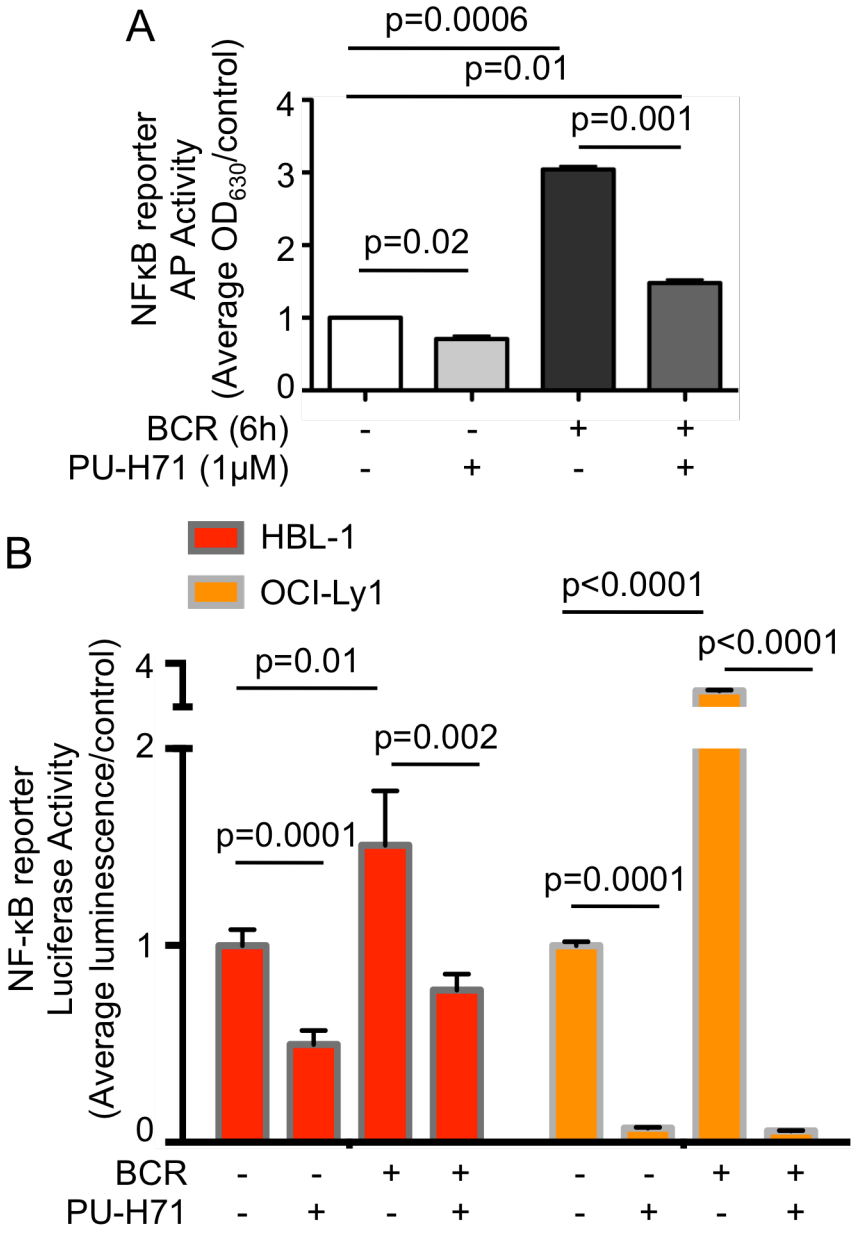

Figure 3.9 Basal and BCR-induced NF-κB activity require teHsp90 function. (A) Ramos-blue cells were treated with vehicle, PU-H71 (1 μM), IgM+IgG (10 μg/mL) or PU-H71 and IgM+IgG (6h). NF-κB reporter activity was measured by colorimetric assay. Unpaired t-test. (B) HBL-1 and OCI-Ly1 transfected with an NF-κB luciferase reporter were treated with PU-H71 (1 μM), IgM+IgG (10 μg/mL) or both (16h) and luciferase activity was assayed. Unpaired t test.

activity in three ABC DLBCL cell lines and a dramatic time-dependent reduction of AKT activity in HBL-1 cells (Figure 3.10).

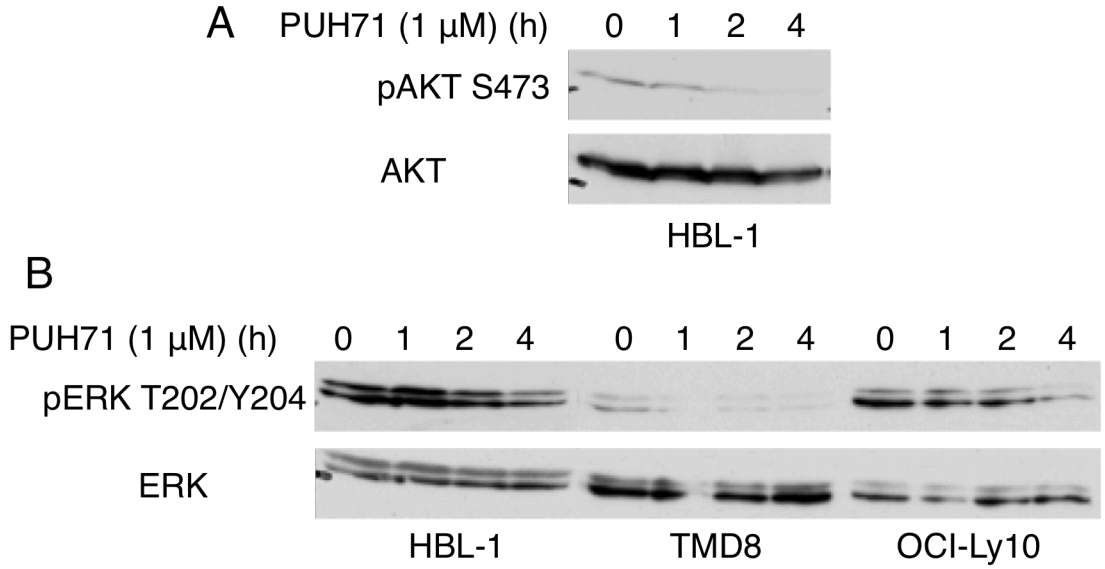

Figure 3.10 PU-H71 induces inhibition of PI3K and ERK pathways in ABC DLBCL. HBL-1, TMD8 and OCI-Ly10 cells were exposed to vehicle or PU-H71 for increasing times as indicated. Lysates were subjected to imunoblotting with anitibodies to pAKT S473 and AKT (A) or pERK T202/Y204 and ERK (B).

2.4 Model of teHsp90 regulation of BCR signaling

Collectively, these data reveal a critical role for teHsp90 stress complexes in BCR signaling. In the presence of PU-H71, the BCR exhibits deficient localization to lipid rafts while concomitantly, SYK and BTK build up on CD79A, the signaling moiety of the BCR, unable to recycle. Due to these effects, and possibly due to additional effects on other signaling mediators of this pathway, there is a resultant loss of calcium flux and NF-κB activity in DLBCL cells (Figure 3.11).

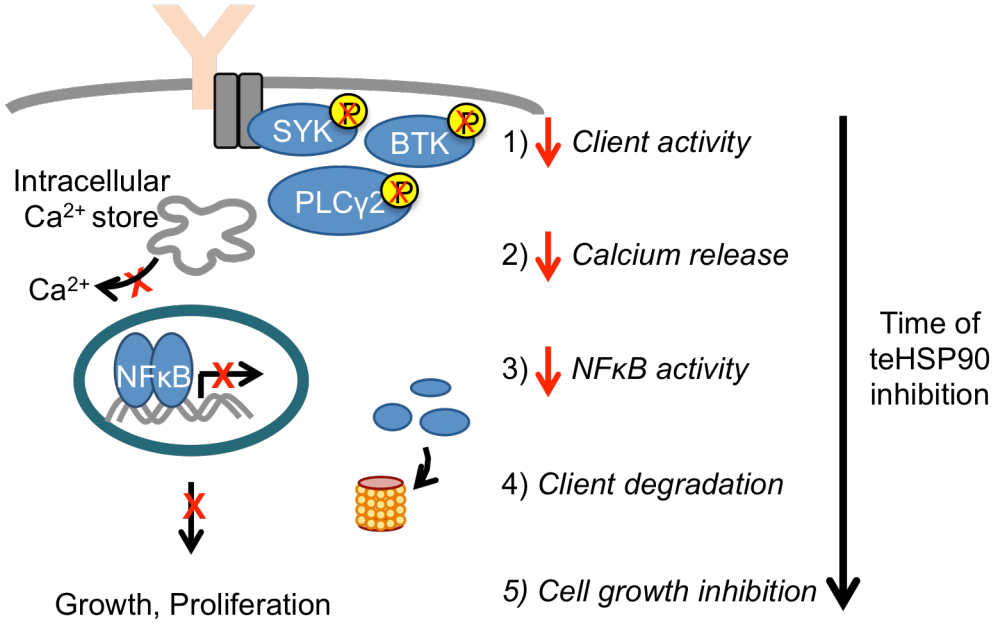

Figure 3.11 Model of PU-H71 effects on BCR signaling at multiple nodes. Inhibition of teHsp90 induces broad attenuation of BCR signaling at multiple nodes including BCR signalosome dynamic recycling, proximal kinase activity, calcium flux and NF-κB activity.

3. Discussion

In this chapter, the scope of previously known Hsp90 functions has been expanded to include binding and facilitating signaling through the BCR signalosome. This function is linked to the tumor-enriched fraction of Hsp90 complexes that can be selectively targeted using the small molecule PU-H71. PU-H71 binds tightly to teHsp90 complexes in an ATP-competitive manner (58). PU-H71 causes teHsp90 to become "locked" in a client protein bound configuration (58). Consistent with the locking effect of PU-H71, exposure of DLBCL cells to this compound resulted in more stable association of CD79A with SYK and BTK as well as disruption of the association of BCR complexes with lipid rafts. Collectively, these data are consistent with the notion that

teHsp90 in some way is required to maintain proper configuration of the BCR signalosome. Moreover, the components of the BCR must dynamically recycle their configuration to promote signaling; teHsp90 may chaperone these dynamics. As actual membrane to cytoplasm vesicle recycling of the BCR is only mildly disturbed by PU-H71 (Figure 3.6), the actions of PU-H71 might be more intimately associated with perturbation of membrane complex protein interaction dynamics. Clearly, in depth structural studies will be required in the future to understand these mechanisms.

Hsp90 isoforms are known to associate with membrane bound proteins such as the BCR. For example, Hsp90N has been shown to contain a putative myristylation sequence, which may explain its membrane localization (207). In T cells, Hsp90 is required for the membrane association of the Src-family kinase Lck (208). Like many other Hsp90 client proteins, activating mutations in Lck increase its dependence on Hsp90 (208). CD79, the signaling moiety of the BCR is often mutated in ABC DLBCLs, resulting in chronic activation of the pathway (150). Though the enzymes of BCR signaling, SYK, BTK and PLCγ2 do not harbor activating mutations, they form the BCR signalosome with CD79 and exhibit increased activity in the ABC DLBCLs. The biochemical and functional dependence of the BCR signalosome on teHsp90 is consistent with the previously demonstrated requirement of teHsp90 to maintain signaling pathways aberrantly activated in human leukemia, lymphoma and solid tumor cells (38, 58, 74, 92). In fact, in avian cells, knockout of Hsp90β was shown to induce multiple defects in BCR signaling including reduction in surface expression of IgM and basal and serum-induced BCR signaling (209). The data herein confirm and underline that teHsp90 stress complexes carry out

specific biochemical functions beyond the classical protein stability and folding functions attributed to Hsp90. Future biochemical approaches probing deeper into the role of teHsp90 in membrane biology and lipid raft functions may provide further insights into the mechanisms described herein.

An important concept that emerges from this work is the notion of teHsp90 as a general facilitator of BCR signaling. The pharmacoproteomic assays described in chapter one indicated extensive interaction of teHsp90 with BCR signaling proteins at multiple levels and throughout multiple branches of the BCR signaling network. These findings correspond with the overall attenuation of BCR signaling, calcium flux and NF-κB activity induced by PU-H71. Moreover, we show that teHsp90 function is required not only for the canonical BCR signaling pathway, but also for lateral signaling pathways within the BCR signaling network including PI3K/AKT and MEK/ERK.

It is worth noting that teHsp90 also associates with BCR components in GCB-type DLBCL cells. In fact, many of the nodes of BCR signaling that are attenuated with PU-H71 are affected equally in GCB and ABC DLBCL cells. It has been shown that GCB DLBCL cells exhibit tonic BCR activity and can be targeted by signaling inhibitors such as SYK inhibitors (23). Hence it is possible that teHsp90 is important for both tonic BCR activity in lymphoma cells as well as chronic active signaling that is more characteristic of ABC-DLBCLs. These data suggest that PU-H71 is a viable therapeutic in the ABC subtype of DLBCL and may affect cell viability through a different mechanism than has been described in GCB DLBCL (38), suggesting the possibility of patient-stratified combinatorial therapies.

4. Materials and methods

Cell lines and reagents

The DLBCL cell lines OCI-Ly1 and OCI-Ly7 were grown in Iscove's Modified Dulbecco's Medium (IMDM) containing 10% FBS and supplemented with peniciliin and streptomycin. OCI-Ly10 was gorwn in IMDM with 20% FBS and penicillin and streptomycin. The DLBCL cell lines HBL-1 and TMD8 were grown in medium containing 90% RPMI and 10% FBS supplemented with L-glutamine, HEPES and penicillin and streptomycin. PU-H71 was synthesized as previously reported (58). Filipin was purchased from Sigma. All human IgM and IgG was purchased from Jackson Immunoresearch. The following antibodies were used: phospho-SYK Y352 #2701, phospho-BTK Y223 #5082, BTK clone D3H5, phospho-PLCγ2 Y759 #3874, phospho-AKT S473 #9271, AKT #2920, phospho-ERK T202/Y204 #9106, and ERK1/2 #9102 (Cell Signaling Technology), SYK clone 4D10, PLCγ2 clone Q-20 (Santa Cruz Biotechnology), Hsp90 ab13495 (Abcam), β-actin clone AC-15 (Sigma Aldrich).

Cell lysis for immunoblot

Cells were counted for viability using Trypan blue dye exclusion, then centrifuged at 1500 rpm for 5 minutes at room temperature and resuspended in fresh medium at a concentration of 2 x 10^6/mL. For lysis, cells were centrifuged for 5 minutes at 1500 rpm at room temperature, then washed with 1X PBS and centrifuged again. Cells were lysed in lysis buffer (10 mM HEPES-KOH pH 7.9, 1.5 mM $MgCl_2$, 10 mM KCl, freshly prepared 1.5 mM $NaMoO_4$, 1% Triton-X, 0.5 mM PMSF, and protease and phosphatase

inhibitors) on ice for 15 minutes, vortexed on high for 15 seconds and centrifuged at 14,000 rpm for 10 minutes at 4°C. Supernatants were measured for protein concentration, mixed with 5X SDS loading buffer and resolved by standard immunoblotting procedures.

Subcellular Fractionation

To isolate membrane fractions, 100 x 10^6 cells were harvested, washed in 1X PBS, and then incubated for 30 minutes at 4°C in 2 mL of hypotonic buffer (42 mM KCl, 10 mM HEPES pH 7.4, 5 mM $MgCL_2$). Cells were homogenized by three rounds of freeze-thawing and centrifuged at 250xg for 10 minutes to remove nuclei and intact cells. The supernatant was centrifugred at 150,000xg for 30 minutes at 4°C to separate cytoplasm from the membrane fraction. The membrane fraction was lysed (1% Triton X-100 in 10 mM Tris-HCl pH7.5, 150 mM NaCl and 5 mM EDTA with protease inhibitors) for 30 minutes on ice. Protein concentration of fractions were quantified using DC Biorad Assay and equal amounts were resolved by standard SDS-PAGE immunoblotting procedure.

Total Internal Reflection Fluorescent Microscopy

Coverslip preparation: Before plating, coverslips were coated with 3.5 μg of Cell-Tak (BD Biosciences) in 300 μL of neutral buffer solution (0.1M sodium bicarbonate pH 8.0) by rocking for 30 minutes at room temperature, then washing twice with distilled water and allowing the coverslips to air dry. After plating, coverslips were centrifuged at 1000 rpm to allow cells to adhere.

Cell plating and treatment: Cells were treated as indicated on the coverslips. After treatment, media was aspirated and cells were fixed by adding warm PHEMO fixative (3.7% formaldehyde, 0.05% glutaraldehyde, 0.5% Triton X-100 in 0.068M PIPES, 0.025M HEPES, 0.015M $EGTANa_2$, 0.003M $MgCl_26H_2O$, 10% DMSO pH 6.8) and incubating for 10 minutes at room temperature. Coverslips were washed 3 times in 1X PBS by shaking gently for 5 minutes. Cells were blocked with 5% normal goat serum in 1X PBS for 10 minutes at room temperature.

Immunostaining: Primary antibodies were diluted in 5% normal goat serum in 1X PBS and incubated overnight at 4°C (Hsp90 Abcam #ab13945, SYK clone 4D10 Santa Cruz Biotechnology) or for 1 hour at room temperature (AlexaFluor 488 goat anti-human IgM, Molecular Probes A21215) then washed 3 times with 1X PBS. Fluorescent conjugated secondary antibodies (Molecular Probes) were diluted in 5% normal goat serum in 1X PBS, added to coverslips and incubated for 1 hour at room temperature in the dark, with shaking. This process was repeated for the second antibody.

Imaging: Cells were imaged on a Nikon TiE inverted microscope with a 100X Apo TIRF objective lens (1.49 NA) and NIS-Elements software using Agilent lasers (488nM = 47mW, 568nM = 58mW) and the Andor Neo sCMOS camera.

Immunoprecipitation

Cells were plated at a concentration of 2 x 10^6/mL and treated with vehicle or PU-H71. Cells were harvested, washed with PBS, and lysed in IP buffer (25 mM HEPES pH 7.5, 150 mM NaCl, 0.2% NP-40, 10% glycerol, 1 mM DTT, 20

mM $NaMoO_4$ and protease inhibitors) for 30 minutes on ice, and then centrifuged at 14,000 rpm for 15 minutes at 4°C to remove insoluble proteins. Protein concentration of supernatants was measured using the DC Protein Assay Kit (Biorad). Input (10 μg) was saved at -20°C. For each IP, 1 mg of protein was precleared for 1 hour at 4°C with 20 μL of Protein G Sepharose beads (Sigma) that were pre-washed three times with IP buffer to remove ethanol. Precleared lysates were precipitated with 10 μg of either αCD79A (Clone HM47, Santa Cruz Biotechnology) or mouse IgG (Abcam ab14813), tumbling overnight at 4°C. Additional Sepharose Protein G beads were blocked overnight tumbling with 1 μg/μL BSA at 4°C. The next day, Sepharose Protein G beads were washed three times with fresh IP buffer and 20 μL was added to each IP and tumbled for one hour at 4°C. IP-bead conjugates were washed three times in IP buffer, resuspended in 20 μL 2X SDS loading buffer, and boiled for 5 minutes at 100°C. 5X SDS loading buffer was added to inputs to achieve a final concentration of 1X and they were boiled for 5 minutes at 100°C. Inputs and immunoprecipitates were resolved by standard immunoblotting procedure and blotted with antibodies to CD79A (clone HM47, Santa Cruz biotechnology), SYK (clone DH35, Santa Cruz Biotechnology), BTK (clone D3H5, Cell Signaling Technology), and Hsp90 (Abcam #ab13495).

BCR-lipid raft colocalization

Cells were treated with vehicle or PU-H71 for 4 hours. After washing with PBS, cells were fixed with 4% paraformaldehyde/0.1% glutaraldehyde/1X PBS for 20 minutes at room temperature. Cells were stained with 10 μg/mL $F(ab')_2$ fragment goat anti-human IgM (Jackson ImmunoResearch 109-006-129) in 0.1% BSA/0.02% sodium azide/1X PBS for 20 minutes at room temperature.

After washing with PBS, cells were stained with 1:1000 Alexa Fluor 647 conjugated donkey anti-goat IgG (Invitrogen A21447) in 0.1% BSA/0.02% sodium azide/1X PBS for 20 minutes at room temperature in the dark. Cells were washed with PBS, and then incubated with 50 μg/mL filipin (Cayman Cheimcal #70440) in PBS for 1 hour at room temperature in the dark. Cells were next affixed to slides by cytocentifugation at 1300 rpm for 5 minutes and mounted with ProLong Gold antifade reagent (Life Technologies). Cells were imaged at 60X using the Fluoview FV10i confocal microscope (Olympus) and analyzed for colocalization using the JACoP plug-in (206) with ImageJ (NIH).

Flow cytometry based BCR internalization assay

Cells were pretreated with vehicle or 1 μM PU-H71 for two hours. To prepare cells, they were first washed with cold 1X PBS, then incubated with 10 μg/mL $F(ab')_2$ fragment goat anti-human IgM (Jackson ImmunoResearch 109-006-129) at a concentration of $2x10^6$ for 30 minutes at 4°C. Cells were washed twice with cold 1X PBS and incubated at 37°C for 0-20 minutes. Internalization was stopped by transferring tubes to ice and adding cold 1% FBS in 1X PBS. To detect receptors remaining on the surface, cells were stained with AlexaFluor 647 donkey anti-goat IgG (Molecular Probes A21447) in 1% FBS in 1X PBS for 20 minutes at room temperature. Cells were washed twice with 1% FBS in 1X PBS, then fixed in 1% paraformaldehyde. Data was acquired on MacsQuant flow cytometer (Miltenyi Biotec) and analyzed using FlowJo software package (TreeStar).

Multicolor intracellular phosphoflow cytometry

Cells were plated at 2 x 10^6/mL and treated with vehicle or 1 μM PU-H71 for 1 hour at 37°C. 10 μg/mL IgG + IgM (Jackson Immunoresearch 309-005-107) was added to treated cells and incubated at 37°C for 15 minutes. Cells were fixed by adding BD Phosflow Fix Buffer I (BD Biosciences) directly to culture medium and incubating for 15 minutes at 37°C. Cells were harvested into eppendorf tubes, centrifuged at 1500 rpm for 5 minutes at room temperature, then permeabilized by adding 250 μL of cold BD Phosflow Perm Buffer III (BD Biosciences) and incubating on ice for 30 minutes, after which 500 μL of wash/stain buffer (1% FBS, 0.09% NaN_3 in 1X PBS) was added. Cells were centrifuged at 1500 rpm for 5 minutes at 4°C, and each sample was divided for staining in equal amounts of either fluorescent-conjugated specific phospho-antibodies (AlexaFluor 488 Mouse anti-SYK pY348 clone I120-722 catalog number 560081, PE Mous anti-BTK pY223 clone N35-86 catalog number 562753, AlexaFluor 647 Mouse anti-PLCγ2 pY759 clone K86-689.37 catalog number 558498, BD Biosciences) or matching isotype controls (AlexaFluor 488 Mouse IgG1 K2317666, PE Mouse IgG1 K 551436, AlexaFluor 647 Mouse IgG1 K 557783 BD Biosciences) in wash/stain buffer on ice. Data was acquired on MacsQuant flow cytometer (Miltenyi Biotec) and analyzed using FlowJo software package (TreeStar).

Calcium Release

Cells were plated at 2 x 10^6 and treated with vehicle or 1 μM PU-H71 for 2 hours at 37°C, then incubated with 2 μM Fluo 4 AM (Invitrogen #F14217) for 30 minutes at 37°C. Fluorescent indicator was washed out cells with fresh media, and cells recovered for 30 minutes at 37°C. Cells were collected in

PBS without calcium, and fluorescence was measured on an LSR-II flow cytometer (BD Biosciences) for 2 minutes. The tube was removed for the addition of 10 μg/mL of IgG + IgM (Jackson Immunoresearch 309-005-107) and one second of vortexing to mix. The tube was replaced and fluorescence measurement continued for at least 5 more minutes. Calcium release was quantified using FlowJo software package (TreeStar) as area under the curve for the first four minutes.

Ramos-blue NF-κB alkaline phosphatase reporter activity assay

Ramos-blue cells (Invivogen) were grown in IMDM containing 10% FBS, supplemented with L-glutamine, penicillin and streptomycin, 100 μg/mL normocin and 100 μg/mL zeocin. To assay, cells were resuspended in medium without selective antibiotics at a concentration of 2 x 10^6/mL, plated in a flat-bottom 96-well plate and treated with vehicle, 1 μM PU-H71, 10 μg/mL IgG + IgM (Jackson Immunoresearch 309-005-107), or PU-H71 and IgG + IgM for 6 hours at 37°C. Following treatment, 40 μL of medium from each treated well was transferred to a new flat-bottom 96-well plate and incubated with 160 μL of QUANTI-Blue reagent overnight at 37°C. Alkaline phosphatase activity was measured by colorimetic assay at 630 nM with the Synergy4 plate reader (BioTek).

NF-κB luciferase reporter assays

In HBL-1 and OCI-Ly1, 1 μg of $(NF\text{-}\kappa B)_5$-Luc2CP-pGL4 per 5 x 10^6 cells were transfected using nucleofection (Amaxa, Lonza). Eight hours after transfection, cells were plated at 2 x 10^6 cells/mL and treated with vehicle, 1 μM PU-H71, 10 μg/mL IgG + IgM (Jackson Immunoresearch 309-005-107), or PU-H71 and

IgG + IgM for 16 hours at 37°C. Cells were harvested and submitted to Dual-Glow luciferase assays following manufacturer's protocol (Promega). Briefly, cells were lysed in 20 μL 1X passive lysis buffer by rocking at room temperature for 20 minutes. 5μL of each sample was added to a white-walled 96 well plate and 50 μL of Luciferase Assay buffer was added before luminescence was read by plate reader (Synergy4, BioTek).

Statistical analysis

Two-tailed unpaired t test was used unless otherwise stated. All statistical analyses were carried out using Prism software (GraphPad).

CHAPTER FOUR

Concomitant inhibition of teHsp90 and the BCR pathway combines to inhibit the growth of DLBCLs

1. Introduction

For many therapeutic targets in cancer achieving a high degree of suppression is imperative to obtain maximal anti-tumor effect. Complex signaling networks like the BCR pathway tend to branch out in many directions, making their complete suppression a challenge. Moreover, complete suppression of the target of a specific inhibitor must be balanced against its off-target effects that can become increasingly problematic with higher doses that may be needed for therapeutic effect. Even if maximal target inhibition is achieved, exposure to targeted compounds over time can lead to acquired resistance in tumors through mutations that prevent drug binding or activate the pathway through another protein in the pathway.

Inhibition of teHsp90 can resolve many of the issues with targeted therapy by simultaneously inhibiting many signaling nodes within multiple pathways. As shown above, PU-H71 inhibition of teHsp90 accomplishes broad attenuation of BCR signaling at multiple nodes, weakening the BCR signaling pathway, and potentially, signaling network. This mechanism of action makes teHsp90 inhibition an ideal platform for rational combination therapies. By combining broad signaling attenuation with focused attack on a key node of oncogenic signaling required for cancer cell survival, maximal target and pathway suppression can be achieved, resulting in increased anti-tumor effect. Specifically, inhibition of teHsp90 and its client proteins can synergize to kill

cancer cells. For example, the combination of PU-H71 and RI-BPI, a peptidomimetic inhibitor of BCL6, the main oncogene in DLBCL and client of teHsp90, synergizes to kill these cancers *in vitro*, *in vivo* and *ex vivo* (194). Further, combined exposure to PU-H71 and obatoclax, an inhibitor of BCL2-family proteins such as MCL-1, a teHsp90 client in PEL, synergized to kill these lymphoma cells (74). After identifying and validating several components of the BCR pathway as clients of teHsp90 in DLBCL, we hypothesized that combinatorial exposure of DLBCLs to the BCR-attenuating activity of PU-H71 together with specific targeted BCR pathway inhibitors would result in additive or synergistic growth inhibition through maximal suppression of the BCR signaling pathway.

2. Results

2.1 PU-H71 and inhibitors of BCR signaling synergize to inhibit growth of DLBCL cells

We set out to determine if PU-H71 synergizes with BCR pathway inhibitors. We selected a panel of BCR pathway inhibitors, prioritizing inhibitors within each class by clinical relevance. The inhibitors chosen for investigation and their targets are listed in Table 4.1.

In order to determine the dosages and schedules that could induce dose-dependent growth inhibition in DLBCL cells, we exposed a panel of DLBCL cell lines to vehicle or a dose curve of each of the BCR pathway inhibitors and assayed for cell viability. We determined that buparlisib and MI-2 could be administered for 48 hours to induce dose-dependent growth inhibition. However R406, ibrutinib and sotrastaurin, had to be administered for 96 hours,

adding drug twice, at 0 and 48 hours to induce the same growth inhibition effect. This slower onset of growth inhibition likely results because these inhibitors are cytostatic, not cytotoxic, and therefore they require more time to induce an effect on cell viability. Our results confirm reports that GCB DLBCLs are resistant to ibrutinib, MI-2 and sotrastaurin but are sensitive to R406 and buparlisib. Although PU-H71 causes dose-dependent growth inhibition within 48 hours of a single dose, we also determined the doses required for longer exposures to be used for combination experiments. Dose curves of each individual drug in a panel of DLBCL cell lines are shown in Figure 4.1.

Table 4.1 Inhibitors selected for combination treatments and their targets

Inhibitor	Target
R406	SYK
Ibrutinib (PCI-32765)	BTK
Buparlisib (BKM120)	PI3K (pan)
MI-2	MALT1
Sotastaurin (AEB071)	PKCβ

In order to determine the growth inhibition effect of PU-H71 in combination with this panel of BCR pathway inhibitors, we exposed a panel of DLBCL cell lines to vehicle, PU-H71, each BCR pathway inhibitor, or the PU-H71-BCR combination. Each drug was administered at 6 doses in 1:2 dilutions, and the combination was administered in constant ratio. We calculated combination effect using the algorithm of Chou and Talalay (210). All of these combinations showed synergistic (combination index (CI) value below 0.9) or additive (CI value between 0.9 and 1.1) effect at concentrations sufficient to inhibit growth

75% (GI_{75}, Figure 4.2). The most potently synergistic combination was PU-H71 and ibrutinib, with marked synergy observed in three ABC DLBCL cell lines (CI $GI_{95} < 0.4$, Figure 4.2).

We observed that GCB DLBCL cell lines respond to some inhibitors of the BCR pathway. In order to determine the combination effect of PU-H71 with inhibitors of the BCR pathway, we exposed GCB DLBCL cell lines to PU-H71, BCR pathway inhibitors or the combination and assayed for viability. For drug combinations where the cell lines respond to the individual BCR pathway inhibitors, we calculated combination effect using the algorithm of Chou and Talalay (210). We observed additive or weakly synergistic effect in combinations of PU-H71 with R406 and buparlisib (Figure 4.3A). In order to calculate combinatorial using this method, a dose effect curve for each individual drug is required. For combinations involving BCR pathway inhibitors that show resistance in GCB DLBCL cell lines, we plotted dose-effect curves of each drug and the combination. We observed no difference between the fraction of growth inhibited in the PU-H71 and combination conditions (Figure 4.3B).

Similarly, the ABC DLBCL cell line OCI-Ly3 has an activating mutation in CARD11, which acts downstream of the BCR signalosome. As such, this cell line is resistant to BCR pathway inhibitors that act upstream of the CBM complex. Though these cells are sensitive to PU-H71, we observed no increased growth inhibition effect when combined with ibrutinib or sotrastaurin (Figure 4.3B). Taken together, our data suggest that synergy with PU-H71 requires sensitivity to BCR pathway inhibitors.

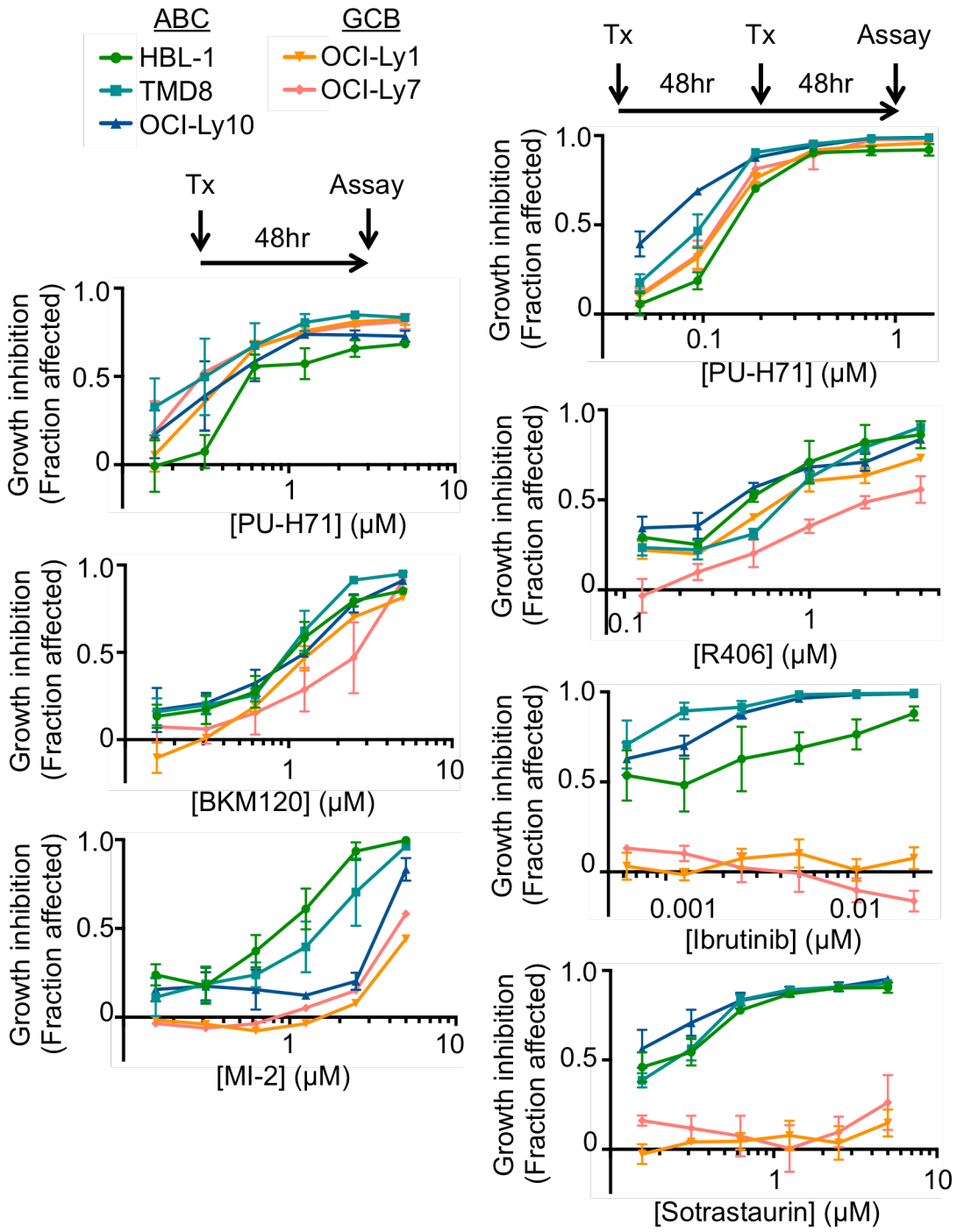

Figure 4.1 Dose response curves of BCR pathway inhibitors in DLBCL cell lines. A panel of DLBCL cell lines was exposed to PU-H71 and various BCR pathway inhibitors in two different schedules and assayed for viability. Growth inhibition was calculated by normalizing drug treated cells to vehicle treated cells.

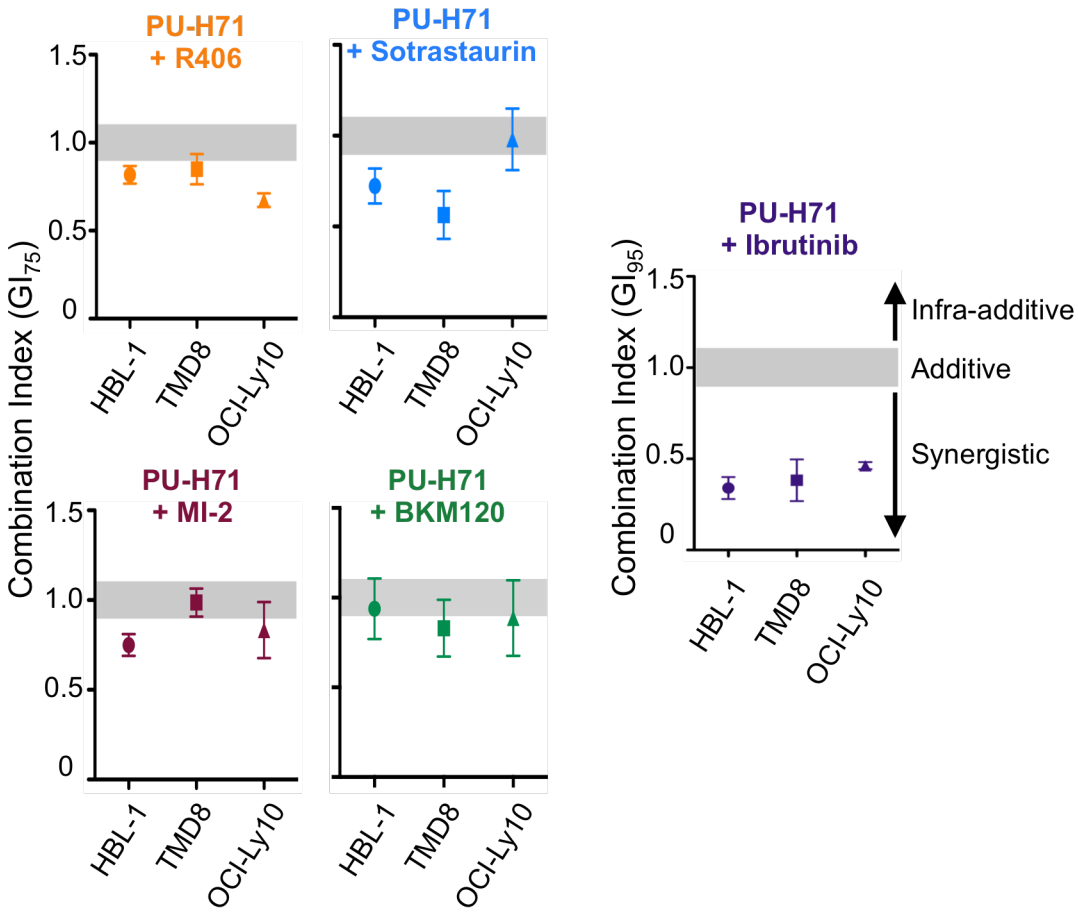

Figure 4.2 PU-H71 combination treatment with BCR pathway inhibitors additively or synergistically kills ABC DLBCLs. A panel of ABC DLBCL cell lines were exposed to PU-H71, a BCR pathway inhibitor or the combination and assayed for cell viability. Dose curves for single and combination drug exposures were plotted and combination index (CI) values were calculated using the algorithm of Chou and Talalay (208). Average CI value (n≥3) ± SEM is plotted. CI value between 0.9 and 1.1 represents additive effect. CI value below 0.9 represents synergistic effect.

Because teHsp90 inhibition disrupts BTK activity, we wondered if the combinatorial effect of PU-H71 with ibrutinib was linked to more powerful inhibition of BTK activity. To test this, we exposed three independent ABC DLBCL cell lines to vehicle, PU-H71, ibrutinib or the combination for 2 hours and measured BTK activity by phospho-immunoblot. The combination of PU-H71 and ibrutinib resulted in additive inhibition of BTK activity (Figure 4.4A).

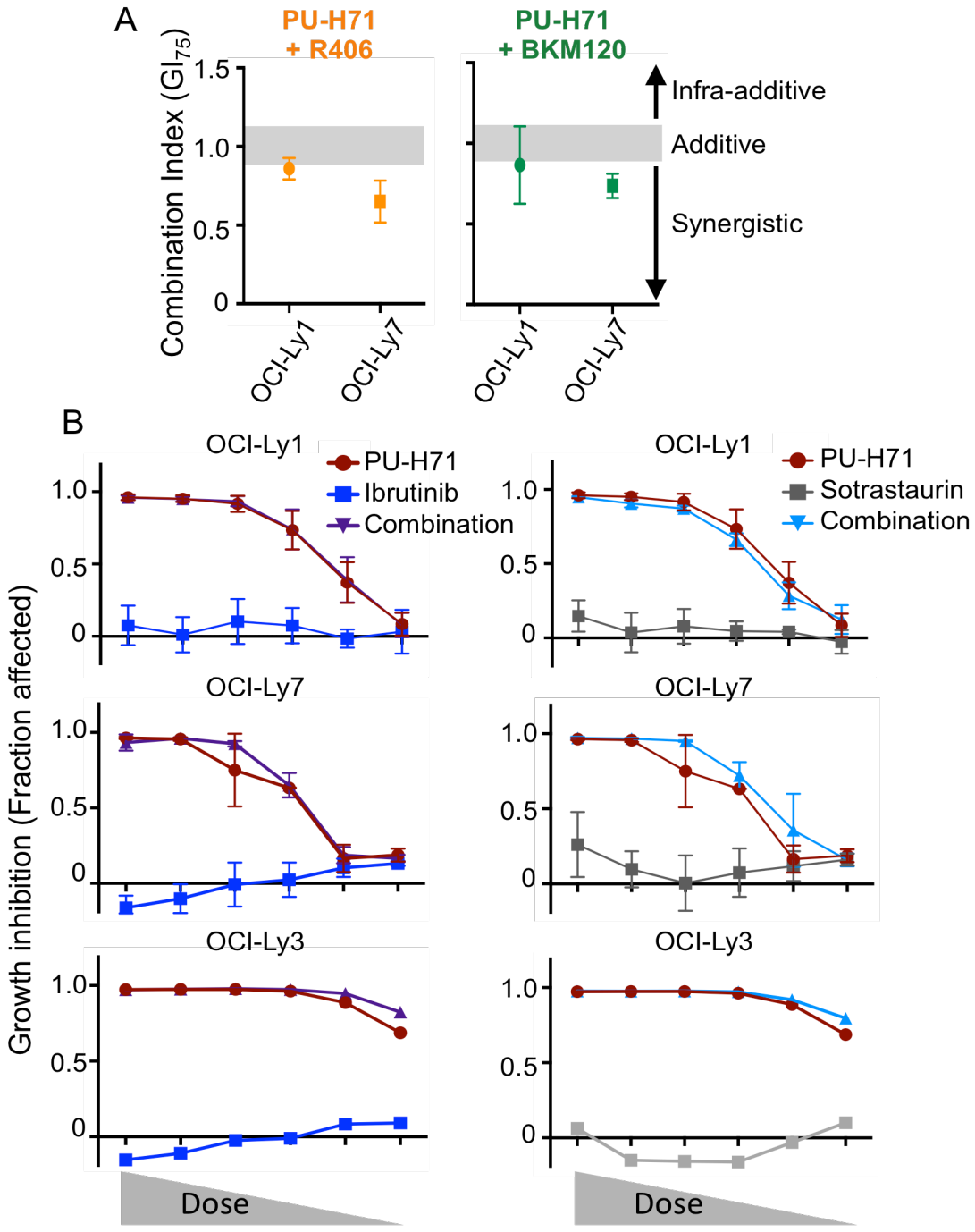

Figure 4.3 Combination effect of PU-H71 with BCR pathway inhibitors in GCB DLBCLs and a CARD11 mutant ABC DLBCL cell line, OCI-Ly3. (A) Average CI ± SEM (n=3) values of OCI-Ly1 and OCI-Ly7 cells exposed to PU-H71, a BCR pathway inhibitor or the combination and assayed for cell viability. (B) Dose-effect curves of OCI-Ly1, OCI-Ly7 and OCI-Ly3 cells exposed to PU-H71, a BCR pathway inhibitor or the combination and assayed for cell viability.

teHsp90 inhibition disrupts NF-κB activity in DLBCL (Figure 3.9), and BTK activity is required for NF-κB activity in ABC DLBCLs. We wondered if the PU-H71-ibrutinib combination more potently suppresses BCR signaling downstream of BTK activity. To test this we used p65 ELISA to measure NF-κB activity in nuclear lysates of two ABC DLBCL cell lines treated with average GI_{50} values of PU-H71, ibrutinib or the combination for 24 hours. At the doses tested, single drugs induced a modest reduction in p65 DNA binding activity. In contrast, the PU-H71-ibrutinib combination significantly decreased p65 activity by 60% in HBL-1 and TMD8 cells in an additive manner (p=0.03, p=0.04, respectively, Figure 4.4B).

As an orthogonal method to test this notion, we used HBL-1 cells transfected with the NF-κB reporter vector $(NF\text{-}\kappa B)_5$-luc2CP-pGL4 which contains five copies of the NF-κB consensus-response element and a destabilized firefly luciferase. Exposure to PU-H71 or ibrutinib decreased NF-κB activity by 65% and 80%, respectively (p=0.0006, p<0.0001, respectively, Figure 4.4C) The PU-H71-ibrutinib combination decreased NF-κB luciferase activity by 90%, and this reduction was significantly more than either ibrutinib or PU-H71 alone (p=0.013, Figure 4.4C). Taken together, our data suggest that the synergistic growth inhibition observed in the PU-H71-ibrutinib combination results from maximal suppression of the BCR pathway, exemplified in BTK and NF-κB activity.

2.2 Ibrutinib enhances PU-H71 anti-lymphoma effect *in vivo*

The PU-H71-ibrutinib combination is particularly suited for clinical translation because PU-H71 is in clinical trials and ibrutinib is an FDA-approved drug,

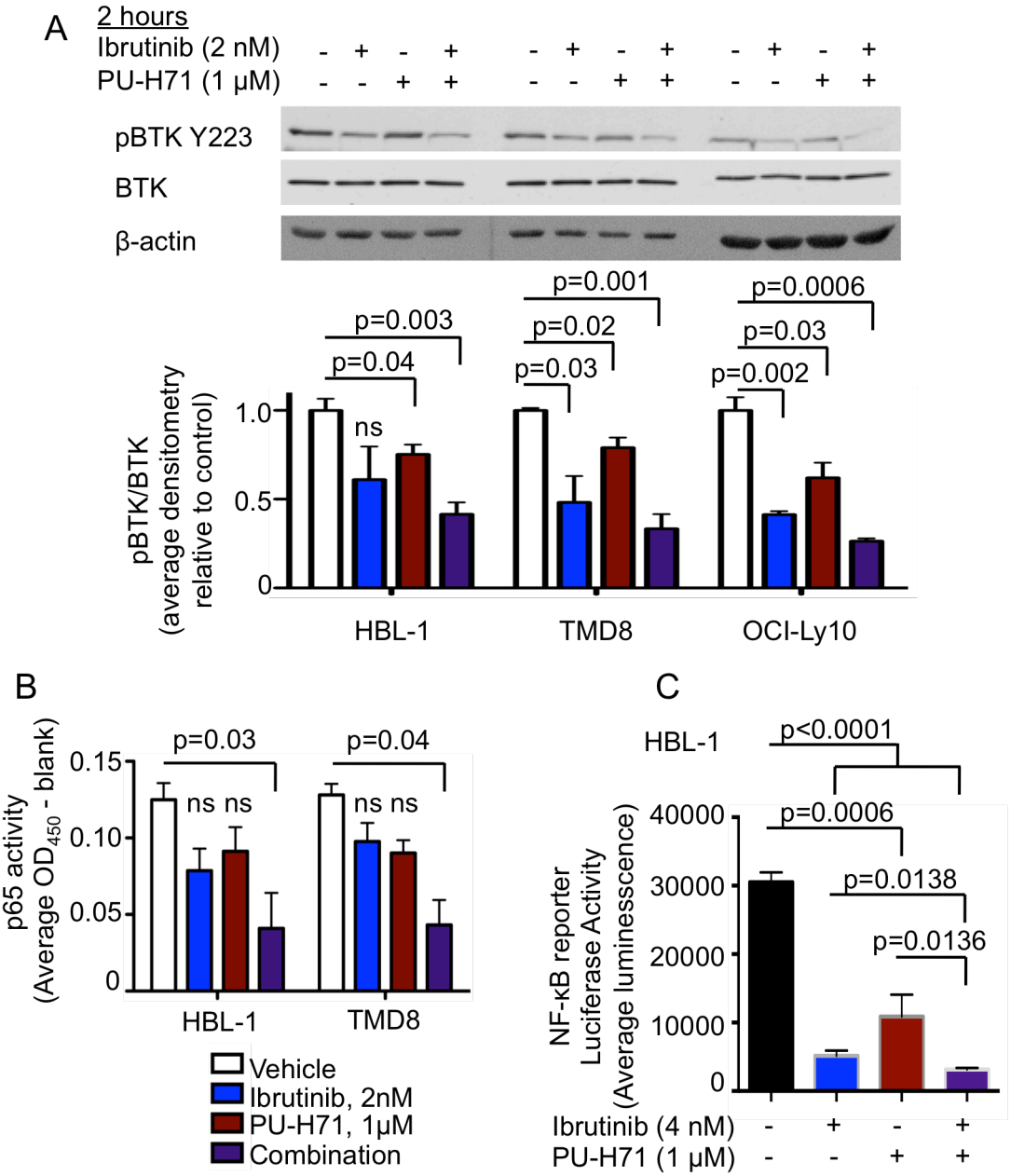

Figure 4.4 PU-H71 and ibrutinib combine to maximally suppress BCR signaling. (A) Lysates of HBL-1, TMD8 and OCI-Ly10 cells treated as indicated were subjected to immunoblotting. Relative protein abundance was quantified using densitometry. Data are presented as mean with SEM, unpaired t test. (B) Nuclear lysates of treated HBL-1 and TMD8 cells were probed for p65 DNA binding activity with TransAM ELISA. Data are presented as mean with SEM n=3, unpaired t test. (C) HBL-1 cells transfected with an NF-κB luciferase reporter were treated for 16h and assayed for luciferase activity. Data represents average with sem, unpaired t test.

prompting us to further investigate this combination treatment in ABC DLBCL *in vivo*. Concentrations of PU-H71 determined in this work to inhibit BCR signaling components (~1 μM) are readily achieved in the tumors of patients using well tolerated doses in our phase I studies (193). We established HBL-1 and TMD8 xenografts in non-obese diabetic/severe combined immunodeficiency (NOD-SCID) mice. After tumors reached an average of 100 mm^3 in volume, mice were randomized to receive vehicle, ibrutinib, PU-H71 or the combination. TMD8 and HBL-1 mice were treated daily with 12.5 mg/kg ibrutinib (ad libitum), 75 mg/kg PU-H71 (intraperitoneal injection) or the combination for 11-13 days (Figure 4.5A). As a single agent, ibrutinib did not significantly inhibit the growth of both TMD8 and HBL-1 xenograft models compared to vehicle. PU-H71 significantly reduced tumor growth in both TMD8 and HBL-1 xenografts as a single agent compared to vehicle ($p<0.0001$ and $p=0.03$, respectively). The PU-H71-ibrutinib combination suppressed TMD8 and HBL-1 xenograft growth significantly more than ibrutinib ($p<0.0001$) or PU-H71 alone ($p=0.0045$ and $p=0.008$, respectively, Figure 4.5B, C).

In order to determine in the combination effect observed *in vivo* was linked to more potent inhibition of BTK activity as was observed in cell lines, we established new HBL-1 and TMD8 xenografts in NOD-SCID mice (n=3/group) and administered a single dose of vehicle, ibrutinib, PU-H71 or the combination. Mice were sacrificed 24 hours after treatment, and tumors were harvested to assay for BTK activity by phospho-immunoblot (Figure 4.6A). In TMD8 xenografts, single doses of each drug had little effect on BTK phosphorylation. In marked contrast, the ibrutinib-PU-H71 combination

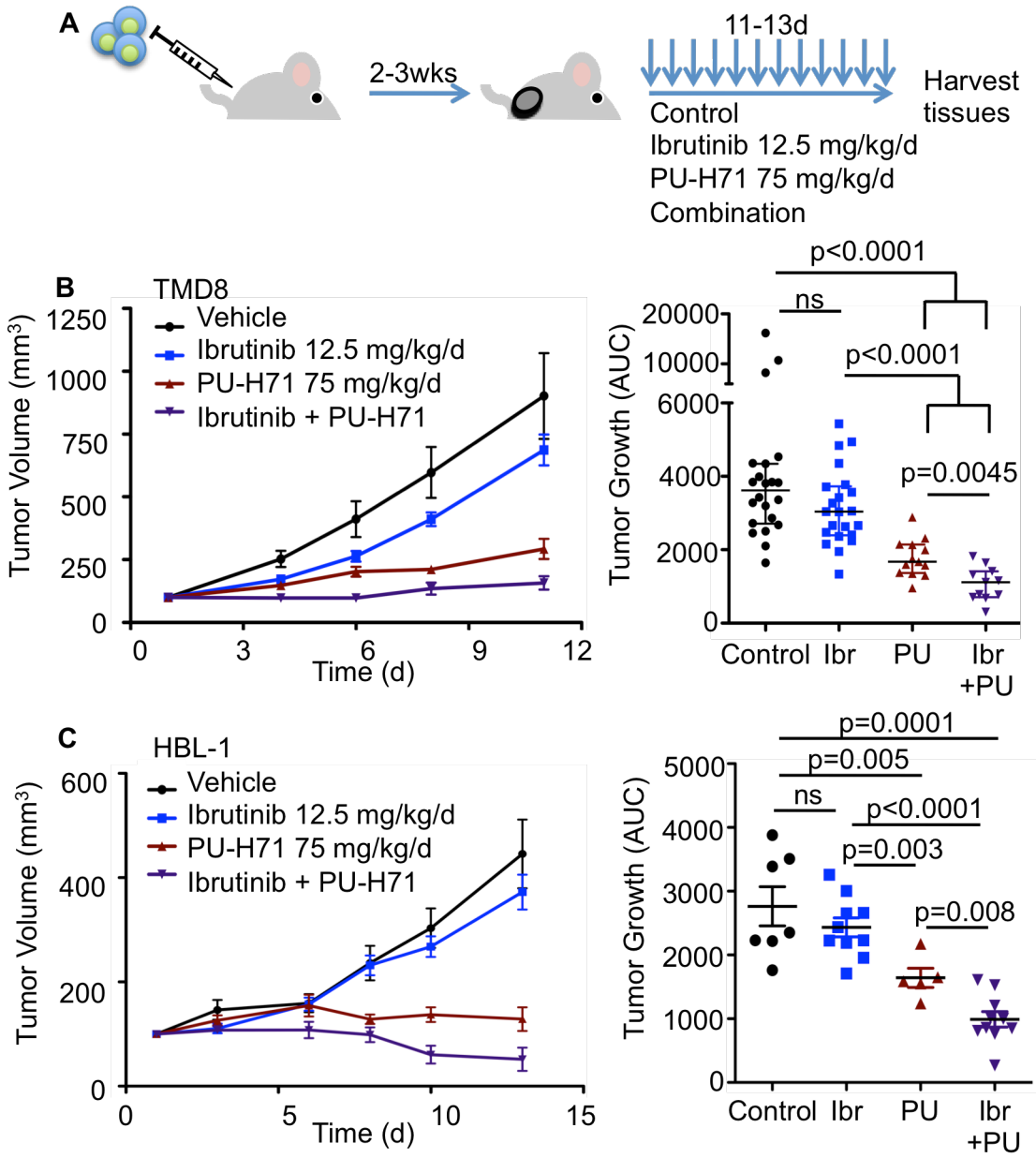

Figure 4.5 PU-H71 potentiates response to ibrutinib in ABC DLBCL in vivo. (A) NOD-SCID mice were subcutaneously injected with 10^6 HBL-1 or TMD8 cells in 1:1 matrigel:PBS. Tumors grew until palpable, and daily treatment began. (B and C) Left panels: Tumor growth plots of TM8 (B) and HBL-1 (C) xenografted mice treated with vehicle (saline, black circles), ibrutinib (12.5 mg/kg in chow, ad libitum, blue squares, Ibr), PU-H71 (75 mg/kg intraperitoneal injection, red triangles, PU) or the combination (purple triangles). Right panels: Growth of each tumor was measured as area under the curve. Average tumor growth is represented on the y-axis (tumor volume (mm^3)/time (days)). Mean ± SEM, Mann-Whitney U test.

significantly suppressed BTK phosphorylation (p=0.04). In HBL-1 xenografts, we observed modest inhibition of BTK in both single agent treatments, but these effects were not statistically significant. In animals treated with the ibrutinib-PU-H71 combination, however, we observed a 75% inhibition of active BTK in their HBL-1 ABC DLBCL tumors (p=0.039, Figure 4.6B) Collectively, the ibrutinib-PU-H71 combination therapy results in enhanced anti-lymphoma effect *in vivo*, and pharmacodynamics studies indicated that this was associated with more potent suppression of BTK activity.

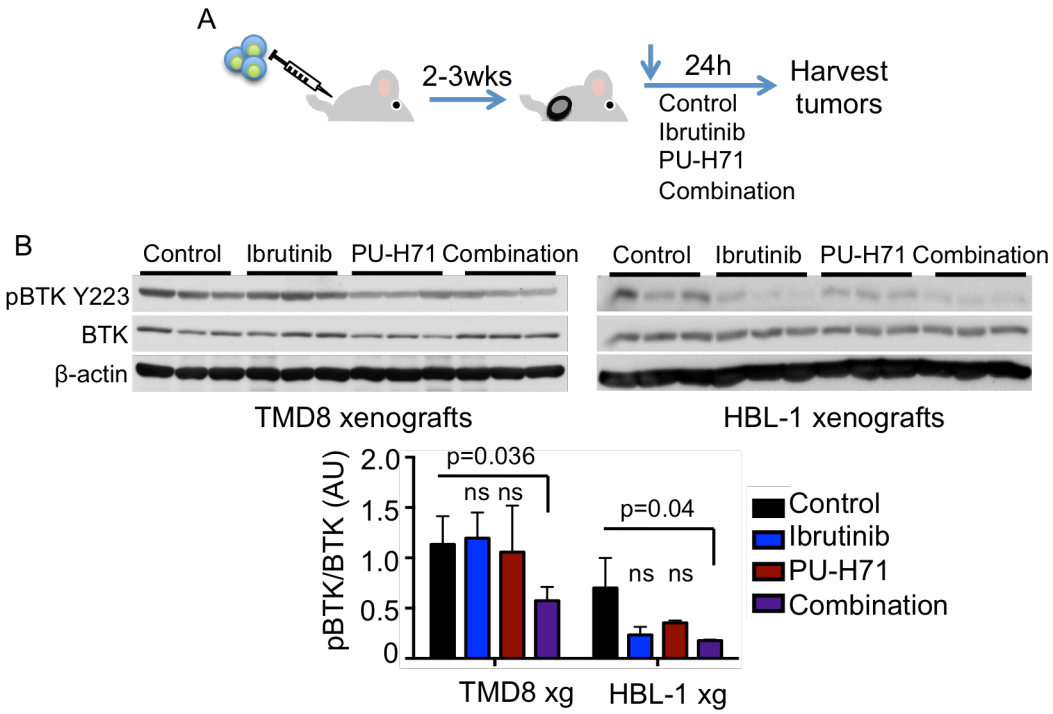

Figure 4.6 PU-H71 and ibrutinib combine to maximally suppress BTK signaling *in vivo*. (A) NOD-SCID mice were xenografted with TMD8 or HBL-1 cells as described and treated for 24 hours. (B) Lysates of tumors harvested from experiments in A were subjected to immunoblot with the antibodies indicated. The relative abundance of phosphor-BTK to total BTK was quantified using densitometry. Mean ± SEM, unpaired t-test.

In order to determine if the PU-H71-ibrutinib combination treatment is toxic, we treated C57 Black mice (n=3/group) for 12 days with vehicle, ibrutinib (12.5 mg/kg ad libitum), PU-H71 (75 mg/kg, intraperitoneal injection) or the combination. A second cohort of mice (n=3/group) were maintained without drug exposure for an additional 14 days to serve as a "washout" comparison group for any observed toxicities in the "treatment" group (Figure 4.7). Animals were weighed daily and sacrificed 24 hours after the last treatment followed by a comprehensive histopathology and molecular analysis.

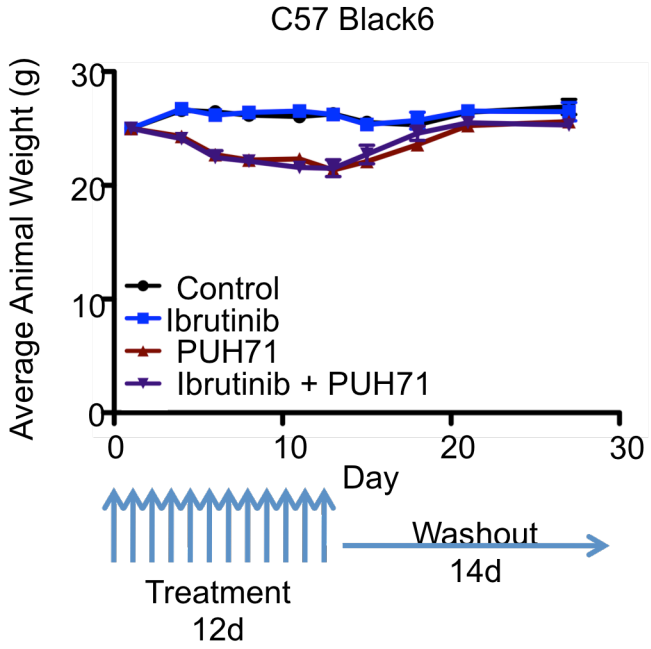

Figure 4.7 Ibrutinib and PU-H71 combination is non-toxic in mice. (A) C57 Black6 mice (n=6/group until day 13) were treated with vehicle, ibrutinib (12.5 mg/kg/d ad libitum), PU-H71 (75 mg/kg/d i.p.) or the combination for 12 days. Animals were weighed every other day. Half of each group (n=3) was sacrificed after treatment for microscopic analysis of organs and blood. The other half (n=3) continued untreated for two weeks to serve as a "washout" group. Animals were weighed every other day until sacrifice for organ and blood analysis.

Table 4.2 Ibrutinib and PU-H71 combination is non-toxic in mice. Blood from mice tested for ibrutinib-PU-H71 toxicity as in Supplementary Figure 2 was collected after 12 days of treatment (Toxicity) and in a second cohort after a 2 week washout period (Washout). Blood was analyzed for differential blood cell count and chemistry panel.

	Toxicity Day 13				Washout Day 27				
Test	**Control**	**Ibrutinib**	**PU-H71**	**Combination**	**Control**	**Ibrutinib**	**PU-H71**	**Combination**	**Reference**
WBC	6.87±2.09	7.78±3.36	4.67±1.82	5.17±0.87	8.17±3.36	6.77±0.76	6.64±3.01	7.12±0.37	6.4±2.5 K/uL
RBC	11.00±0.54	10.49±0.64	10±0.62	9.47±0.42	11.32±0.14	11.46±0.45	9.57±0.48	9.60±0.11	8.53±0.5 M/uL
Hemoglobin	16.03±0.74	15.5±0.53	14.4±0.79	14.33±0.61	16.67±0.25	16.67±0.50	14.63±0.31	14.55±0.07	14.5±1.1 g/dL
Platelets	878±17.35	491.67±138.60	562±229.1	681±230.12	713.67±299.95	612±369.78	1156±692.60	1385±31.11	799-1300 K/uL
Hematocrit	57.8±3.75	54.17±4.40	48.6±3.72	44.83±3.18	56.83±1.98	57.60±2.17	48.83±2.80	48.80±0.42	32-54 %
Neutrophils	1±0.89	0.98±0.97	0.77±0.23	1.54±0.92	1.51±1.81	1.64±1.05	1.04±0.22	1.31±0.28	0-1.8 K/uL
Lymphocytes	5.28±2.04	6.33±2.65	3.71±1.87	3.32±157	6.29±4.47	4.51±1.08	5.08±2.40	5.33±0.64	2.5-10 K/uL
Monocytes	0.35±0.19	0.34±0.15	0.11±0.04	0.22±0.13	0.28±0.33	0.44±0.35	0.31±0.31	0.25±0.00	0-0.2 K/uL
Eosinophils	0.23±0.22	0.12±0.04	0.07±0.07	0.08±0.05	0.08±0.02	0.16±0.01	0.18±0.07	0.24±0.01	0-0.5 K/uL
Basophils	0.01±0.00	0.007±0.006	0.01±0.00	0.02±0.01	0.01±0.00	0.01±0.01	0.02±0.02	0.01±0.01	0-0.4 K/uL
Albumin	4.35±0.07	3.13±0.12	2.7±0.17	3.15±0.64	3.23±0.06	3.87±0.06	3.3±0.61	3.1±0.26	2.5-3.9 g/dL
Total Protein	7.3±0.00	5.53±0.15	4.73±0.45	5.55±0.919	5.6±0.1	6.5±0.00	5.57±0.72	5.43±0.38	4.1-6.4 g/dL
Globulin	3.0±0.07	2.4±0.1	2.03±0.47	2.4±0.28	2.37±0.06	2.63±0.06	2.27±0.12	2.33±0.12	1.3-2.8 g/dL
Total Bilirubin	0.9±0.14	0.27±0.12	0.23±0.06	0.7±0.28	0.27±0.12	0.83±0.05	0.63±0.15	0.43±0.15	0-0.3 mg/dL
Creatinine	0.30±0.07	0.26±0.06	0.16±0.02	0.2±0.07	0.27±0.06	0.26±0.02	0.24±0.02	0.23±0.03	0.1-0.6 mg/dL
Cholesterol	246.5±3.54	111.33±16.01	155.5±23.33	159.5±58.69	95.67±8.74	154±13	117±27	97.67±15.63	70-100 mg/dL

Animals treated with PU-H71 lost a significant amount of weight compared to vehicle and ibrutinib treated animals, but this effect was reversed during the washout period (Figure 4.7). Further, there was no evidence of hematologic, renal or hepatic toxicity, as determined by blood counts, blood chemistry, and liver function testing (Table 4.2). No microscopic evidence of toxicity was observed in the intestines, kidneys, spleens, livers, lungs or hearts harvested from any of the mice. The bone marrow control and ibrutinib treated mice revealed no specific pathological findings, although there was evidence of hypocellularity in 1/3 PU-H71 only and 2/3 combined treatment mice. Bone marrow in all PU-H71 and combination treated mice in the washout group revealed normocellular bone marrow, demonstrating that the observed toxicity is reversible when drug is removed.

2.3 PU-H71 and ibrutinib combination yields enhanced killing of human non-GCB DLCL patient samples *ex vivo*.

Whereas lymphoma cell lines have been used extensively for pre-clinical studies, it is important to underline that these cells may not be fully representative of primary human tumors. We obtained viable primary non-GCB DLBCL specimens classified by Hans immunohistochemistry criteria (211). These patient specimens were plated on a feeder layer of irradiated HK cells and treated with vehicle, 2 nM ibrutinib, 1 μM PU-H71 or the combination for 48 hours. Cell viability was measured by flow cytometry scoring $CD20^+$ B cells for Annexin V and DAPI to determine their viability.

In patient sample 6128 the PU-H71-ibrutinib combination treatment produced significantly enhanced lymphoma-killing effect. In non-GCB DLBCL patient

sample 6938, the PU-H71-ibrutinib combination resulted in even more potent killing relative to each drug alone, although statistics could not be generated since there were insufficient cells to perform multiple replicates (Figure 4.8). In five other non-GCB DLBCL patient samples tested, we observed no response to ibrutinib as a single agent. Although these samples responded to PU-H71, the PU-H71-ibrutinib combination effect observed was equivalent with the effect of PU-H71 as a single agent (Figure 4.8). This result mirrors effects observed in cell lines and may be explained by mutational status of BCR proteins in these patient specimens. Collectively, the efficacy of the PU-H71-ibrutinib combination *in vitro*, *in vivo* and in human patient samples *ex vivo* supports the rationale for translation of this combination therapy in human patients.

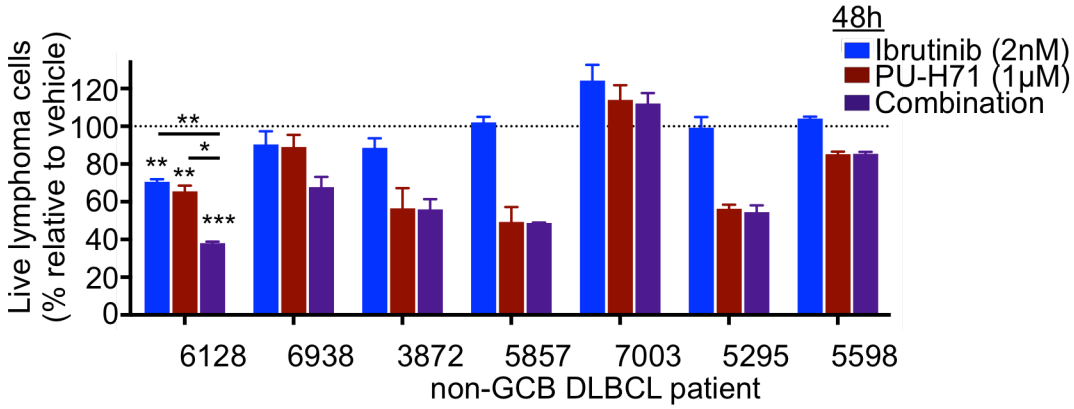

Figure 4.8 PU-H71 and ibrutinib combine to more powerfully kill primary non-GCB DLBCLs *ex vivo*. Human non-GCB DLBCL patient samples were cultured on an irradiated HK cell feeder layer. Cells were exposed to vehicle, ibrutinib (2nM every 24 hours, blue bar), PU-H71 (1μM, red bar) or the combination (purple bar) for 48 hours. Cell viability (represented as percentage of vehicle-treated cells) was measured using flow cytometry and is plotted on the y-axis. Live cells are defined as CD20+/CD3- cells that are Annexin V/DAPI double negative. Sample 6128 was tested in 2 biological replicates, unpaired t test. Other samples were tested in 2 technical replicates. Data are presented as mean with SEM.

3. Discussion

The BCR pathway is well appreciated as a therapeutic target in ABC DLBCLs. Targeting with selective inhibitors against BTK, SYK, PI3K, PKCβ or MALT1 can suppress the growth of ABC DLBCL cells. While potentially effective, the BCR pathway is not linear, but more of an interconnected network of signaling pathways. As a result, targeted therapies against single proteins may not globally suppress all aspects of BCR signaling. For example, a phase II clinical trial of ibrutinib monotherapy in ABC DLBCL patients revealed a 41% overall response rate (181). Moreover, single agent targeted therapies can give rise to resistance. In fact, acquired resistance to ibrutinib has been described in patients with somatic mutations in BTK that block inhibitor binding and in PLCγ2 that activate the pathway downstream of the drug (190, 191). Because of these challenges, single agent targeted therapies are unlikely to be curative in a molecularly heterogeneous disease such as ABC DLBCL. Indeed, a clinical trial of ibrutinib in combination with R-CHOP immunochemotherapy achieved 100% ORR with 60% CR in a clinical study of ABC DLBCL patients (189). However, because R-CHOP treatment is associated with toxicities, immune suppression and secondary malignancies, improved regimens are needed for these patients.

Based on this and the data herein, we propose the clinical translation of regimens that combine the BCR “attenuator” effects of PU-H71 discovered through our pharmacoproteomics approach and described in chapter three, with the more punctual and incisive specific targeted approach represented by ibrutinib and other similar agents. Indeed, the combination of PU-H71 with ibrutinib showed robust synergy in cell lines, and cooperative effect in animal

models and primary human DLBCL cells. In further confirmation of our data, a recent high throughput combinatorial screening study identified Hsp90 inhibitors as one of several classes of drugs that cooperate with ibrutinib to kill ABC DLBCLs (192).

Synergy between PU-H71 and ibrutinib was associated with more potent suppression of BTK and NF-κB activation. Why exactly the combination of PU-H71 with ibrutinib yielded the most potent synergy in inhibiting ABC DLBCL growth remains unclear and could be due to the potency of ibrutinib, the dependence of ABC DLBCLs on BTK, the dependence of BTK on teHsp90 in ABC DLBCLs or some combination of these reasons. Naturally, suppression of other teHsp90 client actions could also contribute to these synergistic effects, such as its effects on the BCL6 transcription factor protein (38). If anything, this adds to the potential appeal of using PU-H71 to anchor combinatorial therapy for DLBCL. By more greatly inhibiting signaling pathways critically required for ABC DLBCL survival, this combination therapy can not only increase the efficacy of treatment, but also potentially minimize the occurrence of resistance through the inhibition of compensatory proteins or pathways. In fact, Hsp90 inhibition has been shown to overcome resistance to a number of targeted therapies. Perhaps if given as a frontline treatment, this combination regimen could decrease the emergence of resistance later on.

An important finding in this work is the lack of toxicity observed in animals exposed to the combination of PU-H71 and ibrutinib. This suggests that this combination would be well tolerated in humans. Moreover, because PU-H71 selectively inhibits the pool of teHsp90 that maintains an oncogenic

phenotype, we expect that targeted therapies combined with PU-H71 will exhibit less toxicity than conventional chemotherapy in patients. PU-H71 is currently completing phase I testing in humans and will be available for phase II studies as a single agent or for rational combination therapy. We expect such studies to yield improved efficacy in humans compared to single BCR agent targeted therapy.

In many of the human ABC DLBCL patient samples tested *ex vivo*, we observed no response to ibrutinib, and, as we observed in viability assays using cell lines that do not respond to ibrutinib as a single agent, the combination effect is no greater than that of PU-H71 alone. These patient samples may harbor mutations in CARD11 or A20 downstream of BTK, preventing their response to ibrutinib, or may require a higher dose to induce some effect. For example, HBL-1 and TMD8 cell lines both respond to ibrutinib, but with a 10-fold difference in GI_{50} values (4 nM and 0.4 nM, respectively). Information about the mutational status of these patients and further testing with other doses of ibrutinib may yield further insights about their response profiles. This information may also provide valuable information for patient stratification for PU-H71-ibrutinib combination therapy.

While ABC DLBCL is the more aggressive subtype with poorer prognosis and greater need for novel therapeutic regimens, some of the combination treatments tested herein yielded combinatorial effect in ABC and GCB DLBCLs. Information about patient mutational status may prove useful in patient stratification of the PU-H71-ibrutinib combination and other PU-H71 anchored combination therapies for DLBCL patients from both subtypes.

Taken together, the efficacy of the PU-H71-ibrutinib combination *in vitro*, *in vivo* and in human patient samples *ex vivo* provides the rationale for translation of this combination therapy in human patients. Other combinatorial regimens anchored with PU-H71 may provide better treatment options for all DLBCL patients.

4. Materials and methods

Cell lines and reagents

The DLBCL cell lines OCI-Ly1 and OCI-Ly7 were grown in Iscove's Modified Dulbecco's Medium (IMDM) containing 10% FBS and supplemented with peniciliin and streptomycin. OCI-Ly10 was grown in IMDM with 20% FBS and penicillin and streptomycin. The DLBCL cell lines HBL-1 and TMD8 were grown in medium containing 90% RPMI and 10% FBS supplemented with L-glutamine, HEPES and penicillin and streptomycin. OCI-Ly3 was grown in RPMI with 20% FBS supplemented with L-glutamine, HEPES and penicillin and streptomycin. PU-H71 was synthesized as previously reported (58). Ibrutinib drug and chow was provided by Pharmacyclics. R406 and sotrastaurin were purchased from Selleck Chemicals. MI-2 was purchased from AMRI. BKM120 was a gift of the Cantley lab. Antibodies to phospho-BTK Y223, and BTK were purchased from Cell Signaling Technology. Antibody to β-actin (clone AC-15) was purchased from Sigma Aldrich.

Cell lysis for immunoblot

Cells were treated at a concentration of 2 x 10^6/mL, harvested, washed with PBS, and resuspended in lysis buffer (10 mM HEPES-KOH pH7.9, 1.5 mM $MgCl_2$, 10 mM KCl, freshly prepared 1.5 mM Na_2MoO_4, 1% Triton-X, 0.5 mM

PMSF, protease and phosphatase inhibitors). Lysates were mixed with 5X SDS loading buffer (1X final) and resolved according to standard immunoblotting procedure.

Cell viability assays and synergy experiments

DLBCL cell lines were played in 384-well white-wall plates at concentrations sufficient to keep untreated cells in exponential growth during the time of drug exposure (50,000/mL for 96 hour exposure, 100,000/mL for 48 hour exposure). Cells were treated with 6 doses of each drug of combination in technical triplicates. For combination treatments, cells were exposed to a dose curve of each drug or their combination in constant ratio. After treatment, a standard curve was made using vehicle treated cells. Cell viability was determined by an ATP luminescent method (CellTiter-Glo, Promega). Luminescence was measured with the Synergy4 microplate reader (BioTek). Cell viability of drug-treated cells was normalized to vehicle treated controls. Compusyn software (Biosoft) was used to plot dose effect curves and calculate combination index values.

NF-κB luciferase reporter assays

In HBL-1, 1 μg of $(NF\text{-}\kappa B)_5$-Luc2CP-pGL4 per 5 x 10^6 cells were transfected using nucleofection (Amaxa, Lonza). Eight hours after transfection, cells were plated at 2 x 10^6 cells/mL and treated with vehicle, 4 nM ibrutinib, 1 μM PU-H71 or the combination for 16 hours at 37°C. Cells were harvested and submitted to Dual-Glow luciferase assays following manufacturer's protocol (Promega). Briefly, cells were lysed in 20 μL 1X passive lysis buffer by rocking at room temperature for 20 minutes. 5μL of each sample was added to a

white-walled 96 well plate and 50 μL of Luciferase Assay buffer was added before luminescence was read with the Synergy4 plate reader (BioTek).

NF-κB ELISA

HBL-1 and TMD8 cells were treated with vehicle, 2 nM ibrutinib, 1 μM PU-H71 or the combination for 24 hours, then harvested and washed in ice-cold PBS. To extract nuclear lysates, cell pellets were resuspended in 1 mL ice-cold hypotonic buffer (20 mM HEPES pH 7.5, 5 mM NaF, 10 μM Na_2MoO_4, 0.1 mM EDTA) and incubated on ice for 15 minute until the addition of 50 μL 10% NP-40. Tubes were vortexed vigorously for 10 seconds. Cells were checked for lysis of the cell membrane under the microscope. Homogenates were centrifuged for 30 seconds at 4°C. Supernatants (cytoplasmic fractions) were removed and saved at -80°C. Pellet were resuspended in 50 μL Complete Lysis Buffer (prepared according to manufacturer's instructions) and rocked gently on ice for 30 minutes on a shaking platform. Tubes were centrifuged for 10 minutes at 14,000 x g at 4°C. Supernatants (nuclear extracts) were saved and measured for protein concentration using the DC Biorad Assay.

Following extraction, 30 μL of Complete Binding Buffer and 5 μg of nuclear extract diluted in 20 μL of Complete Lysis Buffer was added to each well. Complete Lysis Buffer was used as a negative control and 5 μg of provided Raji nuclear extract was used as a positive control. Samples were tested in technical duplicate. Nuclear extracts bound to probes for one hour at room temperature with shaking, and then wells were washed three times with wash buffer. p65 primary antibody bound to extracts in wells for one hour at room temperature followed by three washes with wash buffer. Wells were incubated

with secondary antibody for one hour at room temperature and then washed three times with wash buffer. To develop, 100 μL of developing solution was added to all wells being used and incubated for 2 minutes at room temperature protected from direct light. Then 100 μL of stop solution was added and absorbance was read at 450 nM with the Synergy4 plate reader within 5 minutes (BioTek).

Xenografts

Eight week old NOD-SCID mice were injected subcutanesouly with 10^6 cells in 1:1 PBS:matrigel. Tumors grew until palpable (2-3 wekks) and then treatment began. Mice were injected intraperitoneally with vehicle or 75 mg/kg PU-H71 daily. Ibrutinib was administered via chow at a dose of 12.5 mg/kg/d ad libitum. Control and PU-H71 treated mice were given vehicle chow. Tumors were measured with digital calipers and animals were weighed every other day. Animals were sacrificed after treatment and tumors were weighed and harvested for molecular investigation.

Toxicity

Eight-week old C57 Black 6 mice were treated with vehicle, ibrutinib (12.5 mg/kg/d ad libitum), PU-H71 (75 mg/kg/d i.p. injection) or PU-H71-ibrutinib combination for 12 days (n=6/group). Animals were weighed every other day. After 12 days, 3 animals per group were sacrificed and organs (intestine, spleen, kidney, liver, lung, heart and bone marrow) were harvested. Tissues were fixed in 4% formalin and then washed in 70% ethanol and sent for sectioning and staining with H&E. Stained tissues were microscopically analyzed by specialized pathologists. Blood was also collected at the time of

sacrifice for complete blood count test and chemical analysis. The second half of each group continued without drug for 14 days to serve as a "washout" group. After 14 days, these animals were sacrificed and their organs and blood subjected to the same investigations.

Primary cell treatment

We obtained deidentified human tissues in accordance with and approval from the Institutional Review Board of the New York Presbyterian Hospital. Samples were classified as non-GCB DLBCL using Hans classification (immunohistochemistry for BCL6, CD10 and MUM1 with 30% cutoff for positivity). Single-cell suspensions from lymph node biopsies were thawed and resuspended in Advanced RPMI supplemented with 20% human serum, Glutamax (2X), glycine (5 mM) and penicillin and streptomycin. Cell number and viability was determined by counting with Trypan blue. Irradiated HK cells (2000 rad) in DMEM supplemented with 10% FBS and penicillin and streptomycin were adhered to tissue culture plates at 37°C. Media was aspirated and patient samples were plated on the HK feeder layer. Samples were exposed to vehicle, ibrutinib (2 nM, daily), PU-H71 (1 μM) or the combination for 48 hours, and then stained with FITC-conjugated anti-CD20, PE-Cy7-conjugated anti-CD3 and APC-conjugated anti-Annexin V anti-human antibodies (BD Biosciences). DAPI was used for the exclusion of dead cells. Data was acquired on a MacsQuant flow cytometer (Miltenyi Biotec) and analyzed using FlowJo software package (TreeStar). $CD20^+/CD3^-$ cells that were Annexin V/DAPI double negative were considered live.

Study Approval

Deidentified patient tissues were obtained in accordance with and approval from the Institutional Review Board (IRB) of the Weill Cornell Medical College. The Research Animal Resource Center (RARC) of the Weill Cornell Medical College approved all mouse procedures.

Statistical Analysis

Two-tailed unpaired t test was used unless otherwise stated. Specifically, two-tailed Mann-Whitney U test was used for xenografts growth experiment analysis. All statistical analyses were carried out using Prism software (Graphpad).

CHAPTER FIVE

Additional approaches to Identify combinatorial treatments for ABC DLBCL

1. Introduction

Intracellular signaling pathways drive cell decisions including proliferation, growth and survival. The amplitude and duration of pathway activation is precisely controlled by complex regulatory mechanisms. Because they regulate such important aspects of cell fate, these pathways are often hijacked by activating mutations in signaling activators or deletions of signaling repressors in tumor cells attempting to achieve immortality. Targeted therapies against these transformed proteins and pathways involve the use of small molecule inhibitors of these corrupted signaling effectors to induce apoptosis in tumor cells. The improved precision of targeted therapies over conventional chemotherapy is expected to induce increased efficacy and decreased toxicity in patients..

However, clinical translation of targeted therapies faces several challenges. Prolonged exposure to single drugs can result in acquired drug resistance, and targeted therapies administered as single agents often produce low response rates. The modest efficacy of single agent targeted therapy results in part from the complexity of cellular signaling. Most signaling pathways do not exist in a vacuum, but rather interact with numerous others to form larger signaling networks with pathway crosstalk and compensatory circuits that can allow tumors to bypass single nodes of inhibition. Moreover, many tumors are

molecularly and cellularly heterogeneous. Therefore, it is widely accepted that single agent therapy is unlikely to be curative in cancer.

By simultaneously inhibiting multiple nodes within a broader signaling network, therapies combining multiple inhibitors can completely disable oncogenic signaling and induce more potent and durable responses. The identification of combinations of two or more drugs that cooperate to extinguish oncogenic signaling pathways and networks is critical to improve treatment options for cancer patients. The high complexity of signaling networks and available inhibitors precludes merely guessing which drug combinations will elicit an enhanced combined effect. In this work, we have described a pharmacoproteomic method using teHsp90 inhibitors as bait to identify client proteins as potential partners for therapeutic synergy. In this chapter, we describe additional methods to identify combination treatments using ABC DLBCL as a model system, computational and hypothesis-driven.

ABC DLBCL is characterized by chronic activation of the BCR signaling pathway. These cells are addicted to constitutive activation of survival signals in this pathway including that of NF-κB activation. Many small molecule inhibitors of this pathway have been developed and result in killing of ABC DLBCLs *in vitro* and *in vivo* (140, 150, 164, 165). However, in human patients, these targeted therapies evoke limited responses most likely because of the inherent complexity of the BCR signaling network. Combination therapies that target multiple nodes of the BCR signaling network may improve patient responses. Rather than large, costly experimental screens, an accurate *in silico* model of BCR signaling in ABC DLBCLs may serve as a computational

platform in which to test hundreds of combinations for efficacy. This model may also illuminate combinations that hypothesis-driven experiments would not immediately consider as actionable.

Hypothesis-driven experiments are another approach to identify effective combination therapies for ABC DLBCL. The availability of specific, potent inhibitors of different inhibitors of the BCR pathway is truly an embarrassment of riches. Further, numerous ABC DLBCL cell lines are well characterized for the mutational status of their BCR pathway proteins. Armed with these tools, one can make educated guesses about which agents might more effectively shut down BCR signaling by disrupting known redundancies and feedback loops within the pathway.

In this chapter we present data of different combination treatments for ABC DLBCL predicted by an *in silico* model of BCR signaling and through the hypothesis-driven rational prediction. We observed differential combination growth arrest effects depending on which nodes of the BCR signaling network were concomitantly inhibited and discuss the relevance for future rational design of therapeutic combinations.

2. Results

2.1 A virtual B cell lymphoma model to predict effective combination therapy for ABC DLBCL

A detailed kinetic model of the BCR signaling network parameterized by biochemistry assays and protein concentration quantification was constructed by our collaborator, Wei Du (unpublished). The BCR signaling network was

curated by gathering experimentally validated protein-protein interactions from the literature. The resultant network includes three major signaling pathways downstream of the BCR, namely NF-κB, PI3K/AKT and RAF/RAS/ERK. The model was then parameterized using protein binding affinity and enzyme reaction kinetics measured by published *in vitro* biochemistry assays and cellular protein concentrations.

Next, a tumor growth model was constructed in order to simulate the effect of various small molecule inhibitors of BCR signaling on ABC DLBCL viability and to compare simulation results with published combinatorial drug response data. The model was constructed in the ABC DLBCL cell line TMD8 because of the extensive drug combinatorial data available for it. Published drug-effect viability data from experiments of ibrutinib combined with inhibitors of NF-κB, MEK or AKT was used to parameterize the growth model (192).

Using this model, Du predicted synergistic growth inhibition effect across all possible target pairs. The BCR protein pair predicted to show the most synergistic growth inhibition effect when simultaneously inhibited was SYK and PI3K. To test this *in vitro*, we used three ABC DLBCL cell lines – HBL-1, TMD8 and OCI-Ly10 – exposed to PRT062607 (a SYK inhibitor), a panel of PI3K inhibitors BKM120 (pan-PI3K), BYL719 (PI3Kα), CAL101 (idelalisib, PI3Kδ) and GDC0941 (PI3Kα/δ) or SYK in combination with each of these inhibitors and assayed for cell viability. We observed additive and less than additive growth inhibition effect in most of these combinations (Figure 5.1A), matching the model's prediction of weakly synergistic combination effect (~0.86). The pair predicted to be the next most synergistic was BTK-PI3K; this

therapeutic combination has been shown to exhibit synergistic growth inhibition of ABC DLBCLs (192).

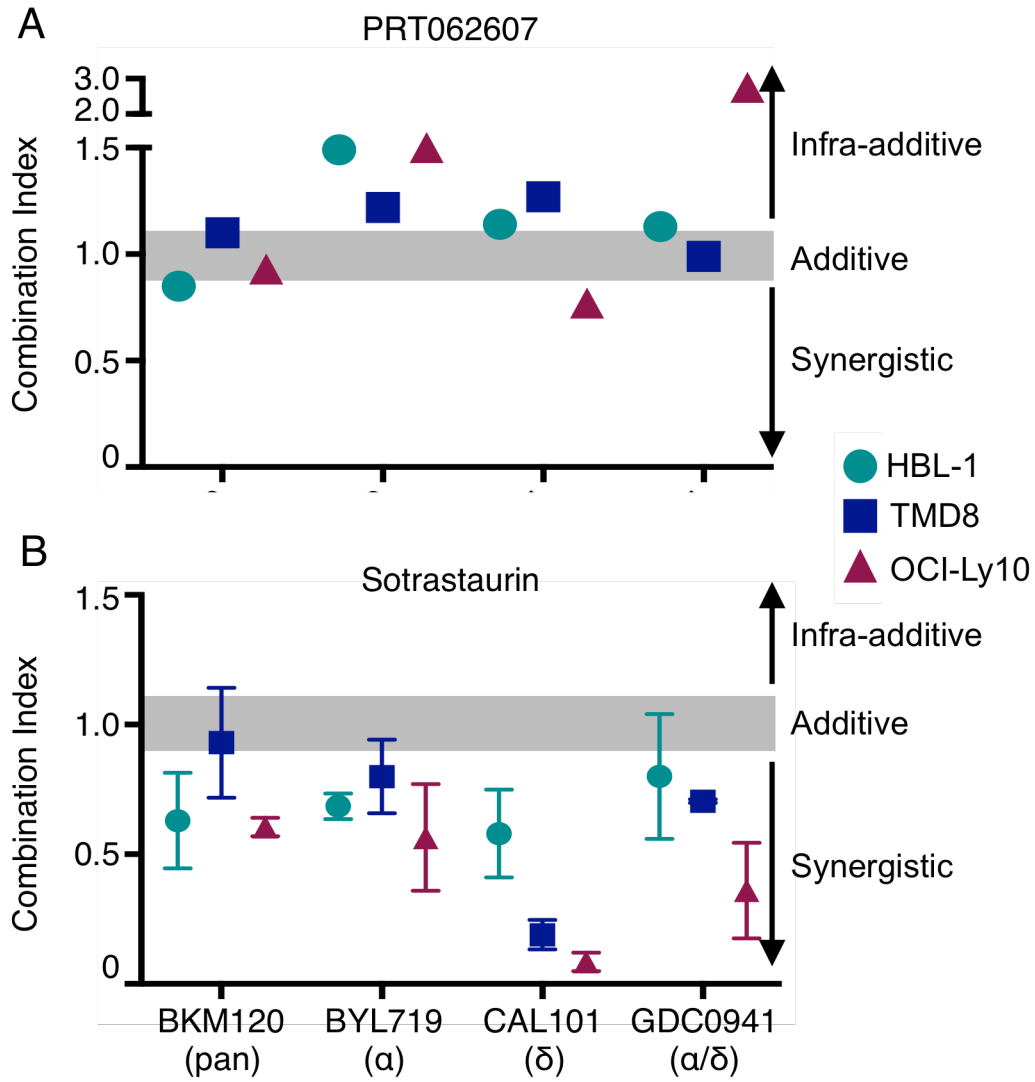

Figure 5.1 SYK and PKCβ inhibitors combine with PI3K inhibition to arrest growth of ABC DLBCL cell lines. HBL-1, TMD8 and OCI-Ly10 cells were exposed to a SYK inhibitor (A), a PKCβ inhibitor (B), a panel of PI3K inhibitors or the combination and assayed for viability. Combination index values were calculated and plotted here. TMD8, OCI-Ly10 (A) GI_{75}, (B)GI_{90} HBL-1 (A) GI_{75} (B)GI_{50} (B) n=2, average ± SEM.

Next, we investigated the PKCβ-PI3K pair, predicted to be the fourth most synergistic possible combination. To test the combination effect, we exposed HBL-1, TMD8 and Ly10 cells to sotrastaurin, a panel of PI3K inhibitors and the combinations and assayed for viability. Nearly all of these combinations proved to be synergistic with combination index values between 0.5 and 0.8 for BKM120, 0.4 and 0.7 for BYL719 and 0.5 and 1.0 for GDC0941. STN combined with CAL101 produced remarkable synergy in TMD8 and OCI-Ly10 cells (CI GI_{90} 0.15, 0.11 respectively, Figure 5.1B) far surpassing the model's predictions (CI ~0.88), and suggesting that with more modifications the *in silico* model may be a very useful tool in identifying effective combination treatments for ABC DLBCL.

2.2 Hypothesis-driven combination therapies with MALT1 inhibition for ABC DLBCL

Recently, our lab developed MI-2, a first in class MALT1 inhibitor, and demonstrated that it selectively kills ABC DLBCL cells *in vitro*, *in vivo* and human patient samples *ex vivo* (165). Because single agents are unlikely to be curative in this molecularly heterogeneous disease, we wondered if combining MI-2 with other BCR pathway inhibitors might induce greater suppression of BCR signaling, leading to additive or synergistic killing of ABC DLBCLs. To test this hypothesis we exposed ABC DLBCL cells to MI-2, BCR pathway inhibitors, or the combination and assayed for viability. We observed additive and weakly synergistic combination effect in these experiments (Figure 5.2) In other experiments combining MI-2 with various PI3K inhibitors in these cell lines, we have observed a more synergistic effect (CI GI_{75} between 0.15 and 0.71). MI-2 combined with the MEK inhibitor selumetinib is also highly

synergistic in these cell lines (CI GI_{75} between 0.3 and 0.4). Other BCR pathway targeted therapies may combine with MI-2 to reveal more effective combinatorial growth inhibition.

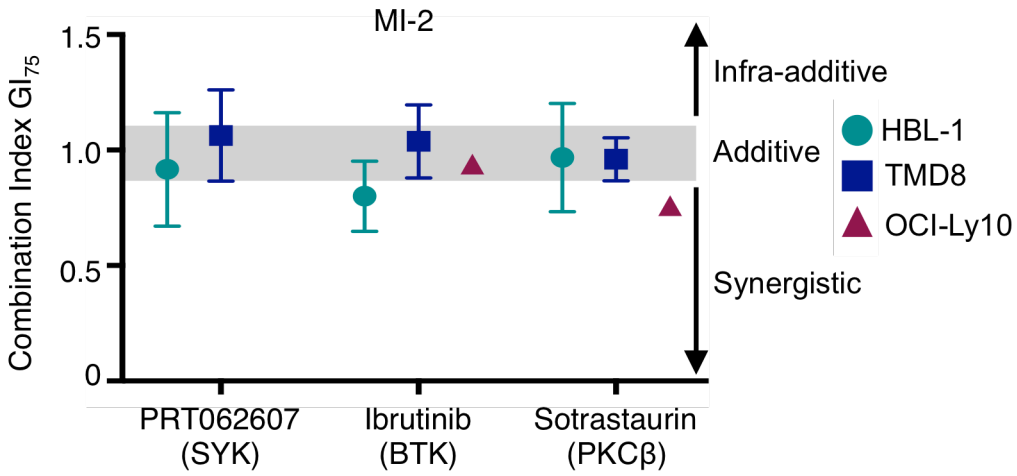

Figure 5.2 MI-2 combines with BCR pathway inhibitors to inhibit ABC DLBCL growth. HBL-1, TMD8 and OCI-Ly10 ABC DLBCL cells were exposed to MI-2, BCR pathway inhibitors, or the combination and assayed for viability. Combination index values were calculated and are plotted here as average ±

3. Discussion

An accurate computational model of BCR signaling that reflects tumor growth and inhibition in the presence of different pathway inhibitors would be of great use in predicting combination therapies for ABC DLBCL. Such a model would provide broad applicability, as cellular testing may be limited to cell line tested and not translatable to highly variable patient tumors. Moreover, thousands of experiments can be performed quickly and affordably *in silico*. *In vitro* experiments of combined SYK-PI3K inhibition resulted in additive growth arrest effect, matching the model's prediction. The PKCβ-PI3K target pair was predicted to have additive growth inhibition effect, but when tested *in vitro* showed astonishingly synergistic growth inhibition. Limitations of the

computational model such including LYN as only a positive regulator of BCR signaling may need to be addressed before the model can accurately predict protein pairs for combination therapy.

While *in vitro* experimental data did not validate the *in silico* predictions, it did reveal a very highly synergistic protein pair for therapeutic combination – PKCβ and PI3K. Of note, combined inhibition of MI-2 and PI3-K also produces highly synergistic growth arrest effects in ABC DLBCL cells. The synergistic effect of combined BTK and PI3K inhibition has also been demonstrated (192). Each of these therapeutic combinations includes inhibition of PI3K and a protein of the canonical BCR signaling pathway – PKCβ, BTK or MALT1. Combined PI3K-IKK inhibition will likely induce synergistic growth arrest in these cells as well. In effect, these treatments achieve inhibition of two signaling branches within the larger BCR signaling network. This effect is echoed in MI-2-selumetinib treatments. By contrast, hitting the same pathway twice – i.e. MI-2 combined with R406, ibrutinib or sotrastaurin – elicits additive growth inhibition effect. It should be mentioned that SYK-PI3K dual inhibition blocks multiple branches while achieving additive growth inhibition effect. This may be due to the selectivity and potency of the inhibitors.

In this work we demonstrated that the PU-H71-ibrutinib therapeutic combination results in maximal inhibition of BTK signaling propagated downstream through NF-κB activity. We also showed that PU-H71 attenuates kinase function of ERK and AKT, perhaps the prototypical teHsp90 client. The basis of PU-H71 synergy with ibrutinib compared to additivity with other BCR pathway inhibitors may be due to the potency and specificity of the inhibitors

used. However, the added inhibition of the PI3K and ERK lateral pathways within the BCR signaling network by PU-H71 undoubtedly contributes to the marked synergy of the PU-H71-ibrutinib combination treatment in ABC DLBCL. Taken together, these experiments show that dual inhibition of a signaling pathway results in additive growth inhibition, but inhibition of multiple branches within a signaling network is required for synergistic growth arrest.

4. Materials and methods

Cell lines and reagents

The DLBCL cell lines HBL-1 and TMD8 were grown in medium containing 90% RPMI and 10% FBS supplemented with L-glutamine, HEPES and penicillin and streptomycin. OCI-Ly10 was grown in IMDM with 20% FBS and penicillin and streptomycin. Ibrutinib was provided by Pharmacyclics. PRT062607, CAL101, and sotrastaurin were purchased from Selleck Chemicals. MI-2 was purchased from AMRI. BYL719, BKM120 and GDC0941 were gifts of the Cantley lab.

Cell viability assays and synergy experiments

DLBCL cell lines were played in 384-well white-wall plates at concentrations sufficient to keep untreated cells in exponential growth during the time of drug exposure. Cells were treated with 6 doses of each drug of combination in technical triplicates. For combination treatments, cells were exposed to a dose curve of each drug or their combination in constant ratio. After treatment, a standard curve was made using vehicle treated cells. Cell viability was determined by an ATP luminescent method (CellTiter-Glo, Promega). Luminescence was measured with the Synergy4 microplate reader (BioTek).

Cell viability of drug-treated cells was normalized to vehicle treated controls. Compusyn software (Biosoft) was used to plot dose effect curves and calculate combination index values.

CHAPTER SIX

References

1. Neckers L. Heat shock protein 90: the cancer chaperone. *Journal of biosciences.* 2007;32(3):517-30.

2. Hartl FU, Bracher A, and Hayer-Hartl M. Molecular chaperones in protein folding and proteostasis. *Nature.* 2011;475(7356):324-32.

3. Queitsch C, Sangster TA, and Lindquist S. Hsp90 as a capacitor of phenotypic variation. *Nature.* 2002;417(6889):618-24.

4. Rutherford SL, and Lindquist S. Hsp90 as a capacitor for morphological evolution. *Nature.* 1998;396(6709):336-42.

5. Hanahan D, and Weinberg RA. The hallmarks of cancer. *Cell.* 2000;100(1):57-70.

6. Zhang H, and Burrows F. Targeting multiple signal transduction pathways through inhibition of Hsp90. *Journal of molecular medicine.* 2004;82(8):488-99.

7. Neckers L. Hsp90 inhibitors as novel cancer chemotherapeutic agents. *Trends in molecular medicine.* 2002;8(4 Suppl):S55-61.

8. Whitesell L, and Lindquist SL. HSP90 and the chaperoning of cancer. *Nature reviews Cancer.* 2005;5(10):761-72.

9. Neckers L, Schulte TW, and Mimnaugh E. Geldanamycin as a potential anti-cancer agent: its molecular target and biochemical activity. *Investigational new drugs.* 1999;17(4):361-73.

10. Schulte TW, and Neckers LM. The benzoquinone ansamycin 17-allylamino-17-demethoxygeldanamycin binds to HSP90 and shares important biologic activities with geldanamycin. *Cancer chemotherapy and pharmacology.* 1998;42(4):273-9.

11. Smith V, Sausville EA, Camalier RF, Fiebig HH, and Burger AM. Comparison of 17-dimethylaminoethylamino-17-demethoxy-geldanamycin (17DMAG) and 17-allylamino-17-demethoxygeldanamycin (17AAG) in vitro: effects on Hsp90 and client

proteins in melanoma models. *Cancer chemotherapy and pharmacology.* 2005;56(2):126-37.

12. Soga S, Shiotsu Y, Akinaga S, and Sharma SV. Development of radicicol analogues. *Current cancer drug targets.* 2003;3(5):359-69.

13. Yamamoto K, Garbaccio RM, Stachel SJ, Solit DB, Chiosis G, Rosen N, and Danishefsky SJ. Total synthesis as a resource in the discovery of potentially valuable antitumor agents: cycloproparadicicol. *Angewandte Chemie.* 2003;42(11):1280-4.

14. Moulin E, Zoete V, Barluenga S, Karplus M, and Winssinger N. Design, synthesis, and biological evaluation of HSP90 inhibitors based on conformational analysis of radicicol and its analogues. *Journal of the American Chemical Society.* 2005;127(19):6999-7004.

15. Chiosis G, Timaul MN, Lucas B, Munster PN, Zheng FF, Sepp-Lorenzino L, and Rosen N. A small molecule designed to bind to the adenine nucleotide pocket of Hsp90 causes Her2 degradation and the growth arrest and differentiation of breast cancer cells. *Chemistry & biology.* 2001;8(3):289-99.

16. Cheung KM, Matthews TP, James K, Rowlands MG, Boxall KJ, Sharp SY, Maloney A, Roe SM, Prodromou C, Pearl LH, et al. The identification, synthesis, protein crystal structure and in vitro biochemical evaluation of a new 3,4-diarylpyrazole class of Hsp90 inhibitors. *Bioorganic & medicinal chemistry letters.* 2005;15(14):3338-43.

17. Marcu MG, Schulte TW, and Neckers L. Novobiocin and related coumarins and depletion of heat shock protein 90-dependent signaling proteins. *Journal of the National Cancer Institute.* 2000;92(3):242-8.

18. Soti C, Racz A, and Csermely P. A Nucleotide-dependent molecular switch controls ATP binding at the C-terminal domain of Hsp90. N-terminal nucleotide binding unmasks a C-terminal binding pocket. *The Journal of biological chemistry.* 2002;277(9):7066-75.

19. Plescia J, Salz W, Xia F, Pennati M, Zaffaroni N, Daidone MG, Meli M, Dohi T, Fortugno P, Nefedova Y, et al. Rational design of shepherdin, a novel anticancer agent. *Cancer Cell.* 2005;7(5):457-68.

20. Yu X, Guo ZS, Marcu MG, Neckers L, Nguyen DM, Chen GA, and Schrump DS. Modulation of p53, ErbB1, ErbB2, and Raf-1 expression in lung cancer cells by depsipeptide FR901228. *Journal of the National Cancer Institute.* 2002;94(7):504-13.

21. George P, Bali P, Annavarapu S, Scuto A, Fiskus W, Guo F, Sigua C, Sondarva G, Moscinski L, Atadja P, et al. Combination of the histone deacetylase inhibitor LBH589 and the hsp90 inhibitor 17-AAG is highly active against human CML-BC cells and AML cells with activating mutation of FLT-3. *Blood.* 2005;105(4):1768-76.

22. Bali P, Pranpat M, Bradner J, Balasis M, Fiskus W, Guo F, Rocha K, Kumaraswamy S, Boyapalle S, Atadja P, et al. Inhibition of histone deacetylase 6 acetylates and disrupts the chaperone function of heat shock protein 90: a novel basis for antileukemia activity of histone deacetylase inhibitors. *The Journal of biological chemistry.* 2005;280(29):26729-34.

23. Murphy PJ, Morishima Y, Kovacs JJ, Yao TP, and Pratt WB. Regulation of the dynamics of hsp90 action on the glucocorticoid receptor by acetylation/deacetylation of the chaperone. *The Journal of biological chemistry.* 2005;280(40):33792-9.

24. Mimnaugh EG, Worland PJ, Whitesell L, and Neckers LM. Possible role for serine/threonine phosphorylation in the regulation of the heteroprotein complex between the hsp90 stress protein and the pp60v-src tyrosine kinase. *The Journal of biological chemistry.* 1995;270(48):28654-9.

25. Zhao YG, Gilmore R, Leone G, Coffey MC, Weber B, and Lee PW. Hsp90 phosphorylation is linked to its chaperoning function. Assembly of the reovirus cell attachment protein. *The Journal of biological chemistry.* 2001;276(35):32822-7.

26. Blank M, Mandel M, Keisari Y, Meruelo D, and Lavie G. Enhanced ubiquitinylation of heat shock protein 90 as a potential mechanism for mitotic cell death in cancer cells induced with hypericin. *Cancer Res.* 2003;63(23):8241-7.

27. Martinez-Ruiz A, Villanueva L, Gonzalez de Orduna C, Lopez-Ferrer D, Higueras MA, Tarin C, Rodriguez-Crespo I, Vazquez J, and Lamas S. S-nitrosylation of Hsp90 promotes the inhibition of its ATPase and

endothelial nitric oxide synthase regulatory activities. *Proc Natl Acad Sci U S A.* 2005;102(24):8525-30.

28. Voss AK, Thomas T, and Gruss P. Mice lacking HSP90beta fail to develop a placental labyrinth. *Development.* 2000;127(1):1-11.

29. He H, Zatorska D, Kim J, Aguirre J, Llauger L, She Y, Wu N, Immormino RM, Gewirth DT, and Chiosis G. Identification of potent water soluble purine-scaffold inhibitors of the heat shock protein 90. *Journal of medicinal chemistry.* 2006;49(1):381-90.

30. Kamal A, Thao L, Sensintaffar J, Zhang L, Boehm MF, Fritz LC, and Burrows FJ. A high-affinity conformation of Hsp90 confers tumour selectivity on Hsp90 inhibitors. *Nature.* 2003;425(6956):407-10.

31. Llauger L, He H, Kim J, Aguirre J, Rosen N, Peters U, Davies P, and Chiosis G. Evaluation of 8-arylsulfanyl, 8-arylsulfoxyl, and 8-arylsulfonyl adenine derivatives as inhibitors of the heat shock protein 90. *Journal of medicinal chemistry.* 2005;48(8):2892-905.

32. Vilenchik M, Solit D, Basso A, Huezo H, Lucas B, He H, Rosen N, Spampinato C, Modrich P, and Chiosis G. Targeting wide-range oncogenic transformation via PU24FCl, a specific inhibitor of tumor Hsp90. *Chemistry & biology.* 2004;11(6):787-97.

33. Biamonte MA, Shi J, Hong K, Hurst DC, Zhang L, Fan J, Busch DJ, Karjian PL, Maldonado AA, Sensintaffar JL, et al. Orally active purine-based inhibitors of the heat shock protein 90. *Journal of medicinal chemistry.* 2006;49(2):817-28.

34. Whitesell L, Shifrin SD, Schwab G, and Neckers LM. Benzoquinonoid ansamycins possess selective tumoricidal activity unrelated to src kinase inhibition. *Cancer Res.* 1992;52(7):1721-8.

35. Soga S, Neckers LM, Schulte TW, Shiotsu Y, Akasaka K, Narumi H, Agatsuma T, Ikuina Y, Murakata C, Tamaoki T, et al. KF25706, a novel oxime derivative of radicicol, exhibits in vivo antitumor activity via selective depletion of Hsp90 binding signaling molecules. *Cancer Res.* 1999;59(12):2931-8.

36. Solit DB, Zheng FF, Drobnjak M, Munster PN, Higgins B, Verbel D, Heller G, Tong W, Cordon-Cardo C, Agus DB, et al. 17-Allylamino-17-demethoxygeldanamycin induces the degradation of androgen receptor

and HER-2/neu and inhibits the growth of prostate cancer xenografts. *Clinical cancer research : an official journal of the American Association for Cancer Research.* 2002;8(5):986-93.

37. Banerji U, Walton M, Raynaud F, Grimshaw R, Kelland L, Valenti M, Judson I, and Workman P. Pharmacokinetic-pharmacodynamic relationships for the heat shock protein 90 molecular chaperone inhibitor 17-allylamino, 17-demethoxygeldanamycin in human ovarian cancer xenograft models. *Clinical cancer research : an official journal of the American Association for Cancer Research.* 2005;11(19 Pt 1):7023-32.

38. Cerchietti LC, Lopes EC, Yang SN, Hatzi K, Bunting KL, Tsikitas LA, Mallik A, Robles AI, Walling J, Varticovski L, et al. A purine scaffold Hsp90 inhibitor destabilizes BCL-6 and has specific antitumor activity in BCL-6-dependent B cell lymphomas. *Nat Med.* 2009;15(12):1369-76.

39. Eiseman JL, Lan J, Lagattuta TF, Hamburger DR, Joseph E, Covey JM, and Egorin MJ. Pharmacokinetics and pharmacodynamics of 17-demethoxy 17-[[(2-dimethylamino)ethyl]amino]geldanamycin (17DMAG, NSC 707545) in C.B-17 SCID mice bearing MDA-MB-231 human breast cancer xenografts. *Cancer chemotherapy and pharmacology.* 2005;55(1):21-32.

40. Sydor JR, Pien, C. S., Zhang, Y., Ali, J., Dembski, M.S., Ge, J., Grenier, L., Hudak, J., Normant, E., Pak, R., Patterson, J., Pink, M., Sang, J., Woodward, C., Mitsiades, C. S., Anderson, K. C., Grayzel, D. S., Wright, J., Tong, J. K., Adams, J., Palombella, V. J., and Barret, J.A. Anti-tumor activity of a novel, water soluble Hsp90 inhibitor IPI-504 in multiple myeloma. *Proc Am Assoc Cancer Res.* 2005;46(

41. Chiosis G, Vilenchik M, Kim J, and Solit D. Hsp90: the vulnerable chaperone. *Drug discovery today.* 2004;9(20):881-8.

42. Brugge JS, Erikson E, and Erikson RL. The specific interaction of the Rous sarcoma virus transforming protein, pp60src, with two cellular proteins. *Cell.* 1981;25(2):363-72.

43. Lees-Miller SP, and Anderson CW. The human double-stranded DNA-activated protein kinase phosphorylates the 90-kDa heat-shock protein, hsp90 alpha at two NH2-terminal threonine residues. *The Journal of biological chemistry.* 1989;264(29):17275-80.

44. Lees-Miller SP, and Anderson CW. Two human 90-kDa heat shock proteins are phosphorylated in vivo at conserved serines that are phosphorylated in vitro by casein kinase II. *The Journal of biological chemistry.* 1989;264(5):2431-7.

45. Walker AI, Hunt T, Jackson RJ, and Anderson CW. Double-stranded DNA induces the phosphorylation of several proteins including the 90 000 mol. wt. heat-shock protein in animal cell extracts. *The EMBO journal.* 1985;4(1):139-45.

46. Lei H, Venkatakrishnan A, Yu S, and Kazlauskas A. Protein kinase A-dependent translocation of Hsp90 alpha impairs endothelial nitric-oxide synthase activity in high glucose and diabetes. *The Journal of biological chemistry.* 2007;282(13):9364-71.

47. Kovacs JJ, Murphy PJ, Gaillard S, Zhao X, Wu JT, Nicchitta CV, Yoshida M, Toft DO, Pratt WB, and Yao TP. HDAC6 regulates Hsp90 acetylation and chaperone-dependent activation of glucocorticoid receptor. *Molecular cell.* 2005;18(5):601-7.

48. Yang Y, Rao R, Shen J, Tang Y, Fiskus W, Nechtman J, Atadja P, and Bhalla K. Role of acetylation and extracellular location of heat shock protein 90alpha in tumor cell invasion. *Cancer Res.* 2008;68(12):4833-42.

49. Scroggins BT, and Neckers L. Post-translational modification of heat-shock protein 90: impact on chaperone function. *Expert opinion on drug discovery.* 2007;2(10):1403-14.

50. Kundrat L, and Regan L. Identification of residues on Hsp70 and Hsp90 ubiquitinated by the cochaperone CHIP. *Journal of molecular biology.* 2010;395(3):587-94.

51. Connell P, Ballinger CA, Jiang J, Wu Y, Thompson LJ, Hohfeld J, and Patterson C. The co-chaperone CHIP regulates protein triage decisions mediated by heat-shock proteins. *Nature cell biology.* 2001;3(1):93-6.

52. Cloutier P, Lavallee-Adam M, Faubert D, Blanchette M, and Coulombe B. A newly uncovered group of distantly related lysine methyltransferases preferentially interact with molecular chaperones to regulate their activity. *PLoS genetics.* 2013;9(1):e1003210.

53. Abu-Farha M, Lanouette S, Elisma F, Tremblay V, Butson J, Figeys D, and Couture JF. Proteomic analyses of the SMYD family interactomes identify HSP90 as a novel target for SMYD2. *Journal of molecular cell biology.* 2011;3(5):301-8.

54. Donlin LT, Andresen C, Just S, Rudensky E, Pappas CT, Kruger M, Jacobs EY, Unger A, Zieseniss A, Dobenecker MW, et al. Smyd2 controls cytoplasmic lysine methylation of Hsp90 and myofilament organization. *Genes & development.* 2012;26(2):114-9.

55. Echtenkamp FJ, and Freeman BC. Expanding the cellular molecular chaperone network through the ubiquitous cochaperones. *Biochimica et biophysica acta.* 2012;1823(3):668-73.

56. Eckl JM, Rutz DA, Haslbeck V, Zierer BK, Reinstein J, and Richter K. Cdc37 (cell division cycle 37) restricts Hsp90 (heat shock protein 90) motility by interaction with N-terminal and middle domain binding sites. *The Journal of biological chemistry.* 2013;288(22):16032-42.

57. Li J, Richter K, Reinstein J, and Buchner J. Integration of the accelerator Aha1 in the Hsp90 co-chaperone cycle. *Nature structural & molecular biology.* 2013;20(3):326-31.

58. Moulick K, Ahn JH, Zong H, Rodina A, Cerchietti L, Gomes DaGama EM, Caldas-Lopes E, Beebe K, Perna F, Hatzi K, et al. Affinity-based proteomics reveal cancer-specific networks coordinated by Hsp90. *Nature chemical biology.* 2011;7(11):818-26.

59. Maroney AC, Marugan JJ, Mezzasalma TM, Barnakov AN, Garrabrant TA, Weaner LE, Jones WJ, Barnakova LA, Koblish HK, Todd MJ, et al. Dihydroquinone ansamycins: toward resolving the conflict between low in vitro affinity and high cellular potency of geldanamycin derivatives. *Biochemistry.* 2006;45(17):5678-85.

60. Bandhakavi S, McCann RO, Hanna DE, and Glover CV. A positive feedback loop between protein kinase CKII and Cdc37 promotes the activity of multiple protein kinases. *The Journal of biological chemistry.* 2003;278(5):2829-36.

61. Kobayashi T, Nakatani Y, Tanioka T, Tsujimoto M, Nakajo S, Nakaya K, Murakami M, and Kudo I. Regulation of cytosolic prostaglandin E synthase by phosphorylation. *The Biochemical journal.* 2004;381(Pt 1):59-69.

62. Lassle M, Blatch GL, Kundra V, Takatori T, and Zetter BR. Stress-inducible, murine protein mSTI1. Characterization of binding domains for heat shock proteins and in vitro phosphorylation by different kinases. *The Journal of biological chemistry.* 1997;272(3):1876-84.

63. Longshaw VM, Dirr HW, Blatch GL, and Lassle M. The in vitro phosphorylation of the co-chaperone mSTI1 by cell cycle kinases substantiates a predicted casein kinase II-p34cdc2-NLS (CcN) motif. *Biological chemistry.* 2000;381(11):1133-8.

64. Vaughan CK, Mollapour M, Smith JR, Truman A, Hu B, Good VM, Panaretou B, Neckers L, Clarke PA, Workman P, et al. Hsp90-dependent activation of protein kinases is regulated by chaperone-targeted dephosphorylation of Cdc37. *Molecular cell.* 2008;31(6):886-95.

65. Gallegos Ruiz MI, Floor K, Roepman P, Rodriguez JA, Meijer GA, Mooi WJ, Jassem E, Niklinski J, Muley T, van Zandwijk N, et al. Integration of gene dosage and gene expression in non-small cell lung cancer, identification of HSP90 as potential target. *PloS one.* 2008;3(3):e0001722.

66. Jolly C, Michelland S, Rocchi M, Robert-Nicoud M, and Vourc'h C. Analysis of the transcriptional activity of amplified genes in tumour cells by fluorescence in situ hybridization. *Human genetics.* 1997;101(1):81-7.

67. McDowell CL, Bryan Sutton R, and Obermann WM. Expression of Hsp90 chaperone [corrected] proteins in human tumor tissue. *International journal of biological macromolecules.* 2009;45(3):310-4.

68. Passarino G, Cavalleri GL, Stecconi R, Franceschi C, Altomare K, Dato S, Greco V, Luca Cavalli Sforza L, Underhill PA, and de Benedictis G. Molecular variation of human HSP90alpha and HSP90beta genes in Caucasians. *Human mutation.* 2003;21(5):554-5.

69. Muller P, Ruckova E, Halada P, Coates PJ, Hrstka R, Lane DP, and Vojtesek B. C-terminal phosphorylation of Hsp70 and Hsp90 regulates alternate binding to co-chaperones CHIP and HOP to determine cellular protein folding/degradation balances. *Oncogene.* 2013;32(25):3101-10.

70. Polier S, Samant RS, Clarke PA, Workman P, Prodromou C, and Pearl LH. ATP-competitive inhibitors block protein kinase recruitment to the Hsp90-Cdc37 system. *Nature chemical biology.* 2013;9(5):307-12.

71. Shipp C, Watson K, and Jones GL. Associations of HSP90 client proteins in human breast cancer. *Anticancer research.* 2011;31(6):2095-101.

72. Chiosis G, and Neckers L. Tumor selectivity of Hsp90 inhibitors: the explanation remains elusive. *ACS chemical biology.* 2006;1(5):279-84.

73. Whitesell L, Mimnaugh EG, De Costa B, Myers CE, and Neckers LM. Inhibition of heat shock protein HSP90-pp60v-src heteroprotein complex formation by benzoquinone ansamycins: essential role for stress proteins in oncogenic transformation. *Proc Natl Acad Sci U S A.* 1994;91(18):8324-8.

74. Nayar U, Lu P, Goldstein RL, Vider J, Ballon G, Rodina A, Taldone T, Erdjument-Bromage H, Chomet M, Blasberg R, et al. Targeting the Hsp90-associated viral oncoproteome in gammaherpesvirus-associated malignancies. *Blood.* 2013;122(16):2837-47.

75. Guasparri I, Keller SA, and Cesarman E. KSHV vFLIP is essential for the survival of infected lymphoma cells. *J Exp Med.* 2004;199(7):993-1003.

76. Bonvini P, Gastaldi T, Falini B, and Rosolen A. Nucleophosmin-anaplastic lymphoma kinase (NPM-ALK), a novel Hsp90-client tyrosine kinase: down-regulation of NPM-ALK expression and tyrosine phosphorylation in ALK(+) CD30(+) lymphoma cells by the Hsp90 antagonist 17-allylamino,17-demethoxygeldanamycin. *Cancer Res.* 2002;62(5):1559-66.

77. Minami Y, Kiyoi H, Yamamoto Y, Yamamoto K, Ueda R, Saito H, and Naoe T. Selective apoptosis of tandemly duplicated FLT3-transformed leukemia cells by Hsp90 inhibitors. *Leukemia.* 2002;16(8):1535-40.

78. An WG, Schulte TW, and Neckers LM. The heat shock protein 90 antagonist geldanamycin alters chaperone association with p210bcr-abl and v-src proteins before their degradation by the proteasome. *Cell growth & differentiation : the molecular biology journal of the American Association for Cancer Research.* 2000;11(7):355-60.

79. Fumo G, Akin C, Metcalfe DD, and Neckers L. 17-Allylamino-17-demethoxygeldanamycin (17-AAG) is effective in down-regulating mutated, constitutively activated KIT protein in human mast cells. *Blood.* 2004;103(3):1078-84.

80. da Rocha Dias S, Friedlos F, Light Y, Springer C, Workman P, and Marais R. Activated B-RAF is an Hsp90 client protein that is targeted by the anticancer drug 17-allylamino-17-demethoxygeldanamycin. *Cancer Res.* 2005;65(23):10686-91.

81. Grbovic OM, Basso AD, Sawai A, Ye Q, Friedlander P, Solit D, and Rosen N. V600E B-Raf requires the Hsp90 chaperone for stability and is degraded in response to Hsp90 inhibitors. *Proc Natl Acad Sci U S A.* 2006;103(1):57-62.

82. Vanaja DK, Mitchell SH, Toft DO, and Young CY. Effect of geldanamycin on androgen receptor function and stability. *Cell stress & chaperones.* 2002;7(1):55-64.

83. Druker BJ, Tamura S, Buchdunger E, Ohno S, Segal GM, Fanning S, Zimmermann J, and Lydon NB. Effects of a selective inhibitor of the Abl tyrosine kinase on the growth of Bcr-Abl positive cells. *Nat Med.* 1996;2(5):561-6.

84. Shah NP, Nicoll JM, Nagar B, Gorre ME, Paquette RL, Kuriyan J, and Sawyers CL. Multiple BCR-ABL kinase domain mutations confer polyclonal resistance to the tyrosine kinase inhibitor imatinib (STI571) in chronic phase and blast crisis chronic myeloid leukemia. *Cancer Cell.* 2002;2(2):117-25.

85. Gorre ME, Ellwood-Yen K, Chiosis G, Rosen N, and Sawyers CL. BCR-ABL point mutants isolated from patients with imatinib mesylate-resistant chronic myeloid leukemia remain sensitive to inhibitors of the BCR-ABL chaperone heat shock protein 90. *Blood.* 2002;100(8):3041-4.

86. Wang S, Pashtan I, Tsutsumi S, Xu W, and Neckers L. Cancer cells harboring MET gene amplification activate alternative signaling pathways to escape MET inhibition but remain sensitive to Hsp90 inhibitors. *Cell cycle.* 2009;8(13):2050-6.

87. Bachleitner-Hofmann T, Sun MY, Chen CT, Liska D, Zeng Z, Viale A, Olshen AB, Mittlboeck M, Christensen JG, Rosen N, et al. Antitumor

activity of SNX-2112, a synthetic heat shock protein-90 inhibitor, in MET-amplified tumor cells with or without resistance to selective MET Inhibition. *Clinical cancer research : an official journal of the American Association for Cancer Research.* 2011;17(1):122-33.

88. Shimamura T, Li D, Ji H, Haringsma HJ, Liniker E, Borgman CL, Lowell AM, Minami Y, McNamara K, Perera SA, et al. Hsp90 inhibition suppresses mutant EGFR-T790M signaling and overcomes kinase inhibitor resistance. *Cancer Res.* 2008;68(14):5827-38.

89. Xu W, Soga S, Beebe K, Lee MJ, Kim YS, Trepel J, and Neckers L. Sensitivity of epidermal growth factor receptor and ErbB2 exon 20 insertion mutants to Hsp90 inhibition. *British journal of cancer.* 2007;97(6):741-4.

90. Katayama R, Khan TM, Benes C, Lifshits E, Ebi H, Rivera VM, Shakespeare WC, Iafrate AJ, Engelman JA, and Shaw AT. Therapeutic strategies to overcome crizotinib resistance in non-small cell lung cancers harboring the fusion oncogene EML4-ALK. *Proc Natl Acad Sci U S A.* 2011;108(18):7535-40.

91. Scaltriti M, Serra V, Normant E, Guzman M, Rodriguez O, Lim AR, Slocum KL, West KA, Rodriguez V, Prudkin L, et al. Antitumor activity of the Hsp90 inhibitor IPI-504 in HER2-positive trastuzumab-resistant breast cancer. *Mol Cancer Ther.* 2011;10(5):817-24.

92. Caldas-Lopes E, Cerchietti L, Ahn JH, Clement CC, Robles AI, Rodina A, Moulick K, Taldone T, Gozman A, Guo Y, et al. Hsp90 inhibitor PU-H71, a multimodal inhibitor of malignancy, induces complete responses in triple-negative breast cancer models. *Proc Natl Acad Sci U S A.* 2009;106(20):8368-73.

93. Roue G, Perez-Galan P, Mozos A, Lopez-Guerra M, Xargay-Torrent S, Rosich L, Saborit-Villarroya I, Normant E, Campo E, and Colomer D. The Hsp90 inhibitor IPI-504 overcomes bortezomib resistance in mantle cell lymphoma in vitro and in vivo by down-regulation of the prosurvival ER chaperone BiP/Grp78. *Blood.* 2011;117(4):1270-9.

94. Supko JG, Hickman RL, Grever MR, and Malspeis L. Preclinical pharmacologic evaluation of geldanamycin as an antitumor agent. *Cancer chemotherapy and pharmacology.* 1995;36(4):305-15.

95. Sydor JR, Normant E, Pien CS, Porter JR, Ge J, Grenier L, Pak RH, Ali JA, Dembski MS, Hudak J, et al. Development of 17-allylamino-17-demethoxygeldanamycin hydroquinone hydrochloride (IPI-504), an anti-cancer agent directed against Hsp90. *Proc Natl Acad Sci U S A.* 2006;103(46):17408-13.

96. Jhaveri K, Ochiana SO, Dunphy MP, Gerecitano JF, Corben AD, Peter RI, Janjigian YY, Gomes-DaGama EM, Koren J, 3rd, Modi S, et al. Heat shock protein 90 inhibitors in the treatment of cancer: current status and future directions. *Expert opinion on investigational drugs.* 2014;23(5):611-28.

97. Kuppers R. Mechanisms of B-cell lymphoma pathogenesis. *Nature reviews Cancer.* 2005;5(4):251-62.

98. Rajewsky K. Clonal selection and learning in the antibody system. *Nature.* 1996;381(6585):751-8.

99. MacLennan IC. Germinal centers. *Annual review of immunology.* 1994;12(117-39.

100. Kuppers R, Zhao M, Hansmann ML, and Rajewsky K. Tracing B cell development in human germinal centres by molecular analysis of single cells picked from histological sections. *The EMBO journal.* 1993;12(13):4955-67.

101. Liu YJ, Arpin C, de Bouteiller O, Guret C, Banchereau J, Martinez-Valdez H, and Lebecque S. Sequential triggering of apoptosis, somatic mutation and isotype switch during germinal center development. *Seminars in immunology.* 1996;8(3):169-77.

102. Cattoretti G, Chang CC, Cechova K, Zhang J, Ye BH, Falini B, Louie DC, Offit K, Chaganti RS, and Dalla-Favera R. BCL-6 protein is expressed in germinal-center B cells. *Blood.* 1995;86(1):45-53.

103. Ye BH, Cattoretti G, Shen Q, Zhang J, Hawe N, de Waard R, Leung C, Nouri-Shirazi M, Orazi A, Chaganti RS, et al. The BCL-6 proto-oncogene controls germinal-centre formation and Th2-type inflammation. *Nat Genet.* 1997;16(2):161-70.

104. Kerfoot SM, Yaari G, Patel JR, Johnson KL, Gonzalez DG, Kleinstein SH, and Haberman AM. Germinal center B cell and T follicular helper

cell development initiates in the interfollicular zone. *Immunity.* 2011;34(6):947-60.

105. Kitano M, Moriyama S, Ando Y, Hikida M, Mori Y, Kurosaki T, and Okada T. Bcl6 protein expression shapes pre-germinal center B cell dynamics and follicular helper T cell heterogeneity. *Immunity.* 2011;34(6):961-72.

106. Phan RT, and Dalla-Favera R. The BCL6 proto-oncogene suppresses p53 expression in germinal-centre B cells. *Nature.* 2004;432(7017):635-9.

107. Phan RT, Saito M, Basso K, Niu H, and Dalla-Favera R. BCL6 interacts with the transcription factor Miz-1 to suppress the cyclin-dependent kinase inhibitor p21 and cell cycle arrest in germinal center B cells. *Nat Immunol.* 2005;6(10):1054-60.

108. Ranuncolo SM, Polo JM, Dierov J, Singer M, Kuo T, Greally J, Green R, Carroll M, and Melnick A. Bcl-6 mediates the germinal center B cell phenotype and lymphomagenesis through transcriptional repression of the DNA-damage sensor ATR. *Nat Immunol.* 2007;8(7):705-14.

109. Ranuncolo SM, Wang L, Polo JM, Dell'Oso T, Dierov J, Gaymes TJ, Rassool F, Carroll M, and Melnick A. BCL6-mediated attenuation of DNA damage sensing triggers growth arrest and senescence through a p53-dependent pathway in a cell context-dependent manner. *The Journal of biological chemistry.* 2008;283(33):22565-72.

110. Phan RT, Saito M, Kitagawa Y, Means AR, and Dalla-Favera R. Genotoxic stress regulates expression of the proto-oncogene Bcl6 in germinal center B cells. *Nat Immunol.* 2007;8(10):1132-9.

111. Harris MB, Chang CC, Berton MT, Danial NN, Zhang J, Kuehner D, Ye BH, Kvatyuk M, Pandolfi PP, Cattoretti G, et al. Transcriptional repression of Stat6-dependent interleukin-4-induced genes by BCL-6: specific regulation of iepsilon transcription and immunoglobulin E switching. *Molecular and cellular biology.* 1999;19(10):7264-75.

112. Li Z, Wang X, Yu RY, Ding BB, Yu JJ, Dai XM, Naganuma A, Stanley ER, and Ye BH. BCL-6 negatively regulates expression of the NF-kappaB1 p105/p50 subunit. *Journal of immunology.* 2005;174(1):205-14.

113. Shaffer AL, Yu X, He Y, Boldrick J, Chan EP, and Staudt LM. BCL-6 represses genes that function in lymphocyte differentiation, inflammation, and cell cycle control. *Immunity.* 2000;13(2):199-212.

114. Niu H, Ye BH, and Dalla-Favera R. Antigen receptor signaling induces MAP kinase-mediated phosphorylation and degradation of the BCL-6 transcription factor. *Genes & development.* 1998;12(13):1953-61.

115. Saito M, Gao J, Basso K, Kitagawa Y, Smith PM, Bhagat G, Pernis A, Pasqualucci L, and Dalla-Favera R. A signaling pathway mediating downregulation of BCL6 in germinal center B cells is blocked by BCL6 gene alterations in B cell lymphoma. *Cancer Cell.* 2007;12(3):280-92.

116. A clinical evaluation of the International Lymphoma Study Group classification of non-Hodgkin's lymphoma. The Non-Hodgkin's Lymphoma Classification Project. *Blood.* 1997;89(11):3909-18.

117. Kuppers R, Klein U, Hansmann ML, and Rajewsky K. Cellular origin of human B-cell lymphomas. *N Engl J Med.* 1999;341(20):1520-9.

118. Stevenson FK, Sahota SS, Ottensmeier CH, Zhu D, Forconi F, and Hamblin TJ. The occurrence and significance of V gene mutations in B cell-derived human malignancy. *Advances in cancer research.* 2001;83(81-116.

119. Alizadeh AA, Eisen MB, Davis RE, Ma C, Lossos IS, Rosenwald A, Boldrick JC, Sabet H, Tran T, Yu X, et al. Distinct types of diffuse large B-cell lymphoma identified by gene expression profiling. *Nature.* 2000;403(6769):503-11.

120. de Jong D, and Enblad G. Inflammatory cells and immune microenvironment in malignant lymphoma. *Journal of internal medicine.* 2008;264(6):528-36.

121. Deriano L, Stracker TH, Baker A, Petrini JH, and Roth DB. Roles for NBS1 in alternative nonhomologous end-joining of V(D)J recombination intermediates. *Molecular cell.* 2009;34(1):13-25.

122. Lee GS, Neiditch MB, Salus SS, and Roth DB. RAG proteins shepherd double-strand breaks to a specific pathway, suppressing error-prone repair, but RAG nicking initiates homologous recombination. *Cell.* 2004;117(2):171-84.

123. Tsai AG, and Lieber MR. Mechanisms of chromosomal rearrangement in the human genome. *BMC genomics.* 2010;11 Suppl 1(S1.

124. Peled JU, Kuang FL, Iglesias-Ussel MD, Roa S, Kalis SL, Goodman MF, and Scharff MD. The biochemistry of somatic hypermutation. *Annual review of immunology.* 2008;26(481-511.

125. Cattoretti G, Mandelbaum J, Lee N, Chaves AH, Mahler AM, Chadburn A, Dalla-Favera R, Pasqualucci L, and MacLennan AJ. Targeted disruption of the S1P2 sphingosine 1-phosphate receptor gene leads to diffuse large B-cell lymphoma formation. *Cancer Res.* 2009;69(22):8686-92.

126. Pasqualucci L, Neumeister P, Goossens T, Nanjangud G, Chaganti RS, Kuppers R, and Dalla-Favera R. Hypermutation of multiple proto-oncogenes in B-cell diffuse large-cell lymphomas. *Nature.* 2001;412(6844):341-6.

127. Butler MP, Iida S, Capello D, Rossi D, Rao PH, Nallasivam P, Louie DC, Chaganti S, Au T, Gascoyne RD, et al. Alternative translocation breakpoint cluster region 5' to BCL-6 in B-cell non-Hodgkin's lymphoma. *Cancer Res.* 2002;62(14):4089-94.

128. Iqbal J, Greiner TC, Patel K, Dave BJ, Smith L, Ji J, Wright G, Sanger WG, Pickering DL, Jain S, et al. Distinctive patterns of BCL6 molecular alterations and their functional consequences in different subgroups of diffuse large B-cell lymphoma. *Leukemia.* 2007;21(11):2332-43.

129. Ci W, Polo JM, Cerchietti L, Shaknovich R, Wang L, Yang SN, Ye K, Farinha P, Horsman DE, Gascoyne RD, et al. The BCL6 transcriptional program features repression of multiple oncogenes in primary B cells and is deregulated in DLBCL. *Blood.* 2009;113(22):5536-48.

130. Baron BW, Anastasi J, Montag A, Huo D, Baron RM, Karrison T, Thirman MJ, Subudhi SK, Chin RK, Felsher DW, et al. The human BCL6 transgene promotes the development of lymphomas in the mouse. *Proc Natl Acad Sci U S A.* 2004;101(39):14198-203.

131. Cattoretti G, Pasqualucci L, Ballon G, Tam W, Nandula SV, Shen Q, Mo T, Murty VV, and Dalla-Favera R. Deregulated BCL6 expression recapitulates the pathogenesis of human diffuse large B cell lymphomas in mice. *Cancer Cell.* 2005;7(5):445-55.

132. Polo JM, Dell'Oso T, Ranuncolo SM, Cerchietti L, Beck D, Da Silva GF, Prive GG, Licht JD, and Melnick A. Specific peptide interference reveals BCL6 transcriptional and oncogenic mechanisms in B-cell lymphoma cells. *Nat Med.* 2004;10(12):1329-35.

133. Lenz G, Wright GW, Emre NC, Kohlhammer H, Dave SS, Davis RE, Carty S, Lam LT, Shaffer AL, Xiao W, et al. Molecular subtypes of diffuse large B-cell lymphoma arise by distinct genetic pathways. *Proc Natl Acad Sci U S A.* 2008;105(36):13520-5.

134. Xiao C, Srinivasan L, Calado DP, Patterson HC, Zhang B, Wang J, Henderson JM, Kutok JL, and Rajewsky K. Lymphoproliferative disease and autoimmunity in mice with increased miR-17-92 expression in lymphocytes. *Nat Immunol.* 2008;9(4):405-14.

135. Young KH, Leroy K, Moller MB, Colleoni GW, Sanchez-Beato M, Kerbauy FR, Haioun C, Eickhoff JC, Young AH, Gaulard P, et al. Structural profiles of TP53 gene mutations predict clinical outcome in diffuse large B-cell lymphoma: an international collaborative study. *Blood.* 2008;112(8):3088-98.

136. Pasqualucci L, Compagno M, Houldsworth J, Monti S, Grunn A, Nandula SV, Aster JC, Murty VV, Shipp MA, and Dalla-Favera R. Inactivation of the PRDM1/BLIMP1 gene in diffuse large B cell lymphoma. *J Exp Med.* 2006;203(2):311-7.

137. Tam W, Gomez M, Chadburn A, Lee JW, Chan WC, and Knowles DM. Mutational analysis of PRDM1 indicates a tumor-suppressor role in diffuse large B-cell lymphomas. *Blood.* 2006;107(10):4090-100.

138. Tagawa H, Suguro M, Tsuzuki S, Matsuo K, Karnan S, Ohshima K, Okamoto M, Morishima Y, Nakamura S, and Seto M. Comparison of genome profiles for identification of distinct subgroups of diffuse large B-cell lymphoma. *Blood.* 2005;106(5):1770-7.

139. Davis RE, Brown KD, Siebenlist U, and Staudt LM. Constitutive nuclear factor kappaB activity is required for survival of activated B cell-like diffuse large B cell lymphoma cells. *J Exp Med.* 2001;194(12):1861-74.

140. Lam LT, Davis RE, Pierce J, Hepperle M, Xu Y, Hottelet M, Nong Y, Wen D, Adams J, Dang L, et al. Small molecule inhibitors of IkappaB kinase are selectively toxic for subgroups of diffuse large B-cell lymphoma defined by gene expression profiling. *Clinical cancer*

research : an official journal of the American Association for Cancer Research. 2005;11(1):28-40.

141. Sciammas R, Shaffer AL, Schatz JH, Zhao H, Staudt LM, and Singh H. Graded expression of interferon regulatory factor-4 coordinates isotype switching with plasma cell differentiation. *Immunity.* 2006;25(2):225-36.

142. Shaffer AL, Emre NC, Lamy L, Ngo VN, Wright G, Xiao W, Powell J, Dave S, Yu X, Zhao H, et al. IRF4 addiction in multiple myeloma. *Nature.* 2008;454(7201):226-31.

143. Iwakoshi NN, Lee AH, and Glimcher LH. It's a good year for Blimp-1 (and plasma cells). *Immunity.* 2003;19(4):466-8.

144. Reimold AM, Iwakoshi NN, Manis J, Vallabhajosyula P, Szomolanyi-Tsuda E, Gravallese EM, Friend D, Grusby MJ, Alt F, and Glimcher LH. Plasma cell differentiation requires the transcription factor XBP-1. *Nature.* 2001;412(6844):300-7.

145. Shaffer AL, Shapiro-Shelef M, Iwakoshi NN, Lee AH, Qian SB, Zhao H, Yu X, Yang L, Tan BK, Rosenwald A, et al. XBP1, downstream of Blimp-1, expands the secretory apparatus and other organelles, and increases protein synthesis in plasma cell differentiation. *Immunity.* 2004;21(1):81-93.

146. Dal Porto JM, Gauld SB, Merrell KT, Mills D, Pugh-Bernard AE, and Cambier J. B cell antigen receptor signaling 101. *Mol Immunol.* 2004;41(6-7):599-613.

147. Lenz G, and Staudt LM. Aggressive lymphomas. *N Engl J Med.* 2010;362(15):1417-29.

148. Ngo VN, Davis RE, Lamy L, Yu X, Zhao H, Lenz G, Lam LT, Dave S, Yang L, Powell J, et al. A loss-of-function RNA interference screen for molecular targets in cancer. *Nature.* 2006;441(7089):106-10.

149. Lenz G, Davis RE, Ngo VN, Lam L, George TC, Wright GW, Dave SS, Zhao H, Xu W, Rosenwald A, et al. Oncogenic CARD11 mutations in human diffuse large B cell lymphoma. *Science.* 2008;319(5870):1676-9.

150. Davis RE, Ngo VN, Lenz G, Tolar P, Young RM, Romesser PB, Kohlhammer H, Lamy L, Zhao H, Yang Y, et al. Chronic active B-cell-

receptor signalling in diffuse large B-cell lymphoma. *Nature.* 2010;463(7277):88-92.

151. Gazumyan A, Reichlin A, and Nussenzweig MC. Ig beta tyrosine residues contribute to the control of B cell receptor signaling by regulating receptor internalization. *J Exp Med.* 2006;203(7):1785-94.

152. Kraus M, Saijo K, Torres RM, and Rajewsky K. Ig-alpha cytoplasmic truncation renders immature B cells more sensitive to antigen contact. *Immunity.* 1999;11(5):537-45.
153. Torres RM, and Hafen K. A negative regulatory role for Ig-alpha during B cell development. *Immunity.* 1999;11(5):527-36.

154. Gauld SB, and Cambier JC. Src-family kinases in B-cell development and signaling. *Oncogene.* 2004;23(48):8001-6.

155. Xu Y, Harder KW, Huntington ND, Hibbs ML, and Tarlinton DM. Lyn tyrosine kinase: accentuating the positive and the negative. *Immunity.* 2005;22(1):9-18.

156. Chan VW, Meng F, Soriano P, DeFranco AL, and Lowell CA. Characterization of the B lymphocyte populations in Lyn-deficient mice and the role of Lyn in signal initiation and down-regulation. *Immunity.* 1997;7(1):69-81.

157. Thome M. CARMA1, BCL-10 and MALT1 in lymphocyte development and activation. *Nat Rev Immunol.* 2004;4(5):348-59.

158. Tolar P, Hanna J, Krueger PD, and Pierce SK. The constant region of the membrane immunoglobulin mediates B cell-receptor clustering and signaling in response to membrane antigens. *Immunity.* 2009;30(1):44-55.

159. Chen L, Juszczynski P, Takeyama K, Aguiar RC, and Shipp MA. Protein tyrosine phosphatase receptor-type O truncated (PTPROt) regulates SYK phosphorylation, proximal B-cell-receptor signaling, and cellular proliferation. *Blood.* 2006;108(10):3428-33.

160. Chen L, Monti S, Juszczynski P, Daley J, Chen W, Witzig TE, Habermann TM, Kutok JL, and Shipp MA. SYK-dependent tonic B-cell receptor signaling is a rational treatment target in diffuse large B-cell lymphoma. *Blood.* 2008;111(4):2230-7.

161. Friedberg JW, Sharman J, Sweetenham J, Johnston PB, Vose JM, Lacasce A, Schaefer-Cutillo J, De Vos S, Sinha R, Leonard JP, et al. Inhibition of Syk with fostamatinib disodium has significant clinical activity in non-Hodgkin lymphoma and chronic lymphocytic leukemia. *Blood.* 2010;115(13):2578-85.

162. Coffey G, Betz A, DeGuzman F, Pak Y, Inagaki M, Baker DC, Hollenbach SJ, Pandey A, and Sinha U. The novel kinase inhibitor PRT062070 (Cerdulatinib) demonstrates efficacy in models of autoimmunity and B-cell cancer. *The Journal of pharmacology and experimental therapeutics.* 2014;351(3):538-48.

163. Milhollen MA, Traore T, Adams-Duffy J, Thomas MP, Berger AJ, Dang L, Dick LR, Garnsey JJ, Koenig E, Langston SP, et al. MLN4924, a NEDD8-activating enzyme inhibitor, is active in diffuse large B-cell lymphoma models: rationale for treatment of NF-{kappa}B-dependent lymphoma. *Blood.* 2010;116(9):1515-23.

164. Naylor TL, Tang H, Ratsch BA, Enns A, Loo A, Chen L, Lenz P, Waters NJ, Schuler W, Dorken B, et al. Protein kinase C inhibitor sotrastaurin selectively inhibits the growth of CD79 mutant diffuse large B-cell lymphomas. *Cancer Res.* 2011;71(7):2643-53.

165. Fontan L, Yang C, Kabaleeswaran V, Volpon L, Osborne MJ, Beltran E, Garcia M, Cerchietti L, Shaknovich R, Yang SN, et al. MALT1 small molecule inhibitors specifically suppress ABC-DLBCL in vitro and in vivo. *Cancer Cell.* 2012;22(6):812-24.

166. Nagel D, Spranger S, Vincendeau M, Grau M, Raffegerst S, Kloo B, Hlahla D, Neuenschwander M, Peter von Kries J, Hadian K, et al. Pharmacologic inhibition of MALT1 protease by phenothiazines as a therapeutic approach for the treatment of aggressive ABC-DLBCL. *Cancer Cell.* 2012;22(6):825-37.

167. Gupta M, Ansell SM, Novak AJ, Kumar S, Kaufmann SH, and Witzig TE. Inhibition of histone deacetylase overcomes rapamycin-mediated resistance in diffuse large B-cell lymphoma by inhibiting Akt signaling through mTORC2. *Blood.* 2009;114(14):2926-35.

168. Yap TA, Garrett MD, Walton MI, Raynaud F, de Bono JS, and Workman P. Targeting the PI3K-AKT-mTOR pathway: progress, pitfalls, and promises. *Curr Opin Pharmacol.* 2008;8(4):393-412.

169. Hudes G, Carducci M, Tomczak P, Dutcher J, Figlin R, Kapoor A, Staroslawska E, Sosman J, McDermott D, Bodrogi I, et al. Temsirolimus, interferon alfa, or both for advanced renal-cell carcinoma. *N Engl J Med.* 2007;356(22):2271-81.

170. Witzig TE, Reeder CB, LaPlant BR, Gupta M, Johnston PB, Micallef IN, Porrata LF, Ansell SM, Colgan JP, Jacobsen ED, et al. A phase II trial of the oral mTOR inhibitor everolimus in relapsed aggressive lymphoma. *Leukemia.* 2011;25(2):341-7.

171. Levy DS, Kahana JA, and Kumar R. AKT inhibitor, GSK690693, induces growth inhibition and apoptosis in acute lymphoblastic leukemia cell lines. *Blood.* 2009;113(8):1723-9.

172. Zang C, Eucker J, Liu H, Coordes A, Lenarz M, Possinger K, and Scholz CW. Inhibition of pan-class I phosphatidyl-inositol-3-kinase by NVP-BKM120 effectively blocks proliferation and induces cell death in diffuse large B-cell lymphoma. *Leukemia & lymphoma.* 2014;55(2):425-34.

173. Castillo JJ, Furman M, and Winer ES. CAL-101: a phosphatidylinositol-3-kinase p110-delta inhibitor for the treatment of lymphoid malignancies. *Expert opinion on investigational drugs.* 2012;21(1):15-22.

174. Kahl B, Byrd JC, Flinn IW, Wagner-Johnston N, Spurgeon S, Benson DM, Jr., Furman RR, Brown JR, Coutre S, Lannutti B, et al. Clinical safety and activity in a phase 1 study of CAL-101, an isoform-selective inhibitor of phosphatidylinositol 3-kinase p110(delta), in patients with relapsed or refractory non-hodgkin lymphoma. *Blood.*116(21):1777.

175. Dai B, Zhao XF, Hagner P, Shapiro P, Mazan-Mamczarz K, Zhao S, Natkunam Y, and Gartenhaus RB. Extracellular signal-regulated kinase positively regulates the oncogenic activity of MCT-1 in diffuse large B-cell lymphoma. *Cancer Res.* 2009;69(19):7835-43.

176. Friday BB, and Adjei AA. Advances in targeting the Ras/Raf/MEK/Erk mitogen-activated protein kinase cascade with MEK inhibitors for cancer therapy. *Clinical cancer research : an official journal of the American Association for Cancer Research.* 2008;14(2):342-6.

177. Bhalla S, Evens AM, Dai B, Prachand S, Gordon LI, and Gartenhaus RB. The novel anti-MEK small molecule AZD6244 induces BIM-

dependent and AKT-independent apoptosis in diffuse large B-cell lymphoma. *Blood.* 2011;118(4):1052-61.

178. Honigberg LA, Smith AM, Sirisawad M, Verner E, Loury D, Chang B, Li S, Pan Z, Thamm DH, Miller RA, et al. The Bruton tyrosine kinase inhibitor PCI-32765 blocks B-cell activation and is efficacious in models of autoimmune disease and B-cell malignancy. *Proc Natl Acad Sci U S A.* 2010;107(29):13075-80.

179. Advani RH, Buggy JJ, Sharman JP, Smith SM, Boyd TE, Grant B, Kolibaba KS, Furman RR, Rodriguez S, Chang BY, et al. Bruton tyrosine kinase inhibitor ibrutinib (PCI-32765) has significant activity in patients with relapsed/refractory B-cell malignancies. *Journal of clinical oncology : official journal of the American Society of Clinical Oncology.* 2013;31(1):88-94.

180. Barrientos J, and Rai K. Ibrutinib: a novel Bruton's tyrosine kinase inhibitor with outstanding responses in patients with chronic lymphocytic leukemia. *Leukemia & lymphoma.* 2013;54(8):1817-20.

181. Wilson WH, Gerecitano JF, Goy A, de Vos S, Kenkre VP, Barr PM, Blum KA, Shustov AR, Advani RH, Lih J, et al. The Bruton's Tyrosine Kinase (BTK) inhbitor, Ibrutinib (PCI-32765), has preferential activity in the ABC subtype of relapsed/refractory de novo diffuse large B-cell lymphoma (DLBCL): Interim results of a multicenter, open-label phase 2 study. *Blood.* 2012;120(21):686.

182. Aue G, Valdez J, Martyr S, Jones J, Soto S, Stetler-Stevenson M, Yuan C, Arthur DC, Thomas F, Tian X, et al. *Single Agent Ibrutinib (PCI-32765) Achieves Equally Good and Durable Responses In Chronic Lymphocytic Leukemia (CLL) Patients With and Without Deletion 17p.* 2013.

183. Burger JA, Keating MJ, Wierda WG, Hartmann E, Hoellenriegel J, Rosin NY, de Weerdt I, Jeyakumar G, Ferrajoli A, Cardenas-Turanzas M, et al. Safety and activity of ibrutinib plus rituximab for patients with high-risk chronic lymphocytic leukaemia: a single-arm, phase 2 study. *The Lancet Oncology.* 2014;15(10):1090-9.

184. Wang ML, Rule S, Martin P, Goy A, Auer R, Kahl BS, Jurczak W, Advani RH, Romaguera JE, Williams ME, et al. Targeting BTK with ibrutinib in relapsed or refractory mantle-cell lymphoma. *N Engl J Med.* 2013;369(6):507-16.

185. Mahajan S, Ghosh S, Sudbeck EA, Zheng Y, Downs S, Hupke M, and Uckun FM. Rational design and synthesis of a novel anti-leukemic agent targeting Bruton's tyrosine kinase (BTK), LFM-A13 [alpha-cyano-beta-hydroxy-beta-methyl-N-(2, 5-dibromophenyl)propenamide]. *The Journal of biological chemistry.* 1999;274(14):9587-99.

186. Uckun F, Dibirdik I, Sarkissian A, and Qazi S. In vitro and in vivo chemosensitizing activity of LFM-A13, a dual-function inhibitor of Bruton's tyrosine kinase and polo-like kinases, against human leukemic B-cell precursors. *Arzneimittel-Forschung.* 2011;61(4):252-9.

187. Wright G, Tan B, Rosenwald A, Hurt EH, Wiestner A, and Staudt LM. A gene expression-based method to diagnose clinically distinct subgroups of diffuse large B cell lymphoma. *Proc Natl Acad Sci U S A.* 2003;100(17):9991-6.

188. Coiffier B, Lepage E, Briere J, Herbrecht R, Tilly H, Bouabdallah R, Morel P, Van Den Neste E, Salles G, Gaulard P, et al. CHOP chemotherapy plus rituximab compared with CHOP alone in elderly patients with diffuse large-B-cell lymphoma. *N Engl J Med.* 2002;346(4):235-42.

189. Younes A, Flinn I, Berdeja J, Friedberg JW, Casulo C, Thieblemont C, Morschhauser F, Westin JR, Seetharam S, Hellemans P, et al. *Combining Ibrutinib With Rituximab, Cyclophosphamide, Doxorubicin, Vincristine, and Prednisone (R-CHOP): Updated Results From a Phase 1b Study In Treatment-Naïve Patients With CD20-Positive B-Cell Non-Hodgkin's Lymphoma (NHL).* 2013.

190. Furman RR, Cheng S, Lu P, Setty M, Perez AR, Guo A, Racchumi J, Xu G, Wu H, Ma J, et al. Ibrutinib resistance in chronic lymphocytic leukemia. *N Engl J Med.* 2014;370(24):2352-4.

191. Woyach JA, Furman RR, Liu TM, Ozer HG, Zapatka M, Ruppert AS, Xue L, Li DH, Steggerda SM, Versele M, et al. Resistance mechanisms for the Bruton's tyrosine kinase inhibitor ibrutinib. *N Engl J Med.* 2014;370(24):2286-94.

192. Mathews Griner LA, Guha R, Shinn P, Young RM, Keller JM, Liu D, Goldlust IS, Yasgar A, McKnight C, Boxer MB, et al. High-throughput combinatorial screening identifies drugs that cooperate with ibrutinib to

kill activated B-cell-like diffuse large B-cell lymphoma cells. *Proc Natl Acad Sci U S A.* 2014;111(6):2349-54.

193. Gerecitano JF, Modi S, Gajria D, Taldone T, Alpaugh M, Gomes DaGama E, Uddin M, Chiosis G, Lewis JS, Larson SM, et al. Using 124I-PU-H71 PET imaging to predict intratumoral concentration in patients on a phase I trial of PU-H71. *ASCO Meeting Abstracts.* 2013;31(15_suppl):11076.

194. Cerchietti LC, Hatzi K, Caldas-Lopes E, Yang SN, Figueroa ME, Morin RD, Hirst M, Mendez L, Shaknovich R, Cole PA, et al. BCL6 repression of EP300 in human diffuse large B cell lymphoma cells provides a basis for rational combinatorial therapy. *J Clin Invest.* 2010.

195. Moorhead GB, Trinkle-Mulcahy L, Nimick M, De Wever V, Campbell DG, Gourlay R, Lam YW, and Lamond AI. Displacement affinity chromatography of protein phosphatase one (PP1) complexes. *BMC biochemistry.* 2008;9(28.

196. Jensen LJ, Kuhn M, Stark M, Chaffron S, Creevey C, Muller J, Doerks T, Julien P, Roth A, Simonovic M, et al. STRING 8--a global view on proteins and their functional interactions in 630 organisms. *Nucleic acids research.* 2009;37(Database issue):D412-6.

197. Zhao R, Davey M, Hsu YC, Kaplanek P, Tong A, Parsons AB, Krogan N, Cagney G, Mai D, Greenblatt J, et al. Navigating the chaperone network: an integrative map of physical and genetic interactions mediated by the hsp90 chaperone. *Cell.* 2005;120(5):715-27.

198. Gano JJ, and Simon JA. A proteomic investigation of ligand-dependent HSP90 complexes reveals CHORDC1 as a novel ADP-dependent HSP90-interacting protein. *Molecular & cellular proteomics : MCP.* 2010;9(2):255-70.

199. Tsaytler PA, Krijgsveld J, Goerdayal SS, Rudiger S, and Egmond MR. Novel Hsp90 partners discovered using complementary proteomic approaches. *Cell stress & chaperones.* 2009;14(6):629-38.

200. Taipale M, Krykbaeva I, Koeva M, Kayatekin C, Westover KD, Karras GI, and Lindquist S. Quantitative analysis of HSP90-client interactions reveals principles of substrate recognition. *Cell.* 2012;150(5):987-1001.

201. Sharma K, Vabulas RM, Macek B, Pinkert S, Cox J, Mann M, and Hartl FU. Quantitative proteomics reveals that Hsp90 inhibition preferentially

targets kinases and the DNA damage response. *Molecular & cellular proteomics : MCP.* 2012;11(3):M111 014654.

202. Cheng PC, Brown BK, Song W, and Pierce SK. Translocation of the B cell antigen receptor into lipid rafts reveals a novel step in signaling. *Journal of immunology.* 2001;166(6):3693-701.

203. Chen L, Monti S, Juszczynski P, Ouyang J, Chapuy B, Neuberg D, Doench JG, Bogusz AM, Habermann TM, Dogan A, et al. SYK inhibition modulates distinct PI3K/AKT- dependent survival pathways and cholesterol biosynthesis in diffuse large B cell lymphomas. *Cancer Cell.* 2013;23(6):826-38.

204. Gimpl G, and Gehrig-Burger K. Cholesterol reporter molecules. *Bioscience reports.* 2007;27(6):335-58.

205. Karnell FG, Brezski RJ, King LB, Silverman MA, and Monroe JG. Membrane cholesterol content accounts for developmental differences in surface B cell receptor compartmentalization and signaling. *The Journal of biological chemistry.* 2005;280(27):25621-8.

206. Bolte S, and Cordelieres FP. A guided tour into subcellular colocalization analysis in light microscopy. *Journal of microscopy.* 2006;224(Pt 3):213-32.

207. Grammatikakis N, Vultur A, Ramana CV, Siganou A, Schweinfest CW, Watson DK, and Raptis L. The role of Hsp90N, a new member of the Hsp90 family, in signal transduction and neoplastic transformation. *The Journal of biological chemistry.* 2002;277(10):8312-20.

208. Bijlmakers MJ, and Marsh M. Hsp90 is essential for the synthesis and subsequent membrane association, but not the maintenance, of the Src-kinase p56(lck). *Molecular biology of the cell.* 2000;11(5):1585-95.

209. Shinozaki F, Minami M, Chiba T, Suzuki M, Yoshimatsu K, Ichikawa Y, Terasawa K, Emori Y, Matsumoto K, Kurosaki T, et al. Depletion of hsp90beta induces multiple defects in B cell receptor signaling. *The Journal of biological chemistry.* 2006;281(24):16361-9.

210. Chou TC, and Talalay P. Quantitative analysis of dose-effect relationships: the combined effects of multiple drugs or enzyme inhibitors. *Advances in enzyme regulation.* 1984;22(27-55.

211. Hans CP, Weisenburger DD, Greiner TC, Gascoyne RD, Delabie J, Ott G, Muller-Hermelink HK, Campo E, Braziel RM, Jaffe ES, et al. Confirmation of the molecular classification of diffuse large B-cell lymphoma by immunohistochemistry using a tissue microarray. *Blood.* 2004;103(1):275-82.